UNIVERSITY OF CALIFORNIA SAN DIEGO

Metabolic regulation of neuronal mitochondria by O-GlcNAcylation

A Dissertation submitted in partial satisfaction of the requirements
for the degree Doctor of Philosophy

in

Biology

by

Seungyoon Blenda Yu

Committee in charge:

Professor Gulcin Pekkurnaz, Chair
Professor Susan Ackerman
Professor Jeffrey Esko
Professor Anthony Molina
Professor Gerald Shadel

2022

The Dissertation of Seungyoon Blenda Yu is approved, and it is acceptable in quality and form for publication on microfilm and electronically.

University of California San Diego

2022

EPIGRAPH

Above all, don’t fear difficult moments. The best comes from them.

-Rita Levi-Montalcini

TABLE OF CONTENTS

DISSERTATION APPROVAL PAGE iii

EPIGRAPH iv

TABLE OF CONTENTS v

LIST OF FIGURES viii

LIST OF TABLES x

LIST OF ABBREVIATIONS xi

ACKNOWLEDGEMENTS xiv

VITA xvi

ABSTRACT OF THE DISSERTATION xvii

CHAPTER 1: INTRODUCTION 1

MITOCHONDRIA AS INDEPENDENT YET COOPERATIVE ENTITIES IN CELLS 1

NEURON'S EXTRAORDINARY ENERGY DEMANDS ARE FULFILLED BY MITOCHONDRIA 2

REGULATION OF MITOCHONDRIAL DYNAMICS AND DISTRIBUTION IN NEURONS 4

HEXOSAMINE BIOSYNTHETIC PATHWAY SIGNALS GLUCOSE AVAILABILITY TO MITOCHONDRIA IN NEURONS 5

METABOLIC REGULATION OF NEURONAL MITOCHONDRIA BY O-GLCNACYLATION 6

FIGURES 8

ACKNOWLEDGEMENTS 9

CHAPTER 2: NEURONAL ACTIVITY-DRIVEN O-GLCNACYLATION PROMOTES MITOCHONDRIAL PLASTICITY 10

INTRODUCTION 10

RESULTS 11

CONCLUDING REMARKS 18

Materials and methods 21

Figures and tables 31

Acknowledgements 53

Author contributions 53

CHAPTER 3: O-GlcNAcylation promotes substrate-specific neuronal excitability 54

INTRODUCTION 54

RESULTS 55

CONCLUDING REMARKS 59

Materials and methods 61

Figures 65

Acknowledgements 70

Author contributions 70

CHAPTER 4: Role of Sirtuin 5 in crosstalk between two post translational modifications 71

INTRODUCTION 71

RESULTS 72

CONCLUDING REMARKS 74

Materials and methods 76

Figures 80

Acknowledgements 85

Author contributions 85

CHAPTER 5: CONCLUSIONS AND FUTURE DIRECTIONS 86

O-GlcNAcylation links neuronal activity and glucose metabolism 87
Glycolytic pathway regulation via O-GlcNAcylation 88
How does mitochondrial O-GlcNAcylation control ATP production? 89
Substrate specific regulation of synaptoenergetics 91
Possible role of O-GlcNAcylation in glutamate metabolism 91
O-GlcNAcylation of SIRT5: Co-regulations of multiple PTMs 93
Concluding perspectives 95

REFERENCES 98

LIST OF FIGURES

Figure 1.1 Overview of two fundamental components of the thesis: neuronal mitochondria and O-GlcNAcylation. 8

Figure 2.1 O-GlcNAcylation is increased in neurons from seizure-induced mice. 31

Figure 2.2 O-GlcNAcylation level increases throughout hippocampal regions and cortex. 32

Figure 2.3 O-GlcNAcylation level increases in association with neural age and excitability. 34

Figure 2.4 Neuronal activity increases O-GlcNAcylation in primary cultured neurons. 35

Figure 2.6 Chronic activity by picrotoxin does not change OGT and OGA expression. 38

Figure 2.7 Transient stimulation of neurons induces glucose flux that mediates O-GlcNAcylation. 39

Figure 2.8 Transient neuronal stimulation is captured with Ca^{2+} influx. 41

Figure 2.9 Neuronal mitochondrial bioenergetics enhanced with O-GlcNAcylation. 43

Figure 2.10 Chronic manipulation of O-GlcNAc level by TMG does not influence mitochondrial protein content. 44

Figure 2.11 O-GlcNAcome in crudely isolated mitochondria from neurons. 45

Figure 2.12 Neuronal O-GlcNAcome entails various membrane-bound organelles. . 46

Figure 2.13 ATP replenishment after neuronal stimulation is O-GlcNAcylation dependent. 48

Figure 2.14 Expression of iATPSnFR in neurons and neuronal stimulation pattern with OSMI4. 50

Figure 3.1 Alterations of neuronal fuel preference and metabolite level via O-GlcNAcylation. 65

Figure 3.2 Ketone body utilization promotes mitochondrial motility while glucose causes motility arrest. 66

Figure 3.3 Representative neuronal activity recording and spike events recorded by microelectrode array. 67

Figure 3.4 Working model of synaptic excitability in neurons fueled by glucose or ketone bodies. 68

Figure 3.5 O-GlcNAcylated proteins involved in glutamate metabolism. 69

Figure 4.1 Regulation of SIRT5 O-GlcNAcylation. 80

Figure 4.2 O-GlcNAcylation does not alter mitochondrial localization of SIRT5. 81

Figure 4.3 SIRT5 enhances mitochondrial respiration. 82

Figure 4.4 Upregulation of O-GlcNAcylation enhances succinylation level in neurons. 83

Figure 4.5 O-GlcNAcylation and succinylation levels mouse brain are altered by feeding. 84

LIST OF TABLES

Table 2.1: Key resources table……..……51

LIST OF ABBREVIATIONS

Acac	Acetoacetate
Acetyl-CoA	Acetyl-Coenzyme A
AMPK	AMP-activated protein kinase
ANT	Adenine nucleotide transporters
ATP	Adenosine triphosphate
BHB	β-Hydroxybutyrate
DIV	Days In Vitro
DNA	Deoxyribonucleic acid
ENO1	Enolase 1
FCCP	carbonyl cyanide-4-(trifluoromethoxy)phenylhydrazone
FBP	Fructose-1,6-bisphosphate
GAPDH	Glyceraldehyde-3-phosphate dehydrogenase
GC-MS	Gas chromatography mass spectrometry
GDH	Glutamate dehydrogenase
GFAT	Fructose-6-phosphate-aminotransferase
GFP	Green fluorescent protein
GLUT4	Glucose transporter 4
GSIS	Glucose-stimulated insulin secretion
GOT2	Glutamate oxaloacetate transaminase 2
HBP	Hexosamine biosynthetic pathway
KA	Kainic acid
O-GlcNAc	O-linked β-N-acetylglucosamine

LC-MS/MS	Liquid chromatography with tandem mass spectrometry
MAS	Malate aspartate shuttle
MEA	Microelectrode array
MICOS	Mitochondrial contact site and cristae organizing system
MPE	Molar percent enrichment
mOGT	Mitochondrial O-GlcNAc transferase
mTOR	Mammalian target of rapamycin
MTS	Mitochondrial targeting sequence
NBQX	2,3-dihydroxy-6-nitro-7-sulphamoyl-benzo(F)quinoxaline
ncOGT	Nucleocytoplasmic O-GlcNAc transferase
OGA	O-GlcNAcase
OGT	O-GlcNAc transferase
OXPHOS	Oxidative phosphorylation
PFK	Phosphofructokinase
PPP	Pentose phorphate pathway
PTM	Post-translational modification
PTX	Picrotoxin
SIRT	Sirtuin
sWGA	Succinylated wheat germ agglutinin
TCA cycle	Tricarboxylic acid cycle
TMG	Thiamet-G
TMRM	Tetramethylrhodamine methyl ester
Tuj1	Neuron-specific class III beta-tubulin

UDP-GlcNAc	Uridine diphosphate N-acetylglucosamine
vGLUT1	Vesicular glutamate transporter 1
2-DG	2-deoxy-D-glucose
ΔΨm	Mitochondrial membrane potential

ACKNOWLEDGEMENTS

I'd like to express my sincerest gratitude to:

Gulcin Pekkurnaz, my thesis advisor, for conveying her passion for science, who always have encouraged me to explore my thoughts. This dissertation is the outcome of numerous conversations and discussions with her that tremendously evolved our original ideas and hypotheses. She has also been the mentor who fostered the perseverance, constantly reminding me of our love for science and our mission for the society.

The current and past members of Pekkurnaz laboratory who have provided me with scientific insights, support, friendship, and valuable life lessons.

Committee members, Susan Ackerman, Anthony Molina, Gerald Shadel, and Jeffrey Esko, for sharing their great expertise in their fields that have meticulously guided our science to an intriguing direction.

My family, especially my mother and father, who are the most formidable advocates for my decision to become a scientist.

Chapter 1, in part, is a reprint of the material as it appears in Yu, S. B. and Pekkurnaz, G. (2018) "Mechanisms orchestrating mitochondrial dynamics for energy homeostasis," *J. Mol. Biol., 430* (21), 3922-3941. The dissertation author was the primary author of this paper.

Chapter 2, in full, is a reprint of the material as it appears in Yu, S. B., Sánchez, R. G., Papich, Z. D., Whisenant, T. C., Koberstein J. N., Stewart, M. L., Stork, P. J. S., Goodman, R., and Pekkurnaz, G. "Neuronal activity-driven O-GlcNAcylation promotes mitochondrial plasticity," being submitted. The dissertation author was the primary investigator and author of this paper.

Chapter 3 contains unpublished material coauthored with Ajit S. Divakaruni and Gulcin Pekkurnaz. The dissertation author was the primary investigator and author of this chapter.

Chapter 4 contains unpublished material coauthored with Arlina de Lugo and Gulcin Pekkurnaz. The dissertation author was the primary investigator and author of this chapter.

VITA

2015 Bachelor of Science in Biological Sciences, Korea Advanced Institute of Science and Technology (KAIST)

2022 Doctor of Philosophy in Biology, University of California San Diego

PUBLICATIONS

Wang, H., Vant, J., Micou, M. L., Yu, S. B., Abushawish, A. A., Sánchez, R. G., Jabbo, M., Zhang, A., Luczak, V., Ghassemian, M., Griffis, E., SinghaRoy, A., & Pekkurnaz, G. "Glycolytic Microcompartment Assembly on Mitochondria via O-GlcNAcylation," manuscript in preparation.

Djaja, N. A., Bracha, T., Yu, S. B., Wang, H., Pekkurnaz, G. "FluxNorm: Toolbox for metabolic flux normalization by in-situ cell counting," manuscript in preparation.

Yu, S. B., Sánchez, R. G., Papich, Z. D., Whisenant, T. C., Koberstein J. N., Stewart, M. L., Stork, P. J. S., Goodman, R., and Pekkurnaz, G. "Neuronal activity-driven O-GlcNAcylation promotes mitochondrial plasticity," being submitted.

Wolf, D., Trudeau, K., Zhou, Z., Xu, S., Segawa, M., Benador, I., Yu, S. B., Taddeo, E., Shum, M., Hevener, A., Anikster, Y., Van der Bliek, A., Liesa, M., Pekkurnaz, G., and Shirihai, O. "Mitochondrial motor adaptor, Milton1, regulates mitochondrial fission and mtDNA distribution," submitted.

Fang, L., Monroe, F., Novak, S. W., Kirk, L., Schiavon, C. R., Yu, S. B., Zhang, T., Wu, M., Kastner, K., Latif, A. A., Lin, Z., Shaw, A., Kubota, Y., Mendenhall, J., Zhang, Z., Pekkurnaz, G., Harris, K., Howard, J., and Manor, U. (2021) "Deep learning-based point-scanning super-resolution imaging," *Nat. Methods*, *18*, 406-416. DOI: 10.1038/s41592-021-01080-z.

Yu, S. B. and Pekkurnaz, G. (2018) "Mechanisms orchestrating mitochondrial dynamics for energy homeostasis," *J. Mol. Biol., 430* (21), 3922-3941. DOI: 10.1016/j.jmb.2018.07.027.

Yu, S. B., Baek, J., Choi, M., Oh, Y., Lee, H. R., Yu S. J., Lee E., Sohn, S.-W., Im, S., Jon, S. (2016) "Polymer thin films with tunable acetylcholine-like functionality enable long-term culture of primary hippocampal neurons," ACS Nano, 10, 9909-9918. DOI: 10.1021/acsnano.6b03527.

ABSTRACT OF THE DISSERTATION

Metabolic regulation of neuronal mitochondria by O-GlcNAcylation

by

Seungyoon Blenda Yu

Doctor of Philosophy in Biology

University of California San Diego, 2022

Professor Gulcin Pekkurnaz, Chair

Neuronal activity consists of a series of molecular events—from action potential firing to synaptic vesicle recycling—which entails high energy input. These energetically expensive processes are supported by glucose flux, followed by consequential glycolytic and mitochondrial ATP generation. However, little is known about how glucose uptake regulates mitochondrial adaptation and its contribution to neuronal activity. Recently, the metabolic sensor enzyme O-GlcNAc transferase (OGT) emerged as a key molecular regulator that signals glucose availability in cells. Here, we first report that O-GlcNAcylation is upregulated by neuronal activity to promote

mitochondrial bioenergetics. We demonstrate that disruption in mitochondrial O-GlcNAcylation fails to replenish ATP and compensate for high energy expenditure after neuronal stimulation. Second, we describe that O-GlcNAc modification facilitates proper neuronal excitability from mitochondria that mainly use glucose as opposed to those dependent on ketone bodies. Finally, we show that SIRT5, one of mitochondrial sirtuins, may be O-GlcNAcylated to work as the mediator of the crosstalk between two PTMs—O-GlcNAcylation and succinylation. To sum up, O-GlcNAcylation provides a cue for mitochondria to actively adapt to the new metabolic state in neurons.

CHAPTER 1: INTRODUCTION

Mitochondria as independent yet cooperative entities in cells

Around one and a half billion years ago, mitochondria evolved from a free-living prokaryotic organism via symbiosis. Although this symbiotic merger occurred a long time ago, mitochondria remained discrete organelles within the cytoplasm and played a critical role in eukaryotic cell evolution. Mitochondria, like bacteria, have a double membrane, contain ribosomes and Deoxyribonucleic acid (DNA), proliferate by division, and move constantly and form a dynamic network through fusion-fission and constant movement. Almost all eukaryotic cells contain hundreds of mitochondria that work together to generate Adenosine triphosphate (ATP); maintain calcium homeostasis; synthesize heme, phospholipids, and extracellular signaling molecules including neurotransmitters; and initiate the cell death process (Yu and Pekkurnaz, 2018).

The recent discovery that mitochondria interact with one another, combined with molecular insights into mitochondrial dynamics, has challenged the traditional view of mitochondria as singular organelles in the cytoplasm. Mitochondria form a dynamic, interconnected network in cells and adapt their morphology rapidly to acute metabolic perturbations. For example, upon nutrient starvation, mitochondria undergo a series of fusion events to become more elongated, which is critical for enhancing bioenergetics efficiency (Lee et al., 2014). Also, changes in mitochondrial morphology—either elongation or fragmentation—are restored easily as cells recover from metabolic insults (Dietrich et al., 2013; Lee et al., 2014; Poole et al., 2008; Ramírez et al., 2017; Schneeberger et al., 2013; Tondera et al., 2009). Thus, morphological and functional plasticity of mitochondria support metabolic homeostasis in cells.

Mitochondrial morphology and content highly vary across cell types in tissues, due to their distinctive energy requirements. For example, in fibroblasts an evenly distributed mitochondrial network occupies ~20% of the total cell volume, whereas in cardiomyocytes mitochondria exhibit a dense network and occupy ~30% of the cytoplasm (Piquereau et al., 2013; Zhang et al., 2012). In neurons, while somatodendritic mitochondria form an extensively connected and motile network, axonal branches contain singular mitochondrion in either a motile or stationary state (Lewis et al., 2018; Misgeld and Schwarz, 2017). The distribution of mitochondria represents the local energy and calcium buffering demands in neurons.

To summarize, mitochondria are multifaceted organelles involved in the coordination of multiple signaling pathways. They support energy homeostasis throughout the cell and sustain spatiotemporal bioenergetics, which is particularly important for large, polarized cells, such as neurons.

Neuron's extraordinary energy demands are fulfilled by mitochondria

The brain uses ~20% of the resting body's energy, although it only accounts for 2% of the body's weight. The excessive energy intake evolved in the primate brain to sustain enhanced cognitive ability and large brain size (Clarke and Sokoloff, 1999; Mink et al., 1981; Raichle and Mintun, 2006). The nervous system comprises two main cell types: neurons and glia. While glial cells play a supportive role, neurons form an interconnected network, which enables them to transfer information and generate thoughts and actions. At the molecular level, neurons come into contact and communicate with each other via specialized structures called synapses. The communication between neurons starts with an action potential. When an action potential reaches the presynaptic *en passant* or *terminaux* boutons in axons, voltage-gated Ca^{2+} channels open and

allow Ca^{2+} into the presynaptic terminals. This presynaptic Ca^{2+} signaling induces neurotransmitter release by synaptic vesicle exocytosis and subsequent endocytosis. Synaptic vesicle recycling and refilling sustains neurotransmission (Li and Sheng, 2022; Südhof, 2018). Neurotransmitters allow chemical signals to be transmitted to the postsynaptic neuron. This line of tasks, both at the pre- and post-synaptic sites, requires a massive amount of energy in the form of ATP (60% of total energy used by a neuron). In addition to synaptic activity, housekeeping tasks—including sustaining cytoskeletal dynamics, protein synthesis, and organelle trafficking, as well as maintaining resting membrane potential—take up ~40% of neuronal energy utilization (Rossi and Pekkurnaz, 2019). Overall, the total ATP consumption rate of a neuron is calculated to be 5 billion ATP/neuron/second in order to maintain basic neuronal functions and neurotransmission (Laughlin et al., 1998). Thus, tight coupling between neuronal activity, energy consumption and generation is essential for the nervous system's function.

There are two key ATP generating pathways in eukaryotic cells: glycolysis and oxidative phosphorylation (OXPHOS) by mitochondria. Glycolysis produces two net molecules of ATP and pyruvate. The end product of glycolysis, pyruvate, fuels the mitochondrial tricarboxylic acid (TCA) cycle and OXPHOS, which produces 36 ATP. Neurons rely heavily on mitochondrial OXPHOS to meet their instantaneous energy demands. Even under resting states, mitochondria provide 93% of the neuronal ATP. When energy demands increase in response to neuronal stimulation, glycolysis plays an important supportive role for rapid ATP synthesis (Hall et al., 2012; Rangaraju et al., 2014; Díaz-García et al., 2017; Cunnane et al., 2020). Compared to the neighboring glial cells, neurons contain more mitochondria and higher levels of TCA cycle enzymes and pyruvate dehydrogenase, which further supports the enhanced use of OXPHOS for

neuronal metabolism (Halim et al., 2010). Therefore, it is not surprising that mitochondrial poisons or mutations cause a rapid decline in neuronal function and health.

Regulation of mitochondrial dynamics and distribution in neurons

The precise distribution of axonal and dendritic mitochondria is critical for neuronal development, function, and survival. During neuronal growth, selective immobilization of mitochondria supports elongation of axons and dendrites. As neurons mature, mitochondria become enriched at high energy demanding areas, such as presynaptic boutons and nodes of Ranvier (Figure 1.1A) (Misgeld and Schwarz, 2017; Rossi and Pekkurnaz, 2019).

Long-range transport of mitochondria in neuronal processes are mediated by microtubule motors and mitochondrial motor adaptor complex proteins Miro and Milton. In active synapses, many mitochondria are off-loaded from microtubules due to intracellular Ca^{2+} levels. Neuronal activity triggers Ca^{2+} influx at the synapse. Ca^{2+} binds to the EF-hands of Miro, causes conformational changes in the mitochondrial motor adaptor complex, and disassociates mitochondria from microtubules. This mechanism allows mitochondria to be captured at the active synapses (Wang and Schwarz, 2009; MacAskill et al., 2009; Vaccaro et al., 2017). In presynaptic boutons, synaptic activity also anchors mitochondria onto actin filaments. Intense action potential firing changes the AMP to ATP ratio at the presynaptic boutons and activates AMP-activated protein kinase (AMPK). AMPK signaling mediates mitochondrial motility arrest via myosin 6 and Syntaphilin (Li et al., 2020). Because actin mediates short distance mitochondrial transport in neurons by preventing microtubule-based transport, the AMPK pathway recruits mitochondria in areas with less ATP to resolve energetic stress. While both microtubule and actin-dependent mitochondrial arrest mechanisms are utilized at the synapse, whether each bouton uses both

pathways requires further investigation. Another key mechanism that regulates mitochondrial positioning in neurons is fuel itself, which will be discussed below.

Hexosamine biosynthetic pathway signals glucose availability to mitochondria in neurons

The brain consumes glucose as its primary fuel source. The constant supply of glucose is facilitated by a tight coupling between cerebral blood flow, neuronal activity, and metabolism. Because neurons have limited glucose stores, a minor disruption of proper glucose delivery leads to a significant compromise in cognitive abilities, and even further to delirium and coma (Graveling et al., 2013; Jackson et al., 2018). At the cellular level, neuronal glucose utilization is also coupled with synaptic activity. Neuronal stimulation transiently increases glucose flux, which is followed by glucose utilization via glycolysis and OXPHOS to produce ATP (Díaz-García et al., 2017). At the presynaptic boutons, an activity-dependent increase in glucose uptake is mediated by the insertion of glucose transporter 4 (GLUT4) to presynaptic plasma membrane (Ashrafi et al., 2017). In addition, subcellular compartmentalization of glucose transporters may cause alterations in local glucose metabolism (Mergenthaler et al., 2013).

Cells sense glucose flux rate and availability through the hexosamine biosynthetic pathway (HBP, Figure 1.1B). While most of the intracellular glucose is being used for ATP generation, a part of it is metabolized through the HBP to produce Uridine-diphosphate-N-acetylglucosamine (UDP-GlcNAc). Alterations of UDP-GlcNAc levels are then recognized by the cytoplasmic metabolic sensor enzyme O-GlcNAc transferase (OGT). OGT catalyzes a reversible post-translational modification of proteins by adding a GlcNAc sugar moiety on serine and threonine residues of proteins. The catalytic activity of OGT is regulated by intracellular UDP-GlcNAc concentration, which fluctuates proportionally in response to glucose flux through HBP. Uniquely,

the hexosamine pathway also integrates multiple metabolites. Thus, OGT translates a cellular metabolic state to its substrate proteins via O-GlcNAcylation. While OGT regulates O-GlcNAc addition, O-GlcNAcase (OGA) reverses this reaction. These two enzymes regulate the dynamic O-GlcNAc modification of >8000 proteins in the cytoplasm, mitochondria and nucleus (Zhu and Hart, 2021). Therefore, O-GlcNAcylation, by acting as a metabolic flux sensor, plays an essential role in the integration of multiple signaling pathways.

OGT, and O-GlcNAcylation, is highly enriched in neurons, especially at synapses (Alfaro et al., 2012; Lagerlöf et al., 2017; Trinidad et al., 2012). The defects in the regulation of O-GlcNAc modifications are involved in neurodegenerative diseases (Wang et al., 2016). O-GlcNAc modification, similar to phosphorylation, is also involved in synaptic plasticity regulation and long-term memory formation (Taylor et al., 2014; Wheatley et al., 2019). O-GlcNAcylation also regulates mitochondrial localization in neurons. Increased glucose availability and HBP pathway activation reduces mitochondrial motility by catalyzing O-GlcNAcylation of the mitochondrial motor adaptor protein Milton (Basu et al., 2021; Pekkurnaz et al., 2014). This OGT-mediated response is an adaptation that allows mitochondria to concentrate at glucose-enriched regions in neurons. While this discovery links nutrient availability to mitochondrial function, it still remains unknown how glucose and OGT-dependent mitochondrial compartmentalization affect neuronal metabolic homeostasis and mitochondrial bioenergetics. These topics will be further addressed in the following chapters.

Metabolic regulation of neuronal mitochondria by O-GlcNAcylation

Throughout my doctoral studies, I have aimed to determine how OGT couples nutrient availability to mitochondrial functions in neurons. I hypothesized that O-GlcNAcylation enriches

mitochondria at the glucose rich domains in neurons to couple nutrient uptake with utilization by mitochondria, and to support local energy needs by regulating mitochondrial bioenergetics. The results of my studies will be discussed in the following chapters. In Chapter 2, I will discuss how neuronal activity regulates mitochondrial O-GlcNAcylation to support "on-demand" ATP synthesis. I demonstrate that neuronal activity boosts mitochondrial bioenergetics by altering mitochondrial O-GlcNAcome to fulfill activity-dependent ATP demand. In Chapter 3, I will describe the differentiating role of O-GlcNAc modification on ketone bodies and glucose metabolism in neurons. Chapter 4 will establish the crosstalk between two PTMs—O-GlcNAcylation and succinylation by focusing on Sirtuin 5 (SIRT5), a candidate protein identified from our mitochondrial O-GlcNAcome. The future directions and broader impacts of these aforementioned chapters will be discussed in Chapter 5. Overall, with this doctoral thesis, I hope to have contributed to elucidating the crosstalk between two key factors of neuronal metabolism—the main neuronal energy source, glucose, and the main energy generator, mitochondrial bioenergetics.

Figures

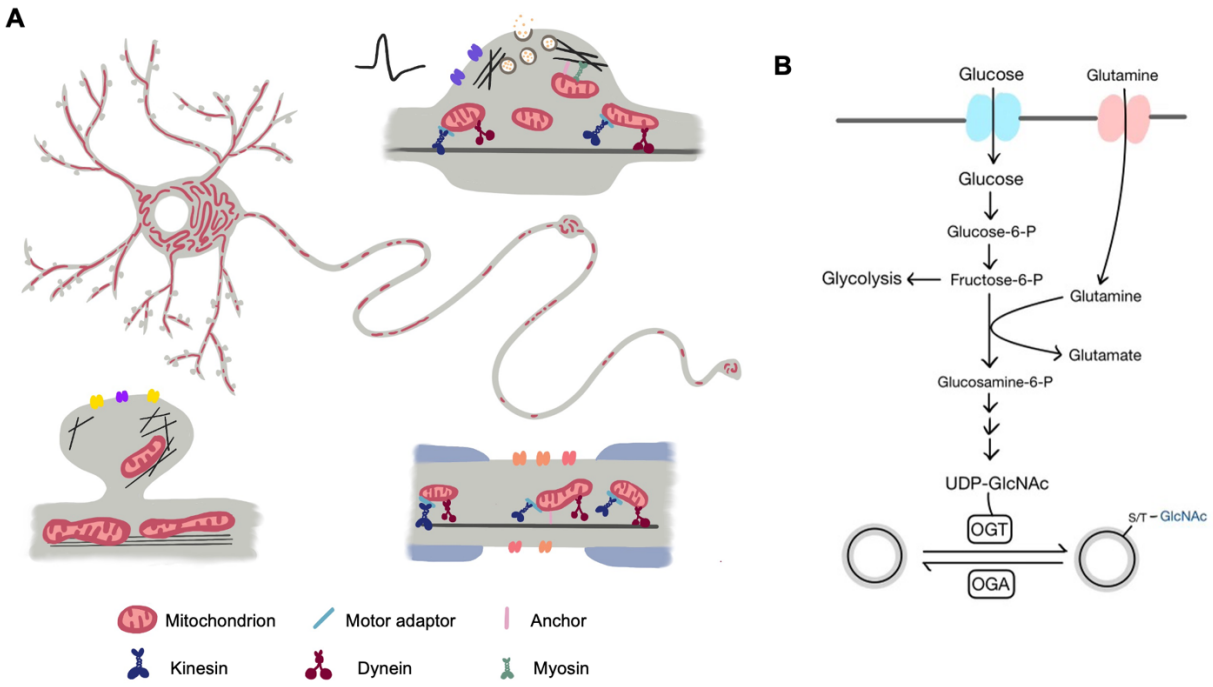

Figure 1.1 Overview of two fundamental components of the thesis: neuronal mitochondria and O-GlcNAcylation.

(A) Mitochondria distribution in neuronal cells, and their concentrated positioning in a presynaptic bouton (top), dendrite (bottom left), and nodes of Ranvier (bottom right). **(B)** General flow of hexosamine biosynthetic pathway (HBP) and O-GlcNAcylation. Glucose and other substrates enter HBP to be metabolized to UDP-GlcNAc, that can be further utilized for O-GlcNAcylation by OGT.

Acknowledgements

Chapter 1, in part, is a reprint of the material as it appears in Yu, S. B. and Pekkurnaz, G. (2018) "Mechanisms orchestrating mitochondrial dynamics for energy homeostasis," *J. Mol. Biol., 430* (21), 3922-3941. The dissertation author was the primary author of this paper.

CHAPTER 2: NEURONAL ACTIVITY-DRIVEN O-GLCNACYLATION PROMOTES MITOCHONDRIAL PLASTICITY

INTRODUCTION

Neuronal activity drives glucose consumption and utilization (Ashrafi and Ryan, 2017; Yellen, 2018). To maintain energy homeostasis, neurons constantly monitor glucose availability and energy level, and appropriately adjust ATP production rate. Continuous fulfillment of this ATP, especially at the synapses, relies on activity-driven mitochondrial ATP synthesis (Li and Sheng, 2022; Rangaraju et al., 2014). However, mechanisms regulating this "on-demand" ATP synthesis, other than the involvement of calcium channels, are unknown (Ashrafi et al., 2020).

As discussed in the Chapter 1 introduction, the metabolic sensor enzyme O-GlcNAc transferase (OGT) emerged as a key molecular regulator that signals glucose availability in cells. Here, we hypothesize that O-GlcNAc cycling provides glucose flux-dependent feedback control in neurons to optimize mitochondrial performance based on neuronal activity and energy demand. To test our hypothesis, we used *in vivo* and *in vitro* approaches to demonstrate how neuronal activity upregulates O-GlcNAc signaling in hippocampal neurons. This global change in O-GlcNAcylation provides a cue for mitochondria to adapt to the new metabolic state, induced by neuronal activity. We show that upregulation of O-GlcNAcylation promotes mitochondrial bioenergetics to compensate for high energy expenditure. To determine which mitochondrial proteins are responsible for these adjustments, we mapped mitochondrial proteome with dynamic O-GlcNAc recycling rate from cultured neurons. A majority of identified proteins participate in oxidative phosphorylation and ATP generation pathways. Finally, we demonstrate that disruption in mitochondrial O-GlcNAcylation fails to replenish ATP after neuronal stimulation. Our findings

suggest that O-GlcNAcylation plays a key role in energy homeostasis by promoting mitochondrial function in response to neuronal activity.

RESULTS

Neuronal activity promotes O-GlcNAcylation

To determine neuronal activity-dependent O-GlcNAc cycling in neurons in vivo, we asked how O-GlcNAc levels respond to strong, widespread neuronal activation by inducing seizures with kainic acid (KA), a glutamate analog (Figure 2.1A). To identify the cellular locus of O-GlcNAc upregulation in the brain, we measured somatic O-GlcNAc levels in sections of mouse hippocampus using immunohistochemistry 1 hour after seizure onset (Figure 2.1A-D), having verified seizure induction visually (Lévesque and Avoli, 2013). We restricted our analysis to the somata of neurons that express the neuronal marker NeuN (Gusel'nikova and Korzhevskiy, 2015) and identified recently active neurons based on expression of the immediate-early gene c-Fos (Liakath-Ali and Südhof, 2021). Using this approach, we found that seizure induction enhanced O-GlcNAcylation in neurons throughout the hippocampus, in addition to the cortex (Figure 2.1A-D and Figure 2.2). Consistent with elevated neuronal activity, KA administration also enhanced the number of c-Fos positive hippocampal neurons (Figure 2.1B and D). To understand the relationship between neuronal activity and O-GlcNAc levels, we plotted the intensity of the c-Fos and O-GlcNAc signals on a neuron-by-neuron basis (Figure 2.1E). Although in some neurons O-GlcNAc levels appeared to vary independently of c-Fos, across the entire population their levels were positively correlated. These results indicate that O-GlcNAcylation is upregulated by neuronal activity in vivo, and importantly, that this occurs in neurons.

O-GlcNAcylation in neuronal processes is regulated by neuronal excitation

In order to determine how neuronal activity regulates O-GlcNAcylation at the subcellular level, we evaluated O-GlcNAc distribution in cultured hippocampal neurons. We first evaluated how O-GlcNAc levels change as neurons mature in vitro. Immunostaining of neurons for O-GlcNAc at 7DIV and 14DIV revealed that neuronal O-GlcNAcylation was enhanced as neurons form a more mature network, not only in the soma, but also in dendrites and axons (Figure 2.3). Next, we elevated network activity for 6 hours by blocking inhibitory synaptic transmission with the GABA-A receptor antagonist picrotoxin (PTX) (Figure 2.4A). This experiment revealed that a prolonged increase in activity leads to a ~2-fold increase in O-GlcNAcylation within neuronal somata, axons, and dendrites (Figure 2.4A-F). Importantly, this PTX-driven activity-dependent O-GlcNAc upregulation was reversed by pharmacological blockade of excitatory synaptic transmission with the selective AMPA receptor antagonist NBQX (Figure 2.4A-F) (Lee and Hablitz, 1989). This results suggest that O-GlcNAcylation is actively altered in neurons experiencing chronical stimulation in a reversible manner.

Activity-driven O-GlcNAc cycling regulates mitochondria in neurons

We next set out to identify the intracellular localization of O-GlcNAcylated proteins in neurons and focused our initial analysis on mitochondria. We hypothesized that neuronal activity-driven O-GlcNAcylation regulates mitochondria to support elevated energy needs. Therefore, we examined the subcellular localization of O-GlcNAc in neuronal processes together with the pan-mitochondrial marker protein Tomm20 (Figure 2.5A-B). When neuronal activity was elevated for 6 hours by PTX treatment, O-GlcNAc co-localization with mitochondria increased in dendritic and axonal processes, and reversed by NBQX treatment (Figure 2.5A-D). To further evaluate

mitochondrial O-GlcNAc levels, we isolated mitochondrial and cytosolic fractions from cultured neurons and analyzed them by immunoblotting. In this case, PTX treatment predominantly increased O-GlcNAcylation of mitochondrial proteins compared to cytosolic proteins (Figure 2.5E-G). The increase in mitochondrial O-GlcNAcylation was not due to alterations of OGT or OGA levels (Figure 2.6A), instead it required enzymatic activity of OGT (Figure 2.6B).

Given that neuronal activity regulates mitochondrial O-GlcNAcylation, we next assessed the impact on neuronal bioenergetics. To measure mitochondrial respiratory activity and glycolytic rate, we cultured neurons under physiological glucose levels and performed respirometry analysis at 12-15 DIV, a time point at which neurons are synaptically mature and functional (Figure 2.6C-E). As primary neuron cultures also include glial cells, we co-stained each well after our measurements with the neuronal marker NeuN and the nuclear dye NucBlue (Figure 2.6D), which revealed that neurons represent 60-80% of cellular population in our cultures. While we did not observe a change in mitochondrial respiration to drive basal mitochondrial ATP synthesis, carbonyl cyanide-4-(trifluoromethoxy)phenylhydrazone (FCCP)–stimulated respiration indicated that neuronal activity increases mitochondrial respiratory capacity (Figure 2.5H-K). When we elevated activity with PTX in the presence of the OGT inhibitor OSMI4 (Figure 2.6B-C), both basal and maximal mitochondrial respiratory capacity were reduced (Figure 2.5H-K). OSMI4-treated neurons also displayed reduced glycolytic capacity (Figure 2.6F-H). These results confirm the involvement of OGT and mitochondrial O-GlcNAcylation in neural activity-induced metabolic flexibility.

Acute neuronal stimulation triggers glycolysis and mitochondrial O-GlcNAcylation

We sought to determine the extent to which neuronal activity-dependent glucose metabolism might contribute to mitochondrial O-GlcNAcylation. To monitor the metabolic changes that occur following neuronal activity, we measured Fructose 1,6-bisphophate (FBP) levels in neuronal processes using HYlight, a fluorescent sensor that reports glycolytic dynamics (Koberstein et al., In press) (Figure 2.7A). Measurements from neuronal processes revealed that even persistent action potential (AP) firing (10Hz, 600 APs) produced only small changes in cytosolic FBP levels. We confirmed that our stimuli induce neuronal activity using the Ca^{2+} sensor GCaMP6s (Figure 2.8A-B). Therefore, either neuronal activity does not enforce significant additional glycolysis or increases in demand are accompanied by activity-driven glucose uptake and consumption. When glycolysis was blocked by exchanging glucose for 2-deoxyglucose (2DG), FBP level slowly declined (τ = 3.007 min). Neuronal stimulation under these conditions caused an additional drop in FBP levels (τ = 1.005 min, Figure 2.7B-D), which implies that FBP levels must be maintained by coupling glucose flux and metabolism.

Given that OGT activity is regulated by glucose flux and the availability of its substrate UDP-GlcNAc (Figure 2.7A) (Pekkurnaz et al., 2014), we hypothesized that neuronal stimulation fuels mitochondrial O-GlcNAcylation. Therefore, we examined O-GlcNAcylation in neurons expressing the mitochondrial marker Mito-DsRed immediately following acute neuronal stimulation (Figure 2.7E). Immunohistochemical analysis of O-GlcNAc localization revealed a local enhancement of mitochondrial O-GlcNAcylation in neuronal processes after induction of neuronal activity (Figure 2.7F-G). Because O-GlcNAcylation is a dynamic post-translational modification, we decided to block the removal of O-GlcNAc from proteins by inhibiting O-GlcNAcase (OGA) with Thiamet-G (TMG) over the course of the stimulation (Figure 2.8D). Ca^{2+}

imaging confirmed that TMG did not alter neural activity induction in response to the stimulus (Figure 2.8E-F). Acute inhibition of OGA intensified the accumulation of mitochondrial O-GlcNAcylation during baseline neuronal activity (Figure 2.8G-H) and this became more prominent upon neuronal stimulation. These results indicate that mitochondrial O-GlcNAcylation is a dynamic process in neurons. Furthermore, it is promoted by neuronal activity and activity-dependent glucose metabolism.

O-GlcNAcylation is sufficient to increase mitochondrial respiration

We next assessed the role of O-GlcNAcylation dynamics in the regulation of mitochondrial bioenergetics. We blocked the removal of O-GlcNAcylation by treating neuronal cultures with the OGA inhibitor TMG overnight and verified that this treatment increased O-GlcNAcylation (Figure 2.10A). First, we evaluated mitochondrial activity by double-labeling neurons with the mitochondrial membrane potential ($\Delta\Psi m$)-sensitive fluorescent dye tetramethylrhodamine methyl ester (TMRM) and the $\Delta\Psi m$ insensitive mitochondrial probe MitoTracker Green (MT Green). At sub-quenching concentrations, TMRM rapidly equilibrates in mitochondria and reflects $\Delta\Psi m$. TMG treatment increased $\Delta\Psi m$, which is quantified as the ratio between TMRM and MT Green intensities (Figure 2.9A-B). To evaluate mitochondrial respiratory capacity, we measured mitochondrial oxygen consumption rate in control and TMG-treated neurons. As demonstrated with neuronal activity (Figure 2.8E-F), we did not observe a change in mitochondrial respiration driving basal mitochondrial ATP synthesis. However, maximal respiratory capacity was enhanced in TMG-treated neurons (Figure 2.9C-E). We confirmed that the mitochondrial activity boost was not due to mitochondrial biogenesis as TMG-treated neuronal mitochondrial protein levels remained constant (Figure 2.10). Thus, our results suggest that modulation of O-GlcNAcylation

plays an important role in ΔΨm regulation and promotes mitochondrial respiratory capacity in neurons.

Mitochondrial O-GlcNAcome reveals adaptive bioenergetic mechanisms

To identify mitochondrial proteins that undergo O-GlcNAc modification when respiratory capacity is enhanced, we compared TMG-treated mitochondrial proteins to the control group. This approach enabled us to recognize the proteins with high or low O-GlcNAcylation dynamics, differentiating our method from previous studies uncovering O-GlcNAc sites of mitochondrial proteins. For the mass spectrometry analysis, mature primary neurons were treated with TMG overnight, followed by crude mitochondrial isolation and O-GlcNAc enrichment using agarose beads coated with succinylated wheat germ agglutinin (sWGA)—a GlcNAc-specific lectin (Fig 2.11A). We confirmed O-GlcNAcylated peptide enrichment from TMG-treated neurons by probing O-GlcNAcylation (Suppl Fig 2.12A). O-GlcNAc enrichment samples from +TMG and control samples were evaluated using a LC-MS/MS-based proteomic analysis. We selected only the proteins identified with at least two unique peptides from our three independent proteomics datasets to ensure the validity of the datasets (Filter 1 from Fig 2.11A). It was confirmed after Filter 1 that more peptides and proteins are enriched within +TMG samples by plotting peptide and protein abundance in each sample (Fig 2.11B and 2.12B). Proteins detected from both +TMG and -TMG samples for proper comparison were included for further analysis ("Total proteome"). To figure out how our total proteome compares to preexisting databases, we examined the overlaps between our total proteome and mitochondrial annotated proteins both by MitoCarta 3.0 and IMPI (Rath et al., 2021; Smith and Robinson, 2019) and the O-GlcNAcylated proteome database from the rat (Malard et al., 2021; Wulff-Fuentes et al., 2021). Out of 770 identified proteins from the

total proteome, only 80 proteins are overlapping with both of the mitochondrial databases and 142 proteins are recognized from the rat O-GlcNAc proteome database (Figure 2.12C). We further determined where in the cells non-mitochondrial proteins were coming from; most of them came from cytosol (23.3%), plasma membrane (10.9%), and endoplasmic reticulum (ER) (10.8%) (Figure 2.12D). This result indicates significant contributions of other membrane-bound organelles while pulling down crude mitochondrial fraction from our cultured neuron lysates, which further led us to apply a filter to take only mitochondrial proteins into account (Figure 2.11A, Filter 2). Selected mitochondrial peptides also displayed a +TMG-enriched trend with overall higher significance shown as a volcano plot (Figure 2.11B). The pathway enrichment analysis further confirmed that identified proteins are mostly involved in cellular respiratory processes as part of electron transport chains and the TCA cycle (Figure 2.11C). Individual protein-protein interaction analysis further revealed the higher degree of interaction between the electron transport chain complex subunits and related metabolism proteins (Figure 2.12E). It was determined that their submitochondrial localization, 48.1% of mitochondrial proteome, was localized on the inner membrane (IMM) followed by the Matrix (19%) (Figure 2.11D). Figure 2.11E demonstrates significant mitochondrial proteins sorted by localization and colored by MitoCarta3.0 annotated MitoPathway. The most representative pathways involved are oxidative phosphorylation (OXPHOS) and mitochondrial small molecule transporters.

O-GlcNAc transferase supports "on-demand" ATP synthesis

The majority of O-GlcNAcylated mitochondrial proteins identified in our proteomics data (Figure 2.11) are involved in ATP synthesis pathways. It led us to hypothesize that O-GlcNAcylation regulates neuronal activity-dependent "on-demand" ATP synthesis. To test our

hypothesis, we expressed the cytoplasmic ATP sensor iATPSnFR1.0-mRuby in neurons and triggered action potential (AP) firing (10 Hz, 600 AP) in the presence of OGT inhibitor OSMI4 (Figure 2.13A and 2.14A). We confirmed that OSMI4 treatment did not alter neuronal activity by imaging intracellular Ca^{2+} with GCaMP6s before and after neuronal stimulation (Figure 2.14B-C). Measurements from neuronal processes revealed that a burst of electrical activity resulted in only a small decrease in ATP levels during the post-stimulus period, which was followed by immediate recovery (Figure 2.13B-D). On the contrary, ATP levels never recovered in OSMI4-treated neurons, which instead displayed a ~30% reduction from the baseline at 10 min post-stimulation (Figure 2.13D). This result, combined with the observation that neuronal activity enhances glucose metabolism as well as mitochondrial O-GlcNAcylation (Figure 2.7), implies that OGT activity is required for neurons to upregulate neuronal bioenergetics (Figure 2.14E).

CONCLUDING REMARKS

Our study provides a compelling mechanism that couple neuronal glucose metabolism and mitochondria to fuel activity-dependent energy needs. We showed that both prolonged and acute neuronal activity enhances mitochondrial O-GlcNAcylation level (Figure 2.5-2.8). It was further proved that O-GlcNAc cycling synchronizes mitochondrial bioenergetics with neuronal activity (Figure 2.9-2.14).

In both prolonged and transient conditions, neuronal activity was sufficient to raise O-GlcNAcylation level. This effect is recapitulated in previous work where they identified global increases of O-GlcNAc in rat cortices injected with KA (Khidekel et al., 2007). However, the demonstrated O-GlcNAc increase was captured within a several hour range from a heterogeneous cell population of cortical tissue. We focused on neuronal O-GlcNAcylation on a time scale

ranging from a minute to several hours and correlated with neuronal activity (c-Fos expression in Figure 1.1E) (Bullitt, 1990). This increment in O-GlcNAcylation was prominent to mitochondria, but not limited to it.

We identified mitochondrial proteins that undergo regulated O-GlcNAcylation by comparing O-GlcNAcase inhibited samples against the baseline state of neurons (Figure 2.11). Our O-GlcNAcome catalog provides mechanistic insight on how O-GlcNAcylation can shift the mitochondrial engine for metabolic adaptations in neurons. I will further elaborate in Chapter 5 how O-GlcNAcylation could change mitochondrial properties at the molecular level. From the O-GlcNAcome data, analyzing mitochondrial proteins involved in mitochondrial bioenergetics and proteins known to be mutated in metabolism-related neurological disorders may pinpoint drug targets and uncover opportunities for metabolism-based therapies.

The enzymes that regulate O-GlcNAc cycling, OGT and OGA (Figure 1.1B), localize within mitochondria as well as in the cytoplasm (Banerjee et al., 2015; Yang and Qian, 2017). OGT is encoded by a single gene and exists in three splice isoforms, including nucleocytoplasmic isoform (ncOGT), mitochondrial isoform (mOGT), and short isoform (sOGT) (Lazarus et al., 2006; Yang and Qian, 2017). mOGT contains mitochondrial targeting sequence (MTS) on its N-terminus, which mediates localization of mOGT in the inner membrane (Banerjee et al., 2015; Hanover et al., 2003; Sacoman et al., 2017). Based on the localization of mitochondrial proteins in our mitochondrial O-GlcNAcome data, we predict that the mitochondrial isoform of OGT is responsible for the regulation of “on demand” ATP generation. I am currently designing experiments to perturb mitochondrial OGT and O-GlcNAcylation. There are several possible ways that mitochondrial O-GlcNAcylation can be manipulated. The first and the most straightforward way is to reduce the expression of mitochondrial OGT. Genetic manipulation of this mOGT can

be achieved by deletion of OGT using floxed OGT mice (OGT^{Fl}). Neurons from OGT^{Fl} will be cultured and expressed with Cre recombinase that can lead complete knock out of OGT in vitro. Then cDNA expression of ncOGT and sOGT by transient transfection would leave neurons lacking mOGT expression. In these experiments, we can expect downregulation in mitochondrial O-GlcNAcylation and observe any changes in mitochondrial bioenergetics. We still cannot rule out a possibility that some of mitochondrial proteins may already be O-GlcNAcylated by the time of import from cytoplasm. Alternatively, we can target OGA to specific compartments of mitochondria using nanobody based approaches. (Ge et al., 2021). These studies will help us reveal the role of specific OGT isoforms in neuronal energy homeostasis.

To sum up, our study explores the capacity of O-GlcNAc modification to link glucose metabolism and mitochondria together in response to neuronal activity. O-GlcNAcylation responded to both chronic and transient activation with their duration of modification somewhat matching that of stimulation schemes. It may suggest an intriguing direction this study can evolve to: how can activity-promoted O-GlcNAcylation be controlled back to normal, homeostatic level in the brain? Discovering its recovery mechanism of O-GlcNAcylation will possibly suggest a new therapeutic target pathway to tackle neurological diseases with disrupted metabolic activities.

Materials and methods

Animals: All animal procedures were conducted in accordance with the protocol approved by Institutional Animal Care and Use Committee (IACUC) at University of California, San Diego.

Kainic acid injection and brain tissue immunohistochemistry: Mature C57BL/6J male mice at 10-12 weeks of age were injected with either 10 mg/kg kainic acid (KA) (Tocris) per dose or equivalent volume of saline as control and monitored for visible signs of seizures (Class 4 behavior from Racine scale). If a mouse injected with KA did not develop epileptic symptoms within 1 hour after initial injection, a booster dose (5 mg/kg) of KA was administered. One hour after the onset of seizure symptoms including rearing and repetitive paw movements, the control and KA injected mice were then anesthetized with Isoflurane (MWI Veterinary, Boise, ID) and perfused with PBS followed by 4% PFA. The perfused brain was further fixated with 4% PFA solution overnight then submerged in 30% sucrose in PBS until dehydrated. The dehydrated brain was embedded and frozen with Tissue Tek OCT Compound (Sakura Finetek USA, Torrance, CA) at least 10 min prior to Cryostat sectioning. The frozen brain tissue was sectioned at 25 μm thickness. The sectioned tissue was blocked in PBS with 5% Goat serum and 0.3% Triton X-100 for 1 hour at room temperature. For primary antibody staining, the tissues were incubated with indicated antibodies in 1% Goat serum and 0.3% Triton X-100 overnight at 4 ºC. Following three PBS washes, secondary antibody staining was done for 1 hour at room temperature. The processed tissues were mounted with DAPI-Fluoromount-G (Southern Biotech, Birmingham, AL) on Super-Frosted microscope slide glasses (Fisher Scientific) for further imaging.

Primary neuron culture and transfection: Hippocampal and cortical neurons were isolated and cultured from E18 embryo of Sprague-Dawley rat (Envigo) as previously described (Lin et al., 2008). Briefly, hippocampal and cortical tissues were isolated from embryonic brains and dissociated with Papain (Roche) and L-cysteine solution followed by three washes with trypsin inhibitor (Sigma-Aldrich) in HBSS (Life Technologies)-based solution. The tissues were then further separated by fire-flamed glass Pasteur pipette to achieve single cell resolution. After cell counting, the dissociated neurons were plated on 12 mm-coverslips and 6-well plates at cell density of 5-7 $\times$ 10^4 cells/cm^2 and 1-2 $\times$ 10^5 cells/cm^2, respectively. Prior to plating, the coverslips (Carolina Biological Supplies) and plates were coated with 20 µg/mL Poly-L-Lysine (Sigma-Aldrich) and 3.5 µg/mL Laminin (Life Technologies) overnight. The plated cells were grown in neuronal maintenance medium (Neurobasal medium (Life Technologies) supplemented with B27 (Life Technologies), GlutaMAX (Life Technologies), and penicillin/streptomycin (Life Technologies)). The glucose level for neuronal cultures was maintained at 5mM, if not indicated separately, by combining 25mM glucose and 0mM glucose neurobasal media to keep constant osmolarity. 2-3 days prior to experiments, indicated DNA plasmids were transfected to the neurons using Lipofectamine 2000 (Life Technologies) in plain neurobasal media.

In vitro neuronal stimulation: For chronic activation of neurons, picrotoxin (PTX, Tocris) at 50 µM was administered to DIV 11-14 cultured neurons for 6 hr to ensure the network activity elevation as previously shown (Bateup et al., 2013). To inhibit activity induction, 10 µM NBQX was incubated together with PTX. For transient stimulation of neurons, electrical field stimulation at 10 Hz, 100 mA for 60 seconds (600 action potentials) was applied on coverslip-cultured neurons in Tyrode's buffer (50mM HEPES (pH 7.4), 119mM NaCl, 2.5mM KCl, 2mM CaCl2, 2mM

MgCl2, 5mM glucose, 2mM pyruvate, and 2mM lactate). To ensure the field stimulation had activated neurons, neurons transfected with GCaMP6s were imaged as time series images.

Immunocytochemistry from in vitro stimulated neurons: For immunocytochemistry, after both chronic and transient stimulation methods, the neurons on coverslips were directly fixated with 4% PFA for 10 min. The fixated cells were blocked with blocking solution (10% goat serum, 1% BSA, and 0.1% Triton X-100 in PBS) for an hour, followed by overnight primary antibody incubation in blocking solution at 4 ºC. After three separate washes in PBS, the samples were incubated with secondary antibodies in blocking solution for 1 hr at room temperature. The activated neurons on coverslips were then mounted on Frosted microscope slide glass (Fisher Scientific) with Fluoromount-G (Southern Biotech).

Western blot from in vitro stimulated neurons: Chronically activated neurons from 6-well plates were used for western blot analysis on DIV 11-12. A week prior to the experiment, on DIV 3, the cells were treated with Ara-C (Cytarabine, Tocris) at 1 μM to prevent excessive glial contamination in the plate. After two days, Ara-C containing medium was partially replaced with fresh maintenance medium. On the day of experiment, mitochondrial isolation buffer (MIB) was prepared freshly by mixing 10mM Tris-HCl (pH 7.4), 10mM KCl, 250mM Sucrose, 1 mM EDTA (pH 8.0) together with 1x Protease Inhibitor Cocktail Set III (Calbiochem), 0.1mM PMSF, and 2mM DTT. Pre-treated neurons were incubated with MIB on ice for 10 minutes, scraped from the cultured plate, and pooled together in dounce homogenizer. After breaking cells open with homogenizer, the lysates were centrifuged at 700 xg, 10min for nuclei and cell debris removal. Supernatants were centrifuged again at 10,000 xg, 10min to collect crude mitochondrial fraction.

Total cell lysates, mitochondrial fractions, and cytoplasmic fractions were then resuspended in MIB with 1x Laemmli buffer, boiled, and ran in SDS-PAGE gel. Separated protein fractions in gel were transferred to nitrocellulose membranes, followed by blocking and probing with indicated antibodies.

Seahorse metabolic flux analysis: The dissociated neurons were plated and cultured on Seahorse XF96e plate at 45K / well until DIV 12-15. On DIV 3, the cells were treated and incubated with Ara-C (Cytarabine, Tocris) at 1 μM for two days. A day before or the day of experiment, the cells are pre-treated with indicated drugs (Figure 2.5-2.6 and 2.9). An hour prior to the Seahorse Mito Stress Test Assay, the neuronal maintenance medium was exchanged two times with XF DMEM Base Medium (pH 7.4) with no phenol red (Agilent) supplemented with 5mM glucose and 2 mM pyruvate. For the first medium exchange, NucBlue dye (Thermo Fisher Scientific) was included to stain nuclei for cell counting after the assay. During the Mito Stress Assay, the respiratory and medium acidification rate was measured before and after injection with 1 μM Oligomycin (Sigma-Aldrich), two times with 0.5 μM FCCP (Sigma-Aldrich), and 0.5 μM Rotenone (Sigma-Aldrich) / Antimycin A (Sigma-Aldrich). After the assay, the whole analyzed plate was imaged by pre-stained NucBlue signal with minimum of three separate regions in one well for further data normalization by cell count and extrapolation pipeline (Manuscript in preparation). For quantification of neuron percentage in each well in Seahorse plate, additional NeuN immunostaining and imaging was carried out after fixating the cells with 4% PFA for 10 min.

HYLight FBP sensor imaging and analysis: Cortical neurons on DIV 11-12 were transfected with wild type and mutant (T152E) CMV-HYLT biosensor plasmids for spatiotemporal fructose-1,6-biphosphate (FBP) detection. Two days after transfection, coverslips with transfected neurons were transferred on 37 ºC temperature-controlled stage with Tyrode's buffer constantly being perfused. To ensure the glucose level and fluorescent signal from the sensor is stabilized, the neurons were pre-incubated on the stage for 10 min before the image acquisition. Time-lapse movies were obtained on Zeiss LSM 780 confocal microscope with C-Apochromat 40x/1.20 W Korr FCS M27 objective. Each frame was acquired every 30 seconds. The indicated manipulations including electrical field stimulation and 2-deoxy-D-glucose (2-DG, Sigma-Aldrich) additions were performed during the image acquisition with constant perfusion of Tyrode's buffer. For conditions with 2-DG additions, 5mM glucose was substituted with 5mM 2-DG. The image acquisition and analysis were performed as previously described (Koberstein et al., In press). To outline the procedures briefly, the neurons were excited separately at 488 nm and 405 nm with emission detection range at 492-598 nm and 490-596 nm, respectively. Then the excitation ratio of mean intensity values of the 488 channel to the 405 channel was calculated ($R = F_{488} / F_{405}$) for each time frame. $\Delta R/R$ was further calculated from $(R_t-R_0) / R_0$ as a readout of temporal changes in FBP level, where R0 indicates the excitation ratio at the starting frame of the experiment.

TMRM staining: Hippocampal neurons ranging from DIV 9-13 were stained with 20 nM TMRM (Invitrogen) overnight with or without 2 μM TMG. 40nM of MitoTracker Green FM was administered to the neurons 20 min prior to the imaging to co-stain mitochondrial morphology that works as a standard. The coverslips with stained cells were imaged in Hibernate E solution with

no phenol red (BrainBits) on Zeiss LSM 780 confocal microscope with Plan-Apochromat 100x/1.40 Oil DIC M27 objective and heated chamber stage at 37 ºC. Although the neurons were live, images were only acquired once per imaging field to prevent photobleaching of TMRM signal. For quantification of each mitochondrion, TMRM signal was normalized based on each mitochondrial ROI defined by MitoTracker Green.

Mitochondrial isolation and O-GlcNAc enrichment from cultured neurons: Cortical neurons were cultured at a density of 1.57 x 10^5 cells/cm^2 in a 6-well plate until DIV12-15. A day before mitochondrial isolation, the neurons were treated with 2 μM TMG or DMSO (Control) and incubated overnight. On the day of isolation, mitochondrial isolation buffer (MIB) was prepared freshly. A total of ~1.5 x 10^7 cells for each condition were collected for crude mitochondrial isolation in MIB using a centrifuge as described above.

The collected mitochondrial pellets were resuspended in lysis buffer (50mM Tris-HCl (pH 7.4), 150 mM NaCl, 1 mM EDTA and 2 % NP-40 with Protease Inhibitor Cocktail Set III, PMSF, and DTT). TMG was added to all conditions to retain O-GlcNAc modification on mitochondrial proteins during the whole enrichment process. The resuspended mitochondrial sample was incubated together with succinylated Wheat Germ Agglutinin (sWGA)-bound agarose beads (Vector Laboratories, Burlingame, CA) for 12hr at 4 ºC for specific binding of O-GlcNAcylated proteins with the beads. After the incubation, the beads were washed thoroughly with lysis buffer 4 times, followed by protein recovery from the beads by boiling at 100 ºC for 5 min in 1x Laemmli buffer. Recovered mitochondrial proteins were then loaded to sterile, pre-cast polyacrylamide gel and run minimally to concentrate proteins within a small amount of gel. SimplyBlue was used to stain and visualize the protein on the gel. Only the gels containing proteins were cut and sent for

mass spectrometry analysis at UCSD Biomolecular and Proteomics Mass Spectrometry Facility (BPMSF).

Mass spectrometry in-gel sample preparation and LC-MS/MS: The prepared gels were sent for trypsin digestion followed by mass spectrometry analysis as previously explained (Shevchenko et al., 1996). Briefly, the gel slices were cut to 1mm by 1 mm cubes and de-stained 3 times by first washing with 100 µl of 100 mM ammonium bicarbonate for 15 minutes, followed by additions of the same volume of acetonitrile (ACN) for 15 minutes. The supernatant was and samples were dried in a speedvac. Samples were then reduced by mixing with 200 µl of 100 mM ammonium bicarbonate-10 mM DTT and incubated at 56 °C for 30 minutes. The liquid was removed and 200 µL of 100 mM ammonium bicarbonate-55mM iodoacetamide was added to gel pieces and incubated at room temperature in the dark for 20 minutes. After removing the supernatant and washing with 100 mM ammonium bicarbonate for 15 minutes, the same volume of ACN was added to dehydrate the gel pieces. The solution was then removed and samples were dried in a speedvac. For digestion, enough solution of ice-cold trypsin (0.01 µg/µL) in 50 mM ammonium bicarbonate was added to cover the gel pieces and set on ice for 30 min. After complete rehydration, the excess trypsin solution was removed, replaced with fresh 50 mM ammonium bicarbonate, and left overnight at 37°C. The peptides were extracted twice by the addition of 50 µl of 0.2% formic acid and 5 % ACN and vortex mixing at room temperature for 30 min. The supernatant was removed and saved. A total of 50 µl of 50% ACN-0.2% formic acid was added to the sample, which was vortexed again at room temperature for 30 min. The supernatant was removed and combined with the supernatant from the first extraction. The combined extractions were analyzed by ultra high pressure liquid chromatography (UPLC) coupled with tandem mass

spectroscopy (LC-MS/MS) using nano-spray ionization. The nanospray ionization experiments were performed using a Orbitrap fusion Lumos hybrid mass spectrometer (Thermo) interfaced with nano-scale reversed-phase UPLC (Thermo Dionex UltiMate™ 3000 RSLC nano System) using a 25 cm, 75-micron ID glass capillary packed with 1.7-µm C18 (130) BEHTM beads (Waters corporation). Peptides were eluted from the C18 column into the mass spectrometer using a linear gradient (5–80%) of ACN (Acetonitrile) at a flow rate of 375 µl/min for one hour. The buffers used to create the ACN gradient were: Buffer A (98% H2O, 2% ACN, 0.1% formic acid) and Buffer B (100% ACN, 0.1% formic acid).

Mass spectrometer parameters are as follows; an MS1 survey scan using the orbitrap detector set to (mass range (m/z): 400-1500 (using quadrupole isolation), 120000 resolution setting, spray voltage of 2200 V, Ion transfer tube temperature of 275 C, AGC target of 400000, and maximum injection time of 50 ms) was followed by data dependent scans (top speed for most intense ions, with charge state set to only include +2-5 ions, and 5 second exclusion time, while selecting ions with minimal intensities of 50000 at in which the collision event was carried out in the high energy collision cell (HCD Collision Energy of 30%). The fragment masses were analyzed in the ion trap mass analyzer (With ion trap scan rate of turbo, first mass m/z was 100, AGC Target 5000 and maximum injection time of 35ms).

Analysis of LC-MS/MS proteomic data: The output of quantified values for each protein in each sample (filtered for unique peptides > 1 and significance > 0) was used as input to the Perseus software package (Tyanova et al., 2016) which performed the following processing steps: filter out low abundance proteins (detected in each group), log transform remaining quantification values, and impute values for abundant proteins in undetected samples. These data were imported

to the R statistical computing environment (www.cran.org) and moderated t-tests from the limma package (Ritchie et al., 2015) were used to compare the two groups. This statistical test was followed by p-value adjustment for multiple testing using the Benjamini-Hochberg method (Benjamini and Hochberg, 1995). Scatter plots and pie charts were made with the ggplot2 package for R (Wickham, 2016, p. 2). Of primary importance in this study were proteins detected in the mitochondrial databases IMPI and Mouse Mitocarta 3.0 (Rath et al., 2021; Smith and Robinson, 2019) and the O-GlcNAc Database (Malard et al., 2021; Wulff-Fuentes et al., 2021). Enrichment analysis was performed with gprofiler2 (Kolberg et al., 2020; Raudvere et al., 2019) within R. Network analysis was performed using the string-db.org web application (Szklarczyk et al., 2021) and exported to Cytoscape (Shannon et al., 2003) for image manipulation and enrichment analysis.

Intracellular ATP level analysis with iATPSnFR imaging: Cortical neurons at DIV 11-12 were transfected with Synapsin-cyto-mRuby3-iATPSnFR1.0 plasmid with Mito-BFP plasmid and incubated for two days to allow enough expression of fluorescent signals for imaging. For transient yet sufficient O-GlcNAc transferase blocking, OSMI4 was administered 1 hr prior to the image acquisition for OSMI4 treated conditions. Time series movies of the neurons were acquired with C-Apochromat 40x/1.20 W Korr FCS M27 objective on a heated chamber stage at 37 ºC. Tyrode's buffer was constantly perfused during live imaging with or without OSMI4. Each frame was acquired every 1 min by using 405 nm, 488 nm, and 568 nm lasers for detecting Mito-BFP, ATP level-dependent GFP, and ATP-independent mRuby3 signals respectively. For quantification of ATP level change, regions of interest were selected for both soma and processes in each neuron. Then the ratio of GFP to mRuby3 channels (Green-to-red ratio) was calculated and further normalized to baseline value before the initial stimulation.

Fixated imaging acquisition and analysis: Neurons fixated and immunostained were mounted on slide glasses for image acquisition with Zeiss LSM 780 confocal microscope using Plan-Apochromat 100x/1.40 Oil DIC M27. To capture signals from the whole cells without excessive background noise, the Z-stack images of the neurons were obtained while the pinhole size was set at 1 airy unit (~90 μm). For the processing of the images, FIJI was used for Z-stacking, linear contrast adjustments, and quantification of acquired images (Schindelin et al., 2012). Quantified values from FIJI were extracted as Excel spreadsheets for further calculations. The final values were imported to GraphPad Prism file to generate corresponding graphs and to perform statistical tests.

Statistical tests: All data presented in this paper was analyzed using Microsoft Excel and GraphPad Prism 8 or R. The graphs throughout the paper were were generated via GraphPad Prism 8, expressed as Min-Max graphs or mean ± SEM with individual values shown. Statistical analyses were performed with GraphPad Prism 8. For comparison of two conditions, two-tailed unpaired non-parametric Mann-Whitney U test was used. Multiple conditions were compared by non-parametric one-way ANOVA test with post hoc Tukey's or Kruskal-Wallis multiple comparison test. All p-values below 0.05 were considered significant and marked on the graphs.

Figures and tables

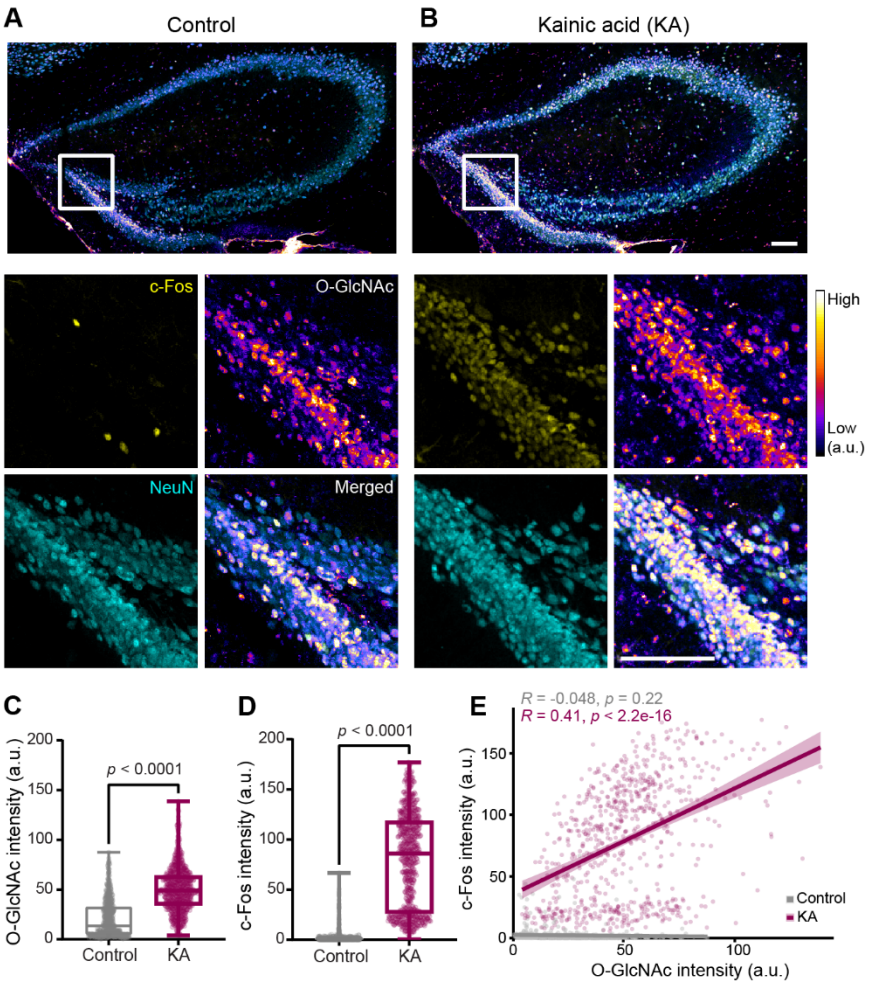

Figure 2.1 O-GlcNAcylation is increased in neurons from seizure-induced mice.

(A and B) Dendate gyrus (DG) in the hippocampus from saline (Control) **(A)** and kainic acid (KA) **(B)** injected mice were immunostained with anti-c-Fos (Yellow), anti-O-GlcNAc (Fire), anti-NeuN (Cyan) and DAPI. **(C)** Quantification of O-GlcNAc intensity from NeuN positive neurons in the DG of Control and KA treated mice. **(D)** Quantifications of c-Fos intensity from NeuN positive neurons in the DG of Control and KA treated mice. All individual values are shown above Min-Max box plot. P-values are as shown in each plot, calculated by Mann-Whitney U test. All scale bars = 100 µm. **(E)** Scatter plot of O-GlcNAc intensity and c-Fos intensity of individual neurons from DG of Control and KA treated brain. Correlation coefficient R values were computed for each condition using Pearson's method. N= 667-720 neurons in DG from three independent animal sets.

Figure 2.2 O-GlcNAcylation level increases throughout hippocampal regions and cortex.

(A) Schematic paradigm of injection and sample collection. **(B)** Map of hippocampal and cortical areas of the imaged section from Bregma -1.22 to -1.34 mm. **(C-E)** Hippocampal regions treated with saline and kainic acid (KA) were immunostained with anti-c-Fos, anti-O-GlcNAc, and anti-NeuN from **(C)** CA1, **(D)** CA3 of hippocampus and **(E)** Layer II/III of motor cortex. O-GlcNAc and c-Fos intensity from NeuN positive neurons were plotted for each condition. P-values are as shown in each plot, calculated by Mann-Whitney U test. N = 655-811 cells (CA1), 508-566 cells (CA3) and 2999-3077 cells (cortex) from three independent animal sets. Scale bar = 100 μm.

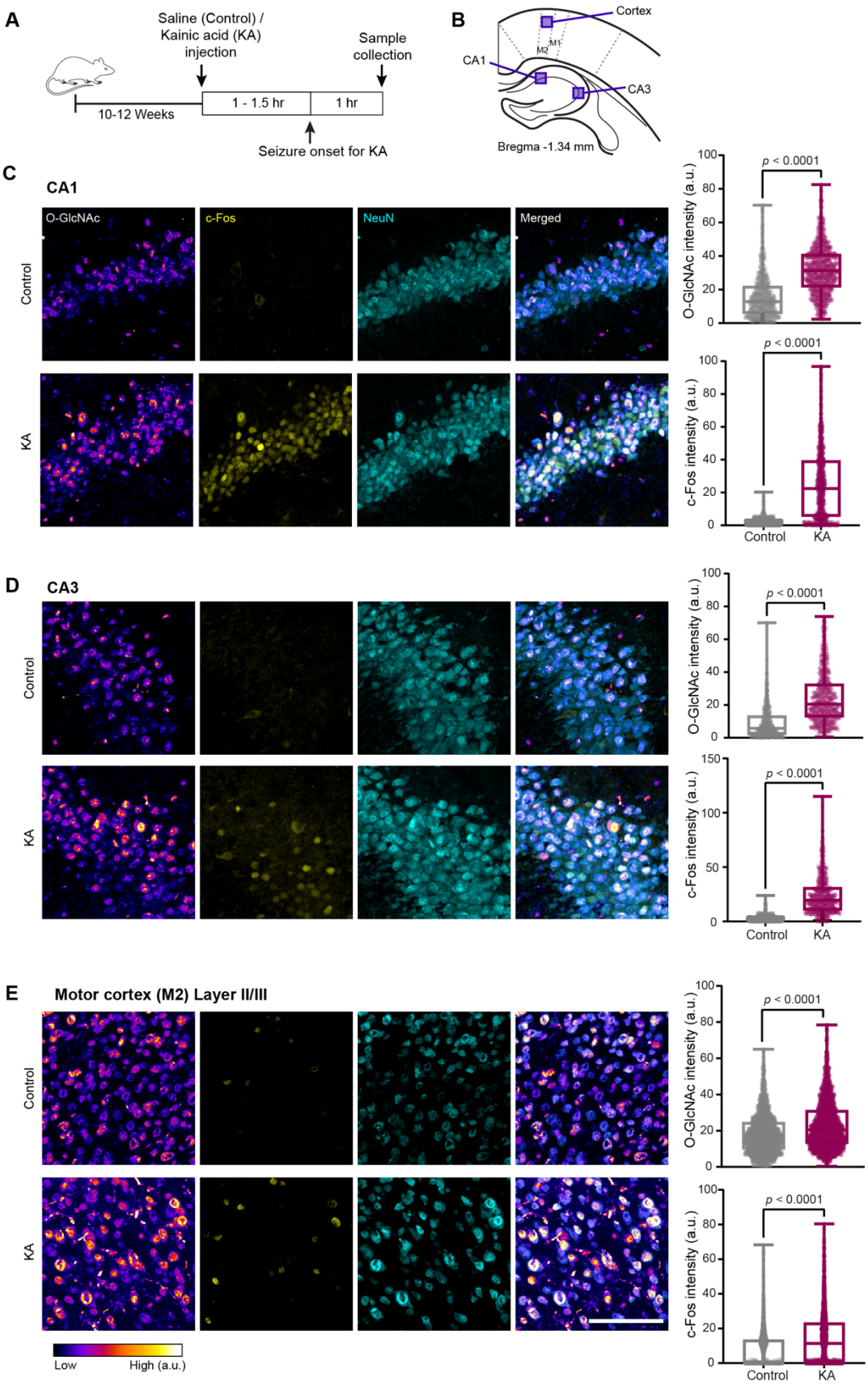
A
Saline (Control) / Kainic acid (KA) injection
Sample collection
10-12 Weeks
1 - 1.5 hr
1 hr
Seizure onset for KA
B
Cortex
M1
M2
CA1
CA3
Bregma -1.34 mm
C
CA1
O-GlcNAc
c-Fos
NeuN
Merged
Control
KA
O-GlcNAc intensity (a.u.)
c-Fos intensity (a.u.)
p < 0.0001
Control
KA
D
CA3
E
Motor cortex (M2) Layer II/III
Low
High (a.u.)

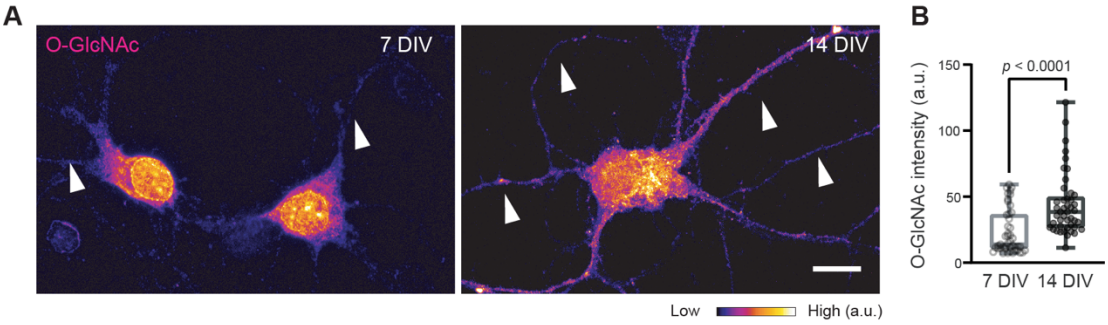

Figure 2.3 O-GlcNAcylation level increases in association with neural age and excitability.

(A) Rat cortical neurons cultured for 7 days in vitro (7 DIV) and 14 days in vitro (14 DIV) were immunostained with anti-O-GlcNAcylation for age-dependent comparison. The arrowheads indicate O-GlcNAc is enriched in processes during neuronal development. Scale bar = 10 µm. **(B)** Quantification of O-GlcNAcylation intensity at 7 and 14 DIV. P-values are as shown in the plot, computed with Mann-Whitney U test. N = 45 cells from each group were analyzed from three independent neuronal dissections.

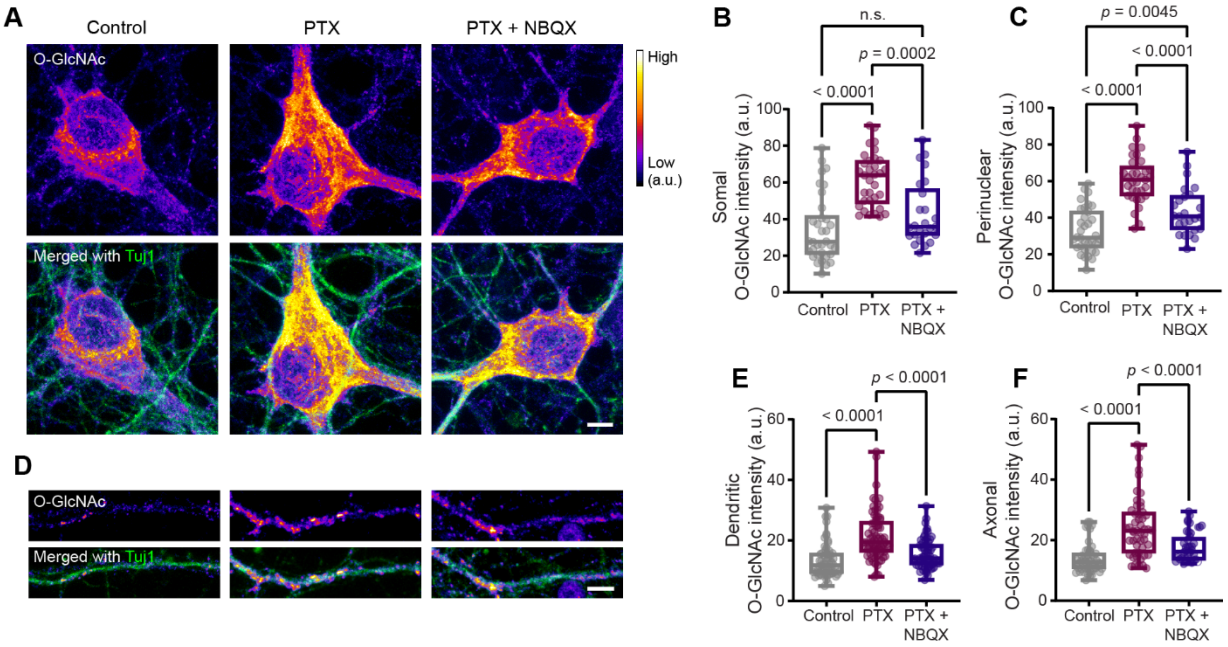

Figure 2.4 Neuronal activity increases O-GlcNAcylation in primary cultured neurons.

(A) Somatic regions of cortical neurons show varied O-GlcNAcylation level by network activity level after 6 hour-treatments of DMSO (Control), Picrotoxin (PTX), and PTX+NBQX. Treated cells were immunostained with anti-O-GlcNAc (Fire) and anti-Tuj1 (Green). (B and C) Quantification of O-GlcNAc intensity from somal (B) and perinulclear regions (C, excluding nuclei) for each condition in cortical neurons. (D) Quantification of dendritic processes from varying conditions, immunostained with anti-O-GlcNAc and anti-Tuj1. (E and F) O-GlcNAcylation intensity plot from dendritic (E) and axonal (F) processes. P-values are as shown in each plot, calculated by one-way ANOVA with post hoc Tukey's multiple comparison test. N = 25-34 neuronal soma, 58-73 dendrites, 36-50 axons from three independent neuronal dissections. All scale bars = 5 μm.

Figure 2.5 Activity-induced O-GlcNAcylation enhances mitochondrial respiration.

(A) Pre-treated neuronal processes were immunostained with anti-O-GlcNAc (Fire) and anti-Tomm20 (Green). Scale bar = 5 μm. **(B)** Immunofluorescence intensity plot of O-GlcNAc and Tomm20 plotted against the neuronal processes. Mitochondrial area was defined as area with mean gray value of 25 and higher Tomm20 immunofluorescence. **(C and D)** Quantification of O-GlcNAcylation intensity of individual dendritic **(C)** and axonal **(D)** mitochondrion from pre-treated neuronal cultures. N=1000-1281 mitochondria analyzed from each group from three independent neuron dissections. **(E-G)** O-GlcNAcylation level changes in isolated fraction of mitochondria and cytoplasm from pre-treated neuronal cell lysates. O-GlcNAc band intensities in the linear range were quantified and normalized to ATP5β band intensity **(F)** and Actin band intensity **(G)** for each condition. N = 4-5 independent neuronal dissections. All values are shown as mean values ± SEM. Significant p-values are shown on the plot, calculated by one-way ANOVA with post hoc Kruskal-Wallis multiple comparison test. **(H)** Traces of oxygen consumption rates (OCRs) of cultured cortical neurons pre-treated with indicated drugs for 6 hrs. The neurons were supplemented with 5mM glucose and 1mM pyruvate by the time of measurement. **(I-K)** Quantification of OCRs at basal **(I)** and maximal respiration timepoints **(J)** and reserve respiratory capacity (difference between maximal and basal respiration) **(K)**. N = 24-32 wells per conditions from three independent neuron dissections.

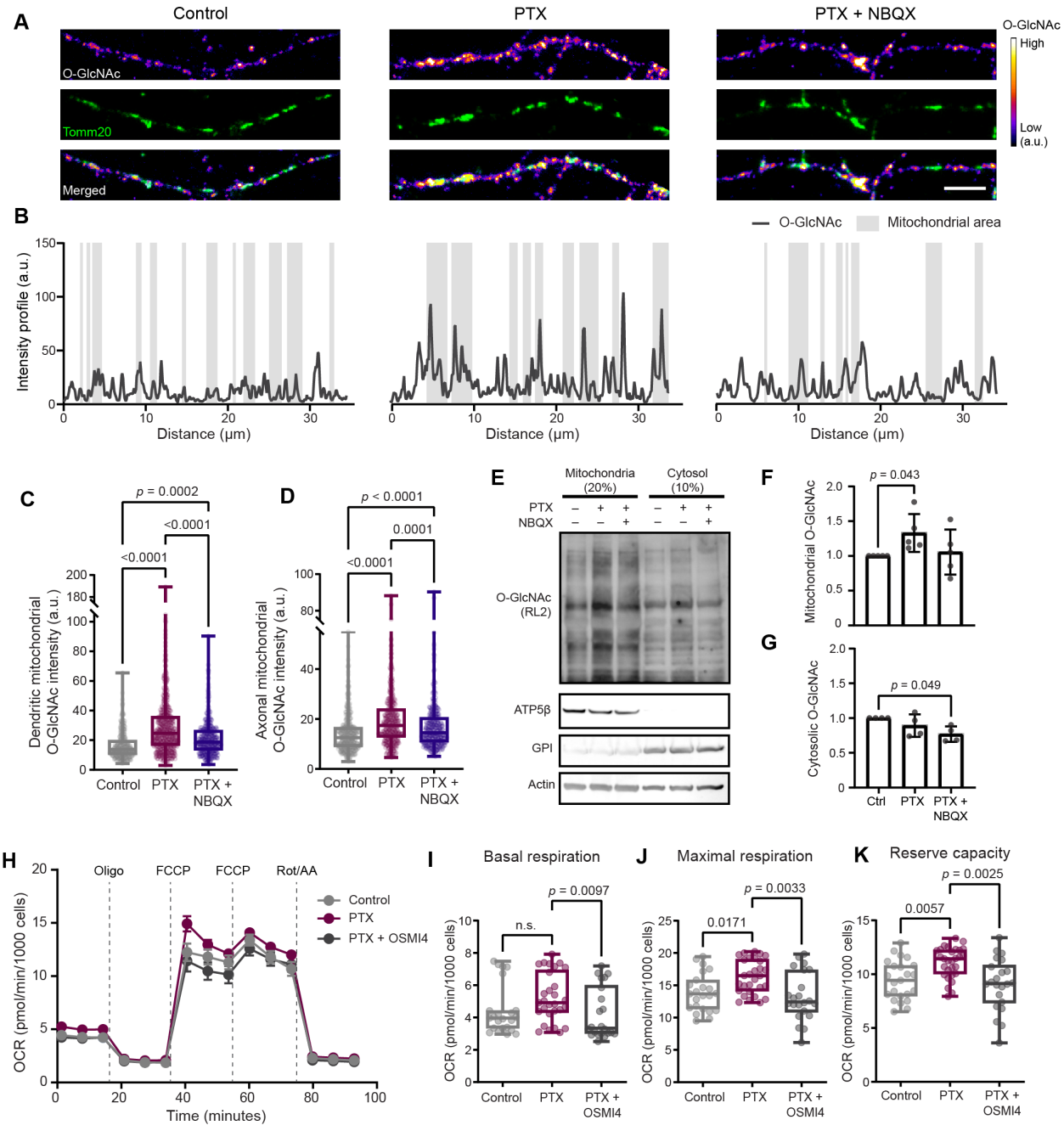
A
Control
PTX
PTX + NBQX
O-GlcNAc
High
Low
(a.u.)
O-GlcNAc
Tomm20
Merged
B
O-GlcNAc
Mitochondrial area
Intensity profile (a.u.)
Distance (μm)
C
p = 0.0002
<0.0001
<0.0001
Dendritic mitochondrial O-GlcNAc intensity (a.u.)
Control
PTX
PTX + NBQX
D
p < 0.0001
0.0001
<0.0001
Axonal mitochondrial O-GlcNAc intensity (a.u.)
Control
PTX
PTX + NBQX
E
Mitochondria (20%)
Cytosol (10%)
PTX
NBQX
O-GlcNAc (RL2)
ATP5β
GPI
Actin
F
p = 0.043
Mitochondrial O-GlcNAc
G
p = 0.049
Cytosolic O-GlcNAc
Ctrl
PTX
PTX + NBQX
H
Oligo
FCCP
FCCP
Rot/AA
Control
PTX
PTX + OSMI4
OCR (pmol/min/1000 cells)
Time (minutes)
I
Basal respiration
p = 0.0097
n.s.
OCR (pmol/min/1000 cells)
Control
PTX
PTX + OSMI4
J
Maximal respiration
p = 0.0033
0.0171
OCR (pmol/min/1000 cells)
Control
PTX
PTX + OSMI4
K
Reserve capacity
p = 0.0025
0.0057
OCR (pmol/min/1000 cells)
Control
PTX
PTX + OSMI4

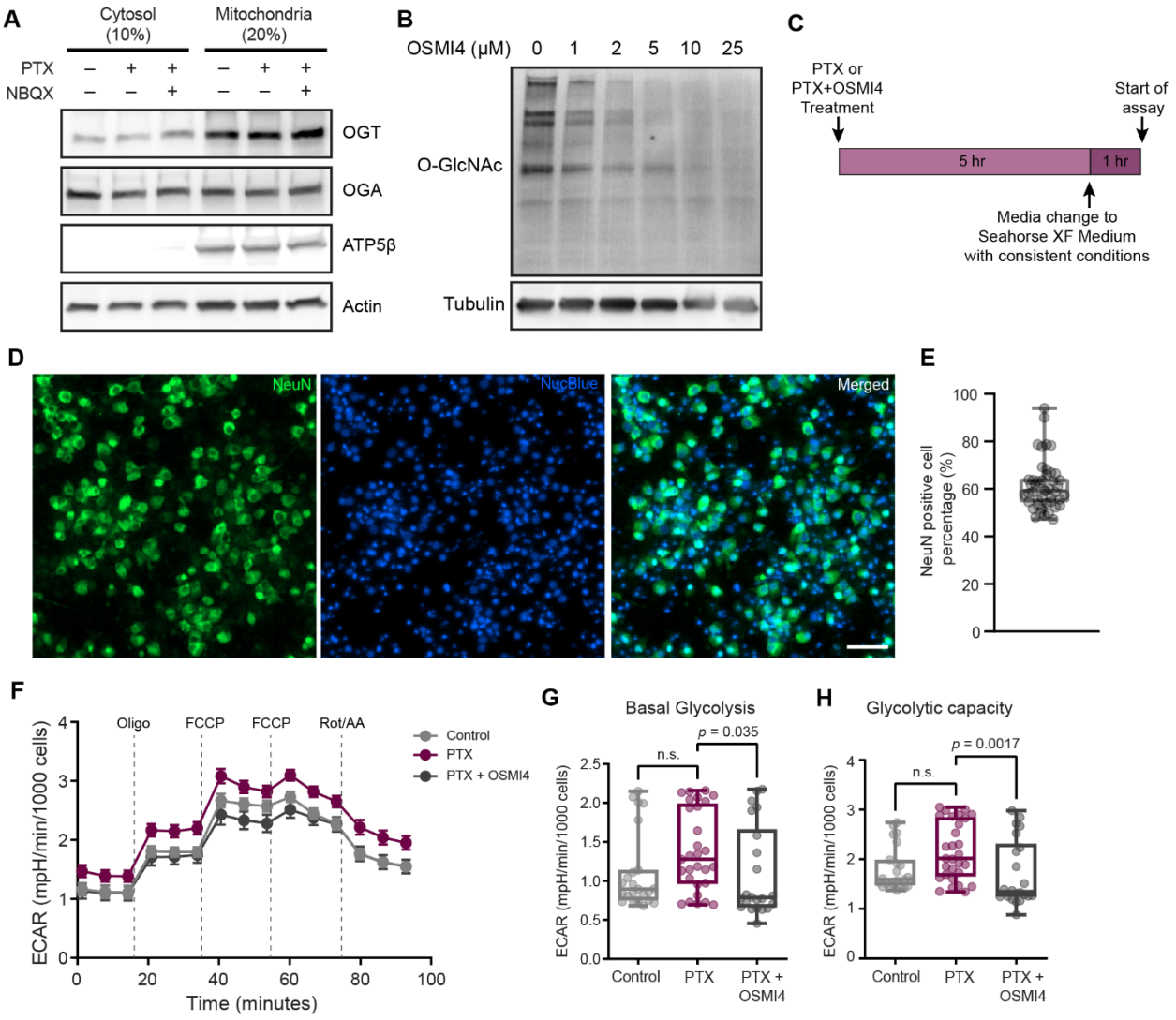

Figure 2.6 Chronic activity by picrotoxin does not change OGT and OGA expression.

(A) Western blot of OGT and OGA expression levels from pre-treated cortical neurons. **(B)** Western blot with O-GlcNAc antibody of cultured cortical neurons treated with varying concentrations of OSMI4 (0, 1, 2, 5, 10, and 25 μM), an OGT inhibitor. **(C)** Schematic paradigm of sample pre-treatment and medium change for Seahorse metabolic flux assay. **(D and E)** Each wells from Seahorse 96 well plates were immunostained with anti-NeuN (Green) and DAPI (Blue) to determine the percentage that NeuN positive neurons take up in each well**. (F)** Traces of extracellular acidification rate (ECARs) of cultured cortical neurons pre-treated with indicated drugs for 6 hrs. **(G and H)** Basal glycolysis **(G)** and glycolytic capacity after oligomycin injection **(H)** values quantified. N = 24-32 wells per conditions from three independent neuron dissections. N = 46 wells analyzed from three independent neuron dissections. Scale bar = 50 μm.

Figure 2.7 Transient stimulation of neurons induces glucose flux that mediates O-GlcNAcylation.

(A) Schematic representation of glucose utilization into glycolytic pathway and hexosamine biosynthetic pathway. Fructose-1,6-biphosphate (FBP) is highlighted in orange color as it is the readout metabolite of HYLT sensor, representing overall intracellular glycolytic flux. **(B)** Traces of intracellular FBP level change measured by HYlight ΔR/R in cultured cortical neurons. R was determined from fluorescence signal as a ratio of 488nm excitation (F_{488}) and 405nm excitation (F_{405}) from each frame. Scale bar = 10 μm. Indicated and color-matched manipulations (arrow) was applied ~10 minutes after the data collection started. All trace values are shown as mean values ± SEM. n = 16-25 individual processes from 7-11 neurons. **(C)** Intracellular FBP level from individual process at three time points just before manipulation (t = 5 min), 3 minutes after manipulation (t = 9 min) and 9 minutes after manipulation (t = 15 min). **(D)** Representative neuronal processes with pseudocolored HYlight R (F_{488} / F_{405}) at the same time points from panel (C). Scale bar = 10 μm. **(E)** Timeline of neuronal transfection with GCaMP6s and MitoDsRed, live cell imaging with stimulation, followed by neuronal fixation and staining for O-GlcNAcylation. **(F and G)** Cultured neurons transfected with MitoDsRed and GCaMP was fixated after stimulation to quantify O-GlcNAcylation with or without electrical stimulation. **(F)** Fixated neurons are immunostained with anti-O-GlcNAc (Fire) that can be overlayed with Mito-DsRed (Green). Scale bar = 5 μm. **(G)** O-GlcNAc signal of individual mitochondrion masked by Mito-DsRed was quantified from non-stimulated or stimulated neuronal processes. N = 646-801 mitochondria from 17-21 neurons. All individual values are shown above Min-Max box plot. P-values are as shown in each plot, calculated by Mann-Whitney U test.

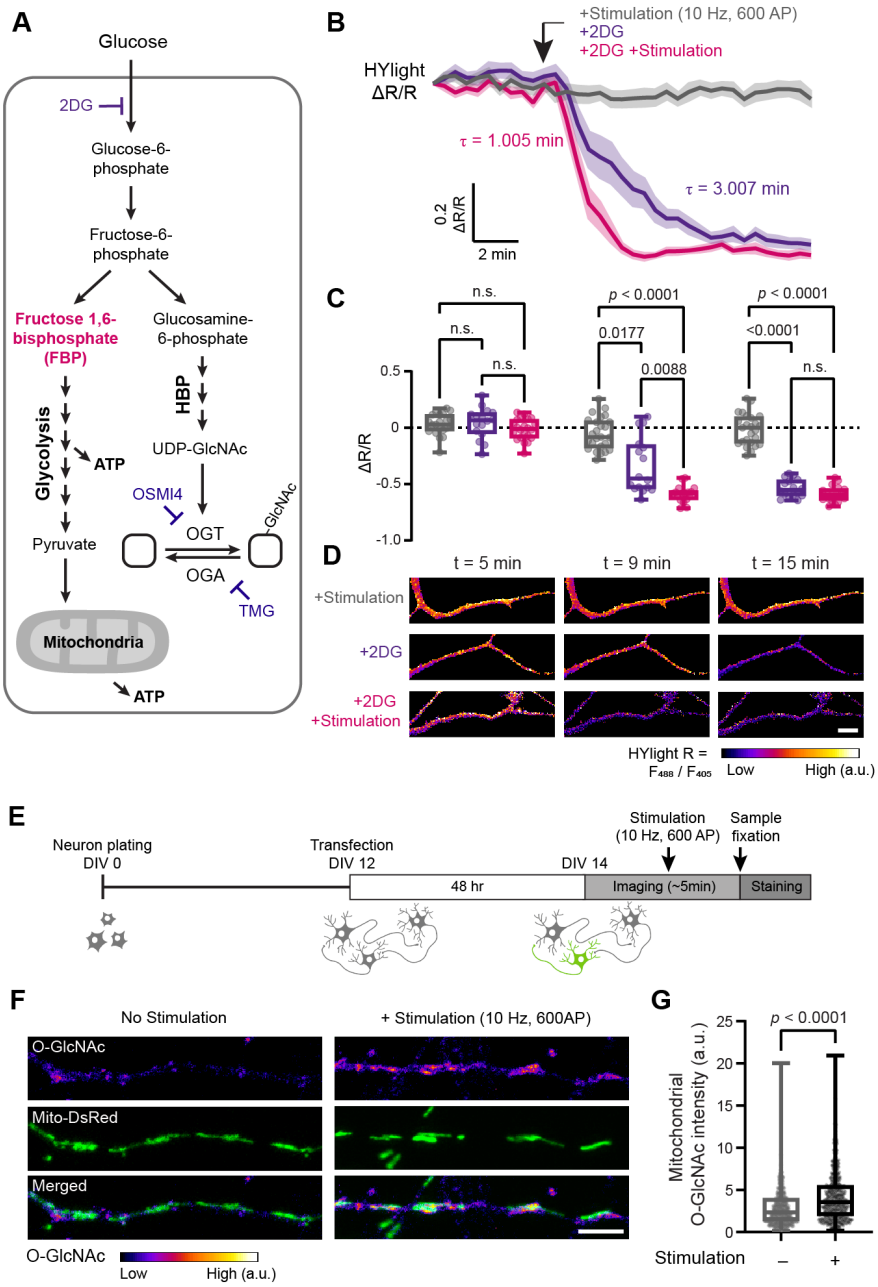
A
Glucose
2DG
Glucose-6-phosphate
Fructose-6-phosphate
Fructose 1,6-bisphosphate (FBP)
Glucosamine-6-phosphate
HBP
Glycolysis
ATP
UDP-GlcNAc
OSMI4
OGT
GlcNAc
Pyruvate
OGA
TMG
Mitochondria
ATP
B
+Stimulation (10 Hz, 600 AP)
+2DG
+2DG +Stimulation
HYlight ΔR/R
τ = 1.005 min
τ = 3.007 min
0.2 ΔR/R
2 min
C
n.s.
n.s.
n.s.
p < 0.0001
0.0177
0.0088
p < 0.0001
<0.0001
n.s.
ΔR/R
0.5
0
-0.5
-1.0
D
t = 5 min
t = 9 min
t = 15 min
+Stimulation
+2DG
+2DG +Stimulation
HYlight R = F488 / F405
Low
High (a.u.)
E
Neuron plating DIV 0
Transfection DIV 12
48 hr
DIV 14
Stimulation (10 Hz, 600 AP)
Sample fixation
Imaging (~5min)
Staining
F
No Stimulation
+ Stimulation (10 Hz, 600AP)
O-GlcNAc
Mito-DsRed
Merged
O-GlcNAc
Low
High (a.u.)
G
p < 0.0001
Mitochondrial O-GlcNAc intensity (a.u.)
25
20
15
10
5
0
Stimulation
–
+

Figure 2.8 Transient neuronal stimulation is captured with Ca^{2+} influx.

(A and B) Cultured cortical neurons transfected with GCaMP6s to ensure Ca2+ influx with the electrical field stimulation. **(A)** Normalized GCaMP6s $\Delta F/F_0$ signals from non-stimulated and stimulated neurons. Graphs represent mean values ± SEM from 5-9 neurons from three independent neuron dissections. **(B)** Pseudocolored representative neuronal GCaMP6s before (t=0min) and after (t=2min) electrical stimulation. Scale bar = 50 μm. **(C)** HYlight transfected neuronal process images were acquired with 488nm excitation (F_{488}) and 405nm excitation (F_{405}) at before (t=10min) and after manipulations (t=14min and 20min). The ratio of F_{488} to F_{405} was represented in Figure 2.7D. Scale bar = 10 μm. **(D)** Schematic of GCaMP6s transfected neuron imaging and fixation, acutely pre-treated with TMG. **(E)** Normalized GCaMP6s $\Delta F/F_0$ signals from non-stimulated and stimulated neurons with the presence of TMG. Graphs represent mean values ± SEM from 5-9 neurons from three independent neuron dissections. **(F)** Pseudocolored representative neuronal GCaMP6s with TMG before (t=0min) and after (t=2min) electrical stimulation. Scale bar = 50 μm. **(G)** Immunostained neuronal processes with anti-O-GlcNAc (Fire LUT) staining and Mito-DsRed (Green) signal. Scale bar = 5 μm. **(H)** More drastic increases in mitochondrial O-GlcNAcylation was quantified from non-stimulated or stimulated neuronal processes. N=568-634 mitochondria from 19-23 neurons. All individual values are shown above Min-Max box plot. P-values are as shown in the plot, calculated by Mann-Whitney U test.

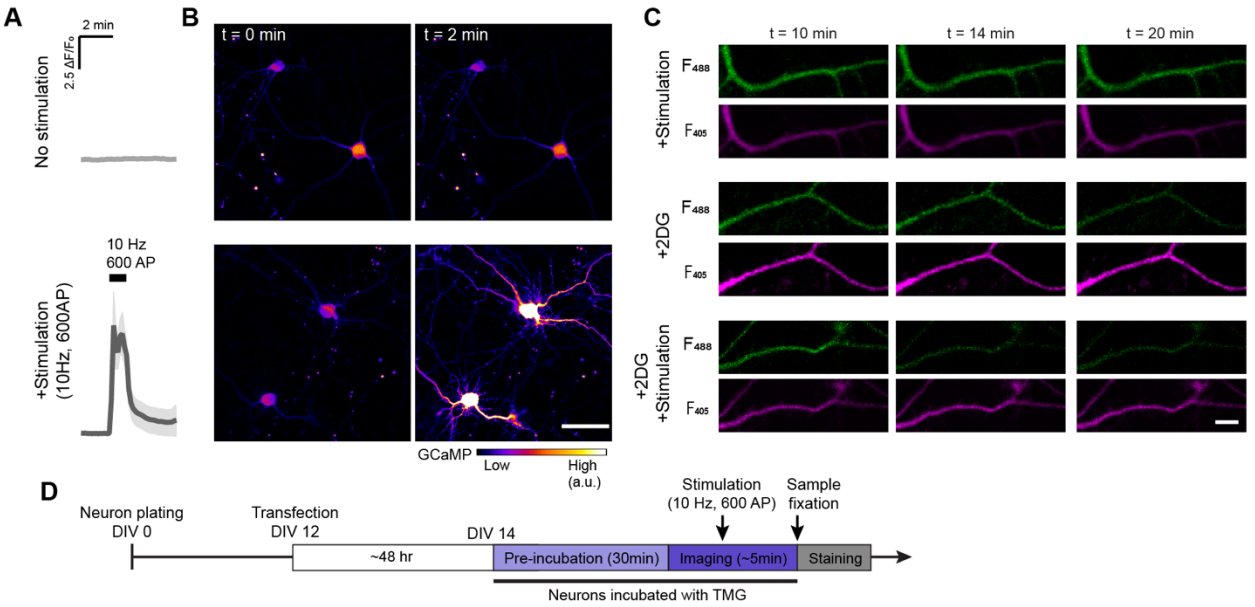
A
2 min
2.5 ΔF/F₀
No stimulation
10 Hz
600 AP
+Stimulation
(10Hz, 600AP)
B
t = 0 min
t = 2 min
GCaMP
Low
High
(a.u.)
C
t = 10 min
t = 14 min
t = 20 min
+Stimulation
+2DG
+2DG
+Stimulation
F488
F405
D
Neuron plating
DIV 0
Transfection
DIV 12
DIV 14
~48 hr
Pre-incubation (30min)
Imaging (~5min)
Staining
Stimulation
(10 Hz, 600 AP)
Sample
fixation
Neurons incubated with TMG

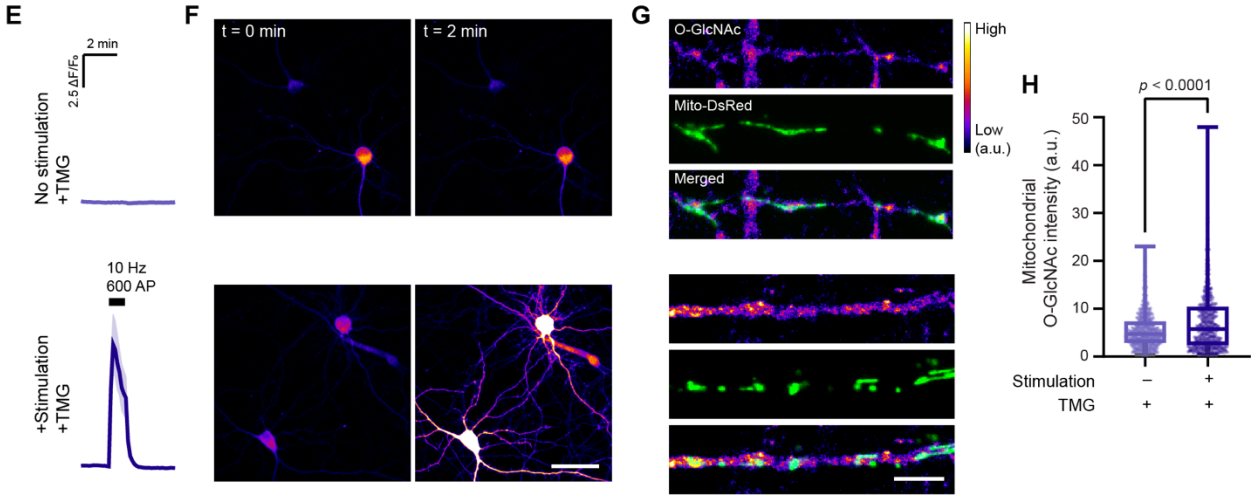
E
2 min
2.5 ΔF/F₀
No stimulation
+TMG
10 Hz
600 AP
+Stimulation
+TMG
F
t = 0 min
t = 2 min
G
O-GlcNAc
Mito-DsRed
Merged
High
Low
(a.u.)
H
p < 0.0001
Mitochondrial
O-GlcNAc intensity (a.u.)
50
40
30
20
10
0
Stimulation
TMG
–
+
+
+

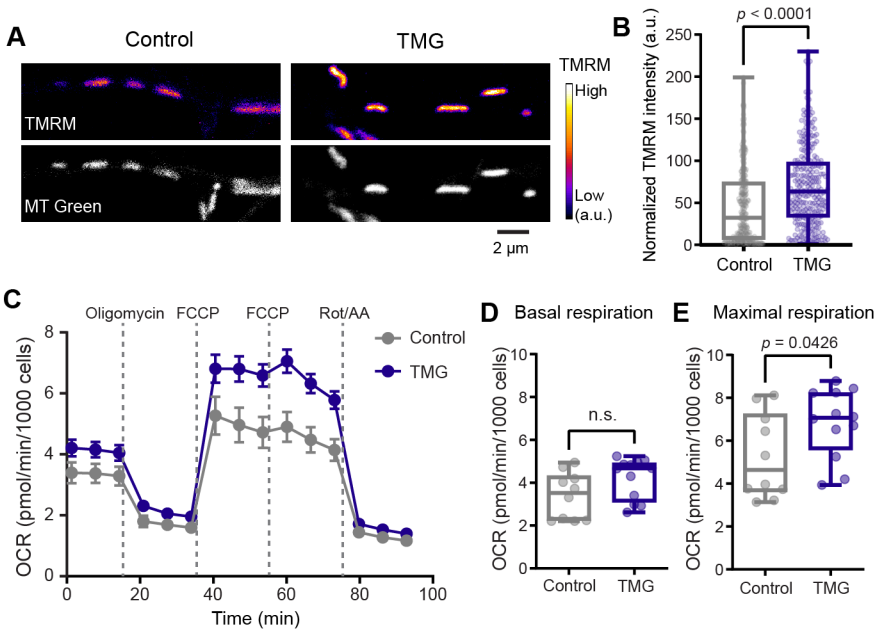

Figure 2.9 Neuronal mitochondrial bioenergetics enhanced with O-GlcNAcylation.

(A and B) Cortical neurons with or without TMG are co-stained with TMRM and MitoTracker (MT) Green. **(A)** Mitochondria from neuronal processes show varied degrees of membrane potential indicated by TMRM intensity. **(B)** TMRM intensities quantified and normalized by MT Green. N=268-281 individual mitochondria from 4 independent neuron dissections. Scale bar = 2 µm. **(C)** Traces of oxygen consumption rates (OCRs) of Control and TMG treated cortical neurons, supplemented with 1mM glucose and 1mM pyruvate. **(D and E)** Comparison of basal **(D)** and maximal **(E)** respiration rates. N=10-12 wells per condition from three independent neuron dissections. All individual values are shown above Min-Max box plot. P-values are as shown in each plot, calculated by Mann-Whitney U test.

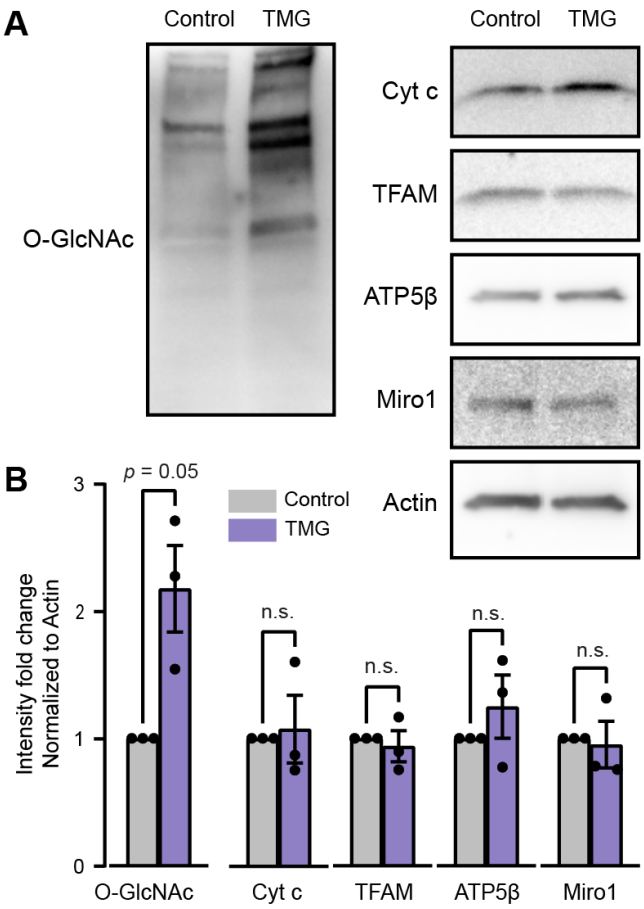

Figure 2.10 Chronic manipulation of O-GlcNAc level by TMG does not influence mitochondrial protein content.

(A) Cell lysates of cortical neurons pre-treated with DMSO (Control) and TMG overnight are probed with multiple mitochondrial proteins to test any chance of mitochondrial biogenesis upon prolonged O-GlcNAcylation. **(B)** Quantification of O-GlcNAcylation level and mitochondrial protein expression between Control and TMG groups are compared as a fold change. N=3 independent neuron dissections. Fold change between Control and TMG were indicated as bar plot with individual datapoints. P values were determined with Mann-Whitney U test.

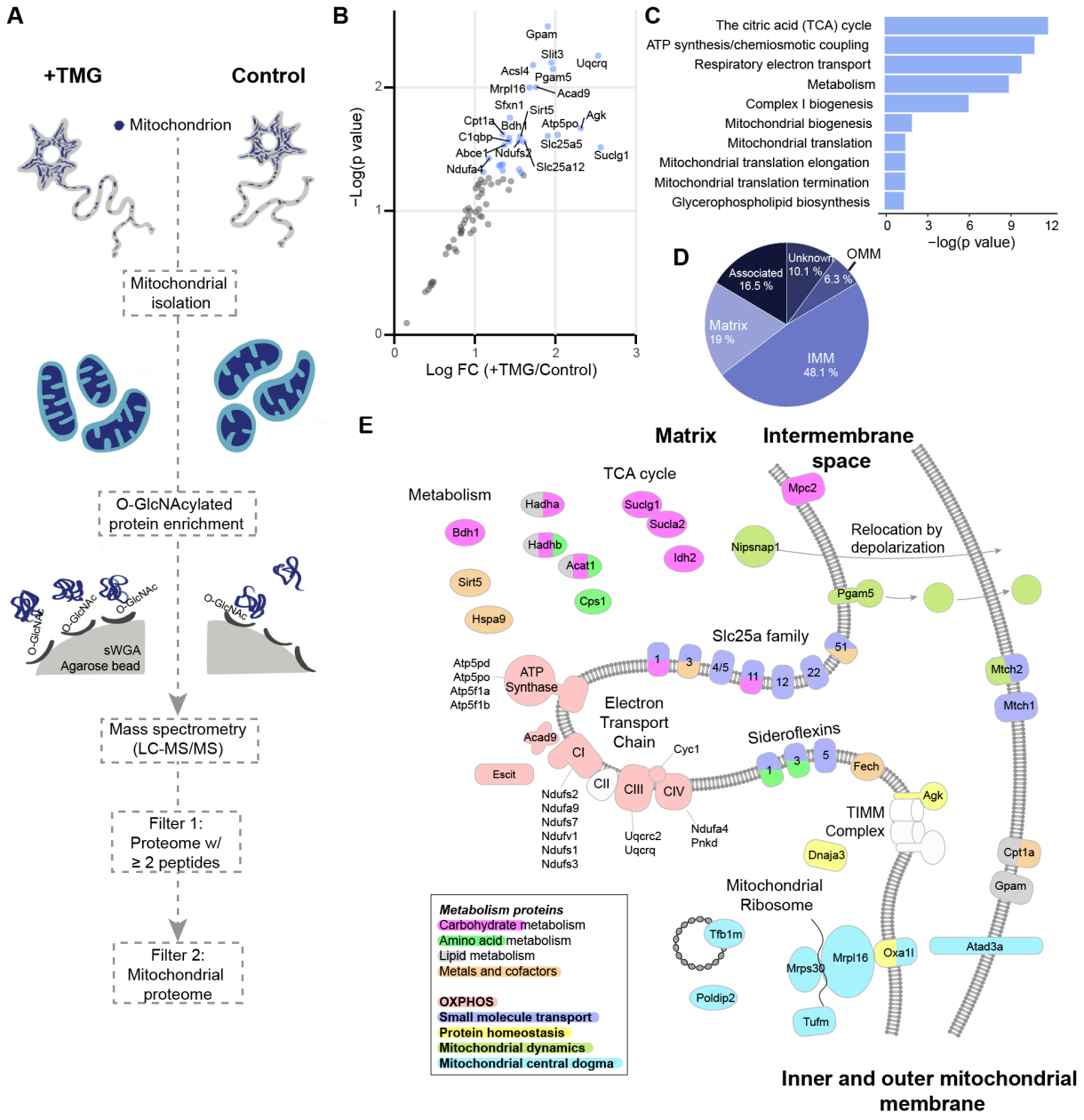

Figure 2.11 O-GlcNAcome in crudely isolated mitochondria from neurons.

(A) Schematic outline of mass spectrometry sample preparation and analysis. **(B)** Volcano plots of identified proteins after Filter 2 (Mitochondrial proteins) with Top 20 gene names by significance (-log(p value)). **(C)** Pathway enrichment analysis of identified mitochondrial proteome. **(D)** Submitochondrial localization of identified mitochondrial proteins. **(E)** Illustration of representative mitochondrial proteins colored by MitoPathway assignments from MitoCarta3.0. N = 3 independent experimental sets.

Figure 2.12 Neuronal O-GlcNAcome entails various membrane-bound organelles.

(A) O-GlcNAc enrichment of isolated crude mitochondrial fractions show higher O-GlcNAcylation level +TMG samples. **(B)** Volcano plot of proteome after Filter 1. **(C)** Venn diagram of overlapping proteins from identified proteins with mitochondrial databases (MitoCarta3.0 and IMPI) and O-GlcNAc database. **(D)** Subcellular location of identified proteins after Filter 1. **(E)** STRING protein-protein interaction analysis of identified mitochondrial proteins with nodes colored by fold change (+TMG / Control).

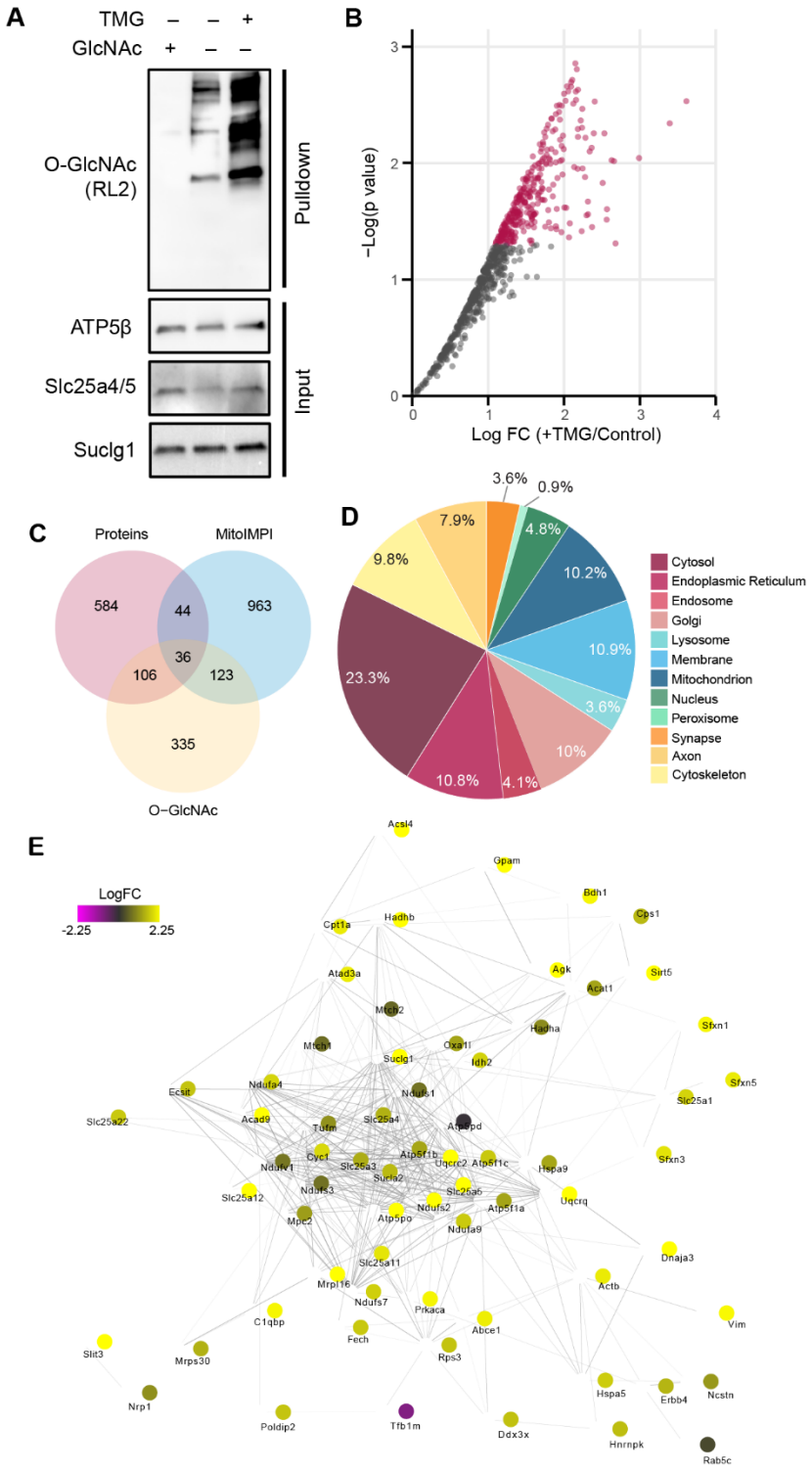
A
TMG – – +
GlcNAc + – –
O-GlcNAc (RL2)
Pulldown
ATP5β
Slc25a4/5
Suclg1
Input
B
−Log(p value)
Log FC (+TMG/Control)
C
Proteins
MitoIMPI
584
44
963
36
106
123
335
O−GlcNAc
D
3.6%
0.9%
7.9%
4.8%
9.8%
10.2%
10.9%
23.3%
3.6%
10%
10.8%
4.1%
Cytosol
Endoplasmic Reticulum
Endosome
Golgi
Lysosome
Membrane
Mitochondrion
Nucleus
Peroxisome
Synapse
Axon
Cytoskeleton
E
LogFC
-2.25
2.25
Acsl4
Gpam
Bdh1
Cps1
Cpt1a
Hadhb
Atad3a
Agk
Sirt5
Acat1
Mccc2
Hadha
Sfxn1
Mccc1
Oxa1l
Suclg1
Idh2
Sfxn5
Ecsit
Ndufa4
Ndufs1
Slc25a1
Slc25a22
Acad9
Tufm
Slc25a4
Atp5pd
Cyc1
Atp5f1b
Uqcrc2
Atp5f1c
Sfxn3
Ndufv1
Slc25a3
Hspa9
Suclg2
Slc25a12
Ndufs3
Slc25a6
Uqcrq
Ndufs2
Atp5f1a
Mpc2
Atp5po
Ndufa9
Dnaja3
Slc25a11
Actb
Mrpl16
Ndufs7
Prkaca
Vim
C1qbp
Abce1
Fech
Slit3
Rps3
Mrps30
Hspa5
Ncstn
Erbb4
Nrp1
Poldip2
Tfb1m
Ddx3x
Hnrnpk
Rab5c

Figure 2.13 ATP replenishment after neuronal stimulation is O-GlcNAcylation dependent.

(A) Timeline for neuronal transfection with iATPSnFR, pre-treatment with DMSO or OSMI4, and imaging. **(B)** Neuronal process images filled with iATPSnFR GFP signal proportionate to ATP level before and 10 minutes after the stimulation. **(C)** Traces of ATP level changes in neuronal processes with the electrical stimulation with or without OSMI4. **(D)** Percent change of normalized iATPSnFR signal 10 minutes after the stimulation from individual processes. N = 20-24 processes from five independent neuron dissections. The graphs are represented as mean values ± SEM. P-values are computed by Mann-Whitney U test. Scale bar = 10 μm. **(E)** Schematic model demonstrating activity induced increase in glucose uptake, downstream glycolysis, and hexosamine biosynthetic pathway (HBP). More UDP-GlcNAc as a product of increased HBP mediates more O-GlcNAcylation on mitochondrial proteins. This eventually results in more ATP synthesis to fuel neuronal activity in neuronal processes.

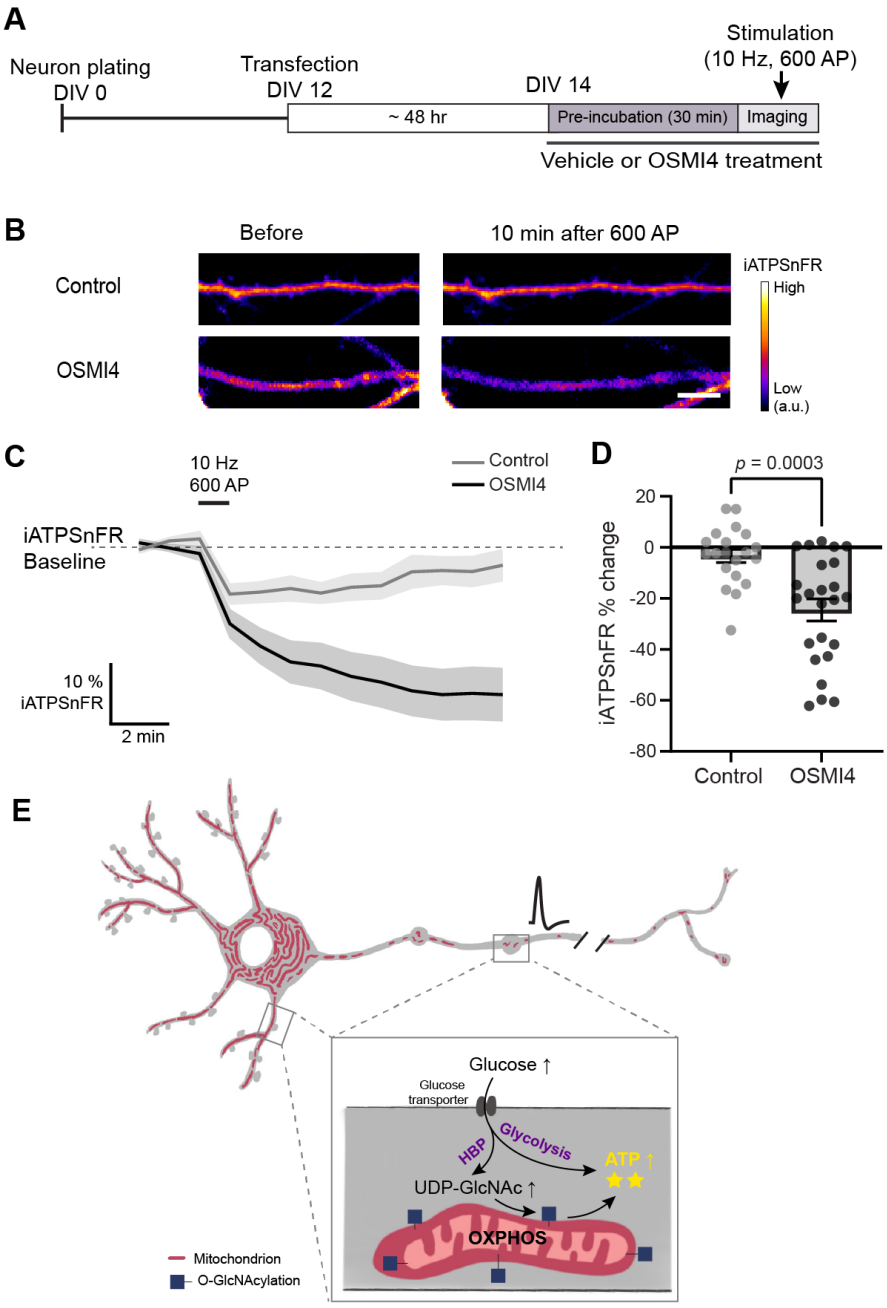
A
Neuron plating
DIV 0
Transfection
DIV 12
DIV 14
Stimulation
(10 Hz, 600 AP)
~ 48 hr
Pre-incubation (30 min)
Imaging
Vehicle or OSMI4 treatment
B
Before
10 min after 600 AP
Control
OSMI4
iATPSnFR
High
Low
(a.u.)
C
10 Hz
600 AP
Control
OSMI4
iATPSnFR
Baseline
10 %
iATPSnFR
2 min
D
p = 0.0003
iATPSnFR % change
20
0
-20
-40
-60
-80
Control
OSMI4
E
Glucose ↑
Glucose
transporter
HBP
Glycolysis
ATP ↑
UDP-GlcNAc ↑
OXPHOS
Mitochondrion
O-GlcNAcylation

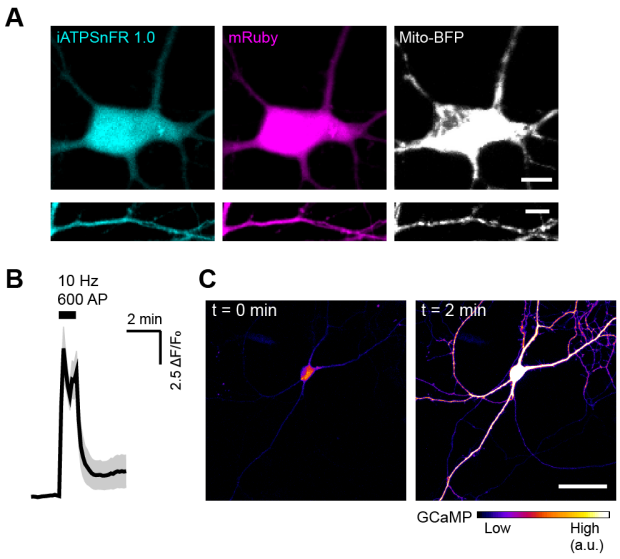

Figure 2.14 Expression of iATPSnFR in neurons and neuronal stimulation pattern with OSMI4.

(A) Neuronal soma and processes transfected with iATPSnFR1.0-mRuby and Mito-BFP. Scale bars = 10 µm. **(B)** Normalized GCaMP6s $\Delta F/F_0$ signal from stimulated cortical neuron with the presence of OSMI4. Graph displays mean GCaMP6s intensity ± SEM from 6 neurons from three independent dissections. **(C)** Neuronal GCaMP6s signals before (t=0min) and after (t=2) electrical stimulation. Scale bar = 50 µm.

Table 2.1: Key resources table

Reagents or Resources	Source	Identifier
Antibodies (Immunoreagents)		
Anti-O-GlcNAc (RL2)	Abcam	Cat # Ab2739
Anti-c-Fos	Synaptic Systems	Cat # 226 003
Anti-NeuN	Sigma-Aldrich	Cat # ABN91
Anti-βIII Tubulin (Tubb3, Tuj1)	Novus Biologicals	Cat # NB100-1612
Anti-Tomm20	Sigma-Aldrich	Cat # HPA011562
Anti-ATP5β	Sigma-Aldrich	Cat # HPA001520
Anti-RHOT1 (Miro1)	Aviva	Cat # ARP44817-P050
Anti-GPI	Invitrogen	Cat # PA5-26787
Anti-Actin	Sigma-Aldrich	Cat # A2228
Anti-Cytochrome c	Abcam	Cat # Ab13575
Anti-TFAM (mtTFA)	Abcam	Cat # Ab131604
Anti-ANT1/2 (Slc25a4/5)	Abcam	Cat # Ab110322
Plasmids		
CMV-HYlight (CggR0-180-PPKE)	Goodman lab, OHSU (In press, PNAS)	N/A
pDsRed2-Mito	Clontech	Cat # 632421
GCaMP6s (AMP resistance)	Addgene (Chen et al., 2013)	Plasmid # 100844
Synapsin-cyto-mRuby3-iATPSnFR1.0	Addgene (Lobas et al., 2019)	Plasmid # 102557
Mito-BFP	(Ashrafi et al., 2014)	
Reagents		
NucBlue Live ReadyProbes Reagent (Hoechst 33342)	Invitrogen	Cat # R37605
Tetramethylrhodamine (TMRM)	Invitrogen	Cat # T668
MitoTracker Green FM	Invitrogen	Cat # M7514
Succinylated Wheat Germ Agglutinin (sWGA), Agarose bound	Vector Laboratories	Cat # AL-1023S
Chemicals		
Kainic acid (KA)	Tocris	Cat # 0222
Picrotoxin (PTX)	Tocris	Cat # 1128
NBQX disodium salt	Tocris	Cat # 1044
Oligomycin A	Sigma-Aldrich	Cat # 75351
Carbonyl cyanide 4-(trifluoromethoxy)phenylhydrazone (FCCP)	Sigma-Aldrich	Cat # C2920
Rotenone	Sigma-Aldrich	Cat # R8875
Antimycin A	Sigma-Aldrich	Cat # A8674
Cytosine β-D-arabinofuranoside (Cytarabine, Ara-C)	Tocris	Cat # 4520
OSMI-4	MedChem Express	Cat # HY-114361
Thiamet-G (TMG)	Calbiochem	Cat # 110165CBC

Table 2.1: Key resources table (continued)

Reagents or Resources	Source	Identifier
Critical commercial assays		
Seahorse XF Cell Mito Stress Test	Agilent	
Experimental models: Organisms/Strains		
C57BL/6J Mouse	The Jackson Laboratory	Strain # 000664
Sprague-Dawley Rat	Envigo	
Software and algorithms		
Fiji	(Schindelin et al., 2012)	https://imagej.net/software/fiji/
GraphPad Prism 8	GraphPad	https://www.graphpad.com
R	R Foundation	https://www.r-project.org/
Cytoscape	National Institute of General Medical Sciences (NIGMS)	https://cytoscape.org/

Acknowledgements

We thank Dr. Majid Ghassemian for technical contributions running and analyzing mass spectrometry analysis; former and current lab members of Pekkurnaz lab for extensive discussion and reviewing the manuscript. We gratefully acknowledge Dr. Baljit Khakh for kind gift of Synapsin-cyto-mRuby3-iATPSnFR1.0. This work was supported by NIH/NIGMS grant no. R35GM128823.

Chapter 2, in full, is a reprint of the material as it appears in Yu, S. B., Sánchez, R. G., Papich, Z. D., Whisenant, T. C., Koberstein J. N., Stewart, M. L., Stork, P. J. S., Goodman, R., and Pekkurnaz, G. "Neuronal activity-driven O-GlcNAcylation promotes mitochondrial plasticity," being submitted. The dissertation author was the primary investigator and author of this paper.

Author contributions

Conceptualization: S.B.Y., G.P.; Methodology: S.B.Y., R.G.S., T.C.W., and G.P.; Data acquisition and analysis: S.B.Y., Z.D.P.; Resources: T.C.W., J.N.K., M.L.S., P.J.S.S., R.G., and G.P.; Writing manuscript: S.B.Y. and G.P.; Supervision: G.P.; Funding acquisition: R.G. and G.P.

CHAPTER 3: O-GLCNACYLATION PROMOTES SUBSTRATE-SPECIFIC NEURONAL EXCITABILITY

INTRODUCTION

Although glucose is the major fuel utilized in the brain, during a prolonged shortage of glucose, the brain is capable of using other fuel sources, especially ketone bodies (Cahill, 2006). Ketone bodies refer to the ketone group-containing soluble molecules produced from fatty acids by the liver. The ketogenesis generates three key substrates that are called ketone bodies: β-hydroxybutyrate (BHB), Acetoacetate (Acac), and acetone. Although they are produced by the liver, they can be released into the blood to be readily transported and taken up by non-hepatic tissues, including the brain. Unlike glucose metabolism, ketone bodies are utilized directly by mitochondria without the generation of cytosolic ATP. Mitochondria convert ketone bodies into acetyl-CoA, which then enters the TCA cycle. Ketone bodies are selectively used by neurons for more efficient ATP generation under starvation conditions (Owen et al., 1967; Chowdhury et al., 2014); thus, metabolite switching from glucose to ketone bodies is an indispensable part of neuronal adaptation for maintaining cognitive performance of the brain during starvation.

When the neuronal fuel source switches to ketone bodies, neurons undergo metabolic rewiring characterized by less excitability. It led to the general notion of a ketogenic diet as a therapeutic treatment to mitigate epileptic seizures (Lutas and Yellen, 2013). Interestingly, this anti-convulsant effect of the ketogenic diet is rapidly reversed by glucose infusion (Huttenlocher, 1976). The study suggested a strong correlation between neuronal excitability and the fuel they are mainly utilizing, yet the molecular mechanism that regulates the fuel switch is unknown. As discussed in Chapter 2, we have identified neuronal mitochondrial O-GlcNAcome. Within our dataset, a number of proteins involved in the transport of ketone bodies and ketolysis are identified to be O-GlcNAcylated (Figure 2.11). Based on these results, we hypothesized that O-

GlcNAcylation, by signaling the enhanced glucose availability on these proteins via post-translational modifications, helps neurons prioritize glucose consumption over ketone bodies. In this Chapter 3, we established methods and studies to test the role of O-GlcNAcylation in neuronal fuel utilization. While these studies are still preliminary, our results suggest that O-GlcNAcylation may play a role in altering ketone body metabolism to maximize glucose utilization and bolster synaptic activity.

RESULTS

O-GlcNAcylation alters amino acids abundance

First, we began evaluating mitochondrial fuel preference upon O-GlcNAcylation by using metabolic tracing assays. The fuel utilization pathways in neurons can be determined by stable isotope tracing and mass spectrometry analysis. For these experiments, we generated neuron culture media containing isotopically labelled [$^{13}C_6$]-Glucose or [$^{13}C_4$]-β–Hydroxybutyrate (BHB). We cultured neurons overnight with these labelled metabolites to allow enough time for neurons to incorporate labeled carbon sources (sample treatment and carbon incorporation schemes for the substrates are depicted in Figure 3.1A). To evaluate how O-GlcNAc upregulation alter fuel preference, we treated neurons with 2 μM Thiamet-G (TMG) prior to incubation with labelled metabolites as demonstrated in Figure 3.1. We specifically isolated hydrophilic metabolites and performed gas chromatography-mass spectrometry (GC-MS) analysis in collaboration with Dr. Ajit Divakaruni's laboratory at the University of California, Los Angeles. These experiments allowed us to determine: (1) percent of ^{13}C incorporation, or mole percent enrichment (MPE), of analayzed metabolites and (2) quantitative abundance of metabolites in the cell. MPE describes a weighted average for how much label from glucose or BHB was

incorporated into intracellular metabolite pool for a given metabolite. Metabolite abundance demonstrates how each intracellular metabolite amount is changed by O-GlcNAcylation upregulation via TMG treatment, as it is an independent factor from isotope incorporation.

In our preliminary analysis, we have not observed any change in incorporation rate of labeled carbon upon TMG treatment from both glucose and BHB (Figure 3.1B). Both substrates were incorporated equally to feed their expected destinations: glycolysis and TCA cycle for glucose and only TCA cycle for BHB. Although we did not observe any difference upon 4 hours pre-treatment of TMG before the labelled metabolite exposure, further optimization of TMG incubation time may be required to reveal O-GlcNAcylation induced changes. The optimization in sample collection timing is also necessary as 20 hours may be enough time for substrates to be completely incorporated and reach equilibrated state. In future experiments, we are planning to collect ^{13}C incorporated samples at shorter time points— such as 1, 2, and 4 hours—to capture acute incorporation rates of the substrates. For our preliminary experiments, we included glucose and ketone bodies together. Providing ketone bodies or glucose alone would be a preferable approach for the upcoming experiments.

From the total abundance of metabolites detected by GC-MS, we observed significant changes in glutamate, aspartate, and threonine levels (Figure 3.1C). Although still preliminary, alterations in these metabolites suggest increase in amino acid metabolism with an elevated O-GlcNAcylation. Intriguingly, glutamate and aspartates are the amino acids that can contribute to neuronal activity directly as excitatory neurotransmitters. It may suggest that O-GlcNAcylation regulates neurotransmission not only by regulating ATP level, but also altering the available neurotransmitter pool, especially at excitatory neurons. If this abundance change in metabolite pool is sheerly coming from more production of the indicated amino acids, we can speculate the

upregulation in amino acid anabolic pathways, specifically for those that can be converted to neurotransmitters. Together, the metabolite abundance data suggest cellular rewiring that can equip neuron for potential robust synaptic activity, expanding our results discussed in Chapter 2.

Fuel source- dependent regulation of mitochondrial transport in neurons

Glucose flux causes mitochondrial motility arrest via O-GlcNAcylation of the mitochondrial motor adaptor protein Milton (Pekkurnaz et al., 2014). Here we investigated whether mitochondrial motility is regulated via ketone body availability instead of glucose. To test whether mitochondrial utilization of ketone bodies alters the mitochondrial transport rate in neurons, we established a neuronal culture model of a ketogenic diet. We established primary hippocampal neuron cultures in 5mM glucose containing media. Then, to mimic physiological starvation conditions, we replaced 5mM culture with media containing 1mM glucose for 24 hours, then treated neurons for 2 hours with media containing either additional 4mM glucose or ketone bodies (Figure 3.2). High glucose caused mitochondrial motility reduction as previously described (Pekkurnaz et al., 2014). However, when we replaced glucose with equal molar of ketone body treatment (4mM BHB), mitochondrial motility was similar to the baseline control; if anything, slightly increased, which was reversed by TMG treatment (Figure 3.2B). These results demonstrate that ketone body utilization does not cause mitochondrial motility arrest. This reduction of the stationary mitochondria pool in neurons may alter spatiotemporal ATP dynamics, especially at the synapse upon ketone body utilization. Our data suggest that when O-GlcNAcylation is upregulated pharmacologically by TMG treatment, it overrides the ketone body dependent mitochondrial motility and enhances the stationary mitochondrial pool in neurons.

O-GlcNAcylation transforms network spiking patterns

Synaptic proteins and their synaptic transmission activities are heavily regulated by O-GlcNAcylation (Alfaro et al., 2012; Trinidad et al., 2012). For example, manipulating O-GlcNAcylation levels in vivo alters both LTP and LTD in the hippocampus, partially owing to its effect on AMPA receptor trafficking in excitatory synapses (Taylor et al., 2014; Yang et al., 2017; Hwang and Rhim, 2019; Stewart et al., 2020). However, it still needs to be elucidated how O-GlcNAcylation modulates excitatory synaptic transmission at the molecular level, especially in the context of glutamate metabolism.

Our preliminary data from metabolite abundance calculations (Figure 3.1) strongly indicates OGT's role in rewiring amino acid metabolism and altering their abundance to support upregulated neuronal functions. Consistent with previously published O-GlcNAcome studies (Lee et al., 2020; Trinidad et al., 2012), our proteomics data also indicates that subunits of all ionotropic and metabotropic glutamate receptors are O-GlcNAc modified (data not shown). Alterations of glutamate abundance, combined with the role of O-GlcNAcylation in glutamate receptor regulation, suggest tight collaboration between neuronal O-GlcNAcylation and excitability. We hypothesized that O-GlcNAcylation upregulates glutamate metabolism in the presence of glucose flux, which may facilitate higher excitability of neurons; this hypothesis requires further investigation.

To directly measure how O-GlcNAcylation alters the spontaneous firing rate of neurons, we utilized microelectrode array (MEA) recordings (Gerber et al., 2021). This system allowed us to culture hippocampal neurons on electrode-coated plates, which can form a neuronal network with spontaneous firing ability. After 13 DIV, we first recorded the spontaneous firing rates of neurons captured by each electrode. There were no changes in spontaneous activity in individual

firing rates. When we stimulated neurons, we detected an increased range of network burst duration upon TMG treatment. Compared to the control, TMG-treated neurons fired more robustly in response to electrical stimulation and displayed increased network burst durations as well as mean inter-spike interval within network bursts (Figure 3.3). These data indicate that global increase in O-GlcNAcylation by the OGA inhibitor TMG treatment primes neurons for efficient firing activity. Although more investigations are needed, our preliminary data suggest that O-GlcNAcylation can reshape neural networks activity and promote more robust synchronous firing.

CONCLUDING REMARKS

Our results indicate that substrate-specific regulation of synaptic energy supply may alter neuronal firing properties via O-GlcNAcylation (Figure 3.4). When neurons use glucose as the major fuel source, O-GlcNAcylation captures mitochondria at the glucose rich pre-synaptic boutons. Furthermore, O-GlcNAc modification of mitochondrial proteins promotes ATP synthesis to sustain synaptic activity, as discussed in Chapter 2 (Figure 2.13). In addition to ATP, we propose that O-GlcNAcylation plays a role in glutamate metabolism. Thus, O-GlcNAcylation supports excitatory neurotransmission by regulating both ATP and glutamate levels in neurons.

Under starvation conditions, neurons utilize ketone bodies as an alternative fuel source. We demonstrated that unlike glucose metabolism, mitochondrial motility persists when ketone bodies are used as a fuel source. This difference in mitochondrial motility may cause less local ATP availability at the synapse, especially at the presynaptic sites. Reduction of glucose levels also decreases O-GlcNAcylation (Ansari and Emerald, 2019; Pinho et al., 2018), which may lead to alterations in glutamate levels. A ketogenic diet has profound effects on reducing neuronal

excitability and epileptic seizure. Our results may provide mechanistic insight into how ketone body utilization by regulating mitochondrial O-GlcNAcylation directly impacts neuronal activity.

Materials and methods

Stable isotope tracing treatments of neuronal cultures and metabolite extraction/analysis: Rat cortical neurons were isolated from the E18 rat (Envigo) embryos and plated at a density of 1-2 × 10^5 cells/cm^2 on 6-well plates coated with 20 μg/mL poly-L-lysine and 3.5 μg/mL Laminin. Neuron cultures were maintained in Neurobasal medium supplemented with B27, GlutaMAX, and penicillin/streptomycin for 12 days in vitro (DIV). For metabolite tracing experiments, 2 μM OGA inhibitor TMG was applied 4 hours before replacing the culture medium with the medium containing stable isotope tracers [U- $^{13}C_6$] glucose and/or [U-$^{13}C_4$] β-hydroxy-butyrate substrates. For metabolite tracing experiments, neuronal maintenance media contained 5mM glucose, 2mM BHB, and 0.22mM pyruvate as substrates either with or without the ^{13}C tracers as indicated in Figure 3.1. The neurons were cultured in medium containing specific metabolite tracer for 20 additional hours to ensure isotopic label incorporation. Metabolite extraction was performed on DIV 13 as described previously (Cordes and Metallo, 2019; Divakaruni et al., 2017). Briefly, 6-well plates containing cultured neurons were rinsed with ice-cold 0.9% (wt/vol) NaCl solution. Then ice-cold methanol containing 1 μg of Norvaline (as an internal standard of metabolites) was added to as an extraction solvent. After a 1-2 min incubation period, each well containing the neurons was scraped with cell lifter and collected into 1.5 mL tubes with interlocking cap. After the addition of 500 μL ice-cold chloroform, each tube vortexed for 5 minutes. Then samples were centrifuged at 10,000xg for 6 min at 4 °C. Only upper methanol / H_2O layers were collected for the polar metabolites, which were transferred to GC/MS sample vials to evaporate liquids for further MOX-TBDMS derivatization for GC-MS processing. The samples were stored at -80 ^0C and shipped on dry ice for GC-MS analysis by the Dr. Ajit Divakaruni's laboratory at University

of California, Los Angeles. The MPE of the isotopes were calculated as the percentage of all atoms within the metabolite pool as described previously (Divakaruni et al., 2017).

Live cell imaging of neurons cultured with different nutrients and mitochondrial motility analysis: Hippocampal neurons were isolated from the E18 rat (Envigo) embryos as previously described, and plated on coverslips coated with 20 μg/ml poly-L-lysine and 3.5 μg/ml Laminin at a density of 5-7 × 10^4 cells/cm^2 (Nie and Sahin, 2012). Neuron cultures were maintained in Neurobasal medium containing 5mM glucose, supplemented with B27, L-glutamine and penicillin/streptomycin for 12 days in vitro (DIV). 13 DIV hippocampal neurons were transfected with Mito-DsRed using Lipofectamine 2000 and imaged 2 days after. Neuronal cultures were established in media containing 5mM glucose. 24 hours prior to imaging, culture media was replaced with 1mM glucose-containing medium. Before the live-cell imaging experiments, neurons were pretreated for 2 hours with 1mM glucose, 5mM glucose, 1mM glucose with 4mM BHB-containing medium. For the conditions containing OGA inhibitor TMG, the TMG treatment began when the initial medium change to 1mM glucose was conducted. For the live cell imaging, neurons were transferred to a Hibernate E (BrainBits) medium containing the same composition of glucose and BHB. The time-lapse movies were acquired on the Zeiss LSM 780 confocal microscopy system equipped with a temperature-controlled stage at 37 °C and with C-Apochromat 40x/1.20 W Korr FCS M27 objective. Images were acquired every 5 seconds. A custom-made Image J macro "Kymolyzer" was used to analyze time-lapse movies as described previously for kymography-based mitochondrial motility tracking (Basu et al., 2020). Briefly, kymographs were generated from selected neuronal axons, and motility parameters were calculated based on

manually drawn traces on the kymographs. Velocities smaller than 0.05 μm/sec were considered zero. The "percent time spent in motion" values were calculated for each traced mitochondrion.

Neuronal plating and activity acquisition on an MEA plate: MEA plates (Axion Biosystems) were coated with 0.1% polyethylenimine (PEI, Sigma-Aldrich) in borate buffer 24 hours. Specifically, 10 μL droplet of PEI coating solution was applied on MEA electrode area on MEA plate and incubated for 1hr at 37 °C. The coating solution was washed four times with 200 μL sterilized ddH_2O and dried overnight in a biosafety cabinet. Two hours before the neuronal plating, 20 μg/mL of Laminin in Neurobasal medium was applied by 5 μL droplet on MEA electrode area as a secondary coating. The plate was incubated for two hours at 37 °C while checking every 30 minutes to prevent evaporation to preserve Laminin droplet on MEA electrode area, and autoclaved ddH_2O was added to the area surrounding the MEA reservoir to as needed to provide humidified environment. Primary hippocampal neurons were isolated from the E18 rat (Envigo) embryos as previously described at a density of 1.6×10^7 cells/mL (= 40,000 cells/5 μL). After removing Laminin droplet, 5 μL of the neuron suspension was applied onto MEA electrode area. The plate with seeded neurons were incubated at 37 °C, 5% CO_2 incubator for an hour. Then, additional 200 μL of neuronal maintenance medium was applied gently in each well to not to disrupt the adhered neurons on MEA surface. Additional 300 μL of maintenance medium was applied again to reach the total volume of 500 μL in each well. The neurons were then incubated for 12 days in vitro with media change every three days. A day before the recording, the neurons were treated with 2 μM TMG or DMSO (Control) overnight. On DIV12, neuronal activity recording was performed with the Maestro Edge MEA and Impedence system (Axion Biosystems). For neuronal stimulation, an electrical pulse of 400 AP, 500 mV, 50 μA max current was applied

every 7 seconds from the stimulation electrode at the bottom right corner of MEA. The acquired data were further analyzed with AxIS Navigator software (Axion Biosystems). With the software, mean firing rate, burst frequency, network burst frequency, and synchrony index were analyzed.

Figures

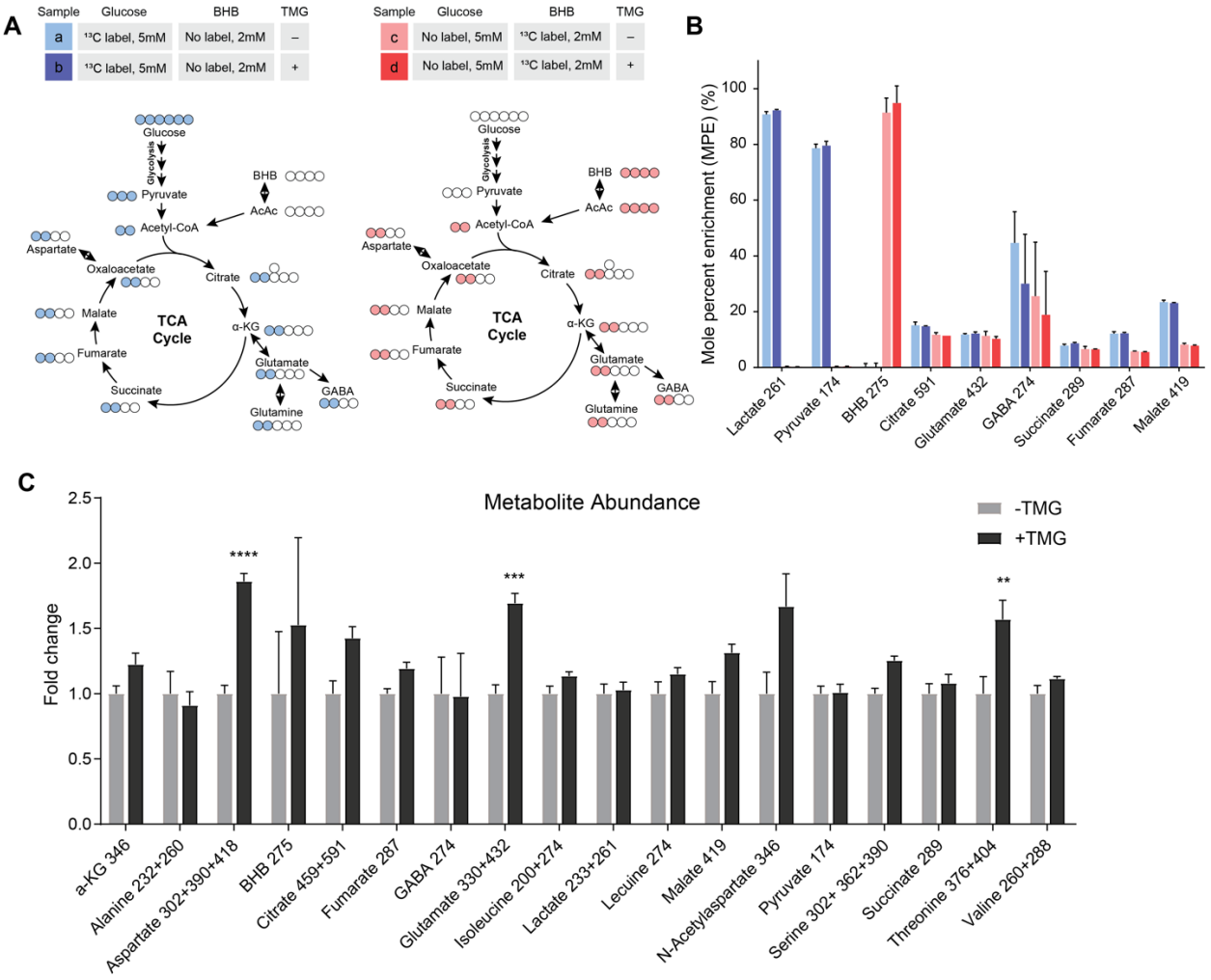

Figure 3.1 Alterations of neuronal fuel preference and metabolite level via O-GlcNAcylation.

(A) Table of summarizing the neuronal culture media composition, and their incorporation routes into the TCA cycle. **(B)** Percentage of each metabolite labeled with [^{13}C] glucose or BHB as indicated in (A). N=3 technical replica per each condition. **(C)** Total metabolite abundance from control or TMG treated samples. N=6 technical replica per each condition, from 1 independent primary neuron culture. **P < 0.01, ***P < 0.001, and ****P < 0.0001; Sidak's multiple comparisons test. All bar graphs represent mean values ± SEM.

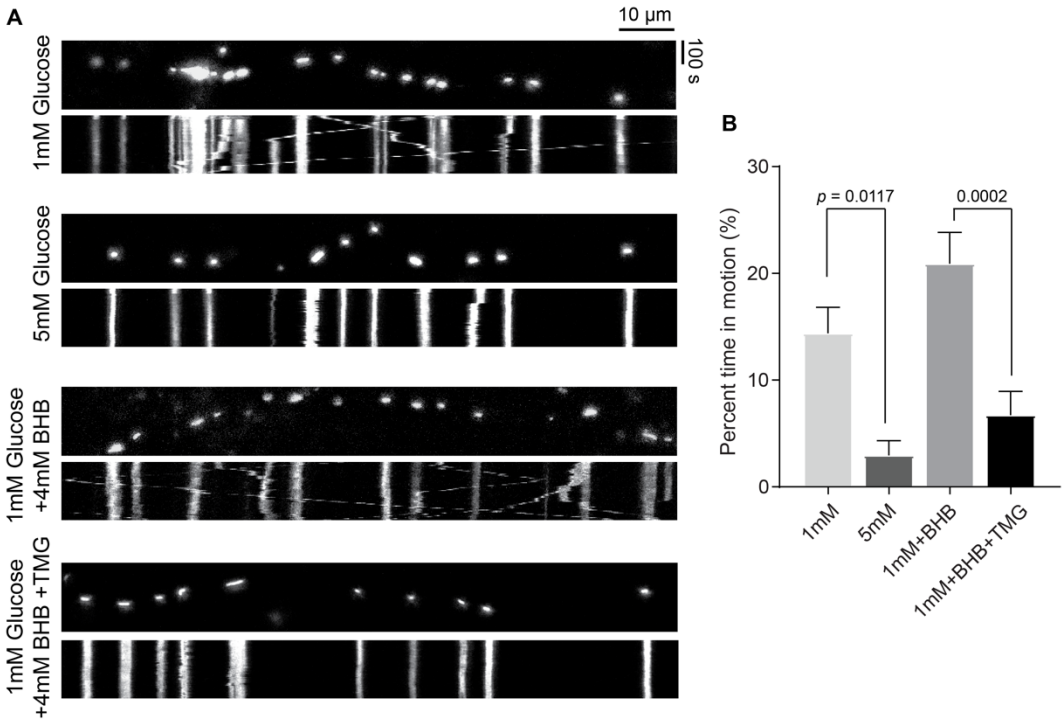

Figure 3.2 Ketone body utilization promotes mitochondrial motility while glucose causes motility arrest.

(A) Hippocampal neurons were transfected with Mito-DsRed for 2 days and treated with indicated conditions for 2 hours. To assess the effect of different nutrients on mitochondrial motility, live-cell imaging was performed for 3-5min. Selected axonal regions containing mitochondria and associated kymographs were illustrated together. **(B)** Percentage of time mitochondria spent in motion was calculated from kymographs. Bar graphs represent mean values ±SEM with indicated p-values computed from a non-parametric one-way ANOVA test with post hoc Kruskal-Wallis multiple comparison test. N=45-130 individual mitochondrial motility from 8-10 axons, from 3 independent neuronal dissections.

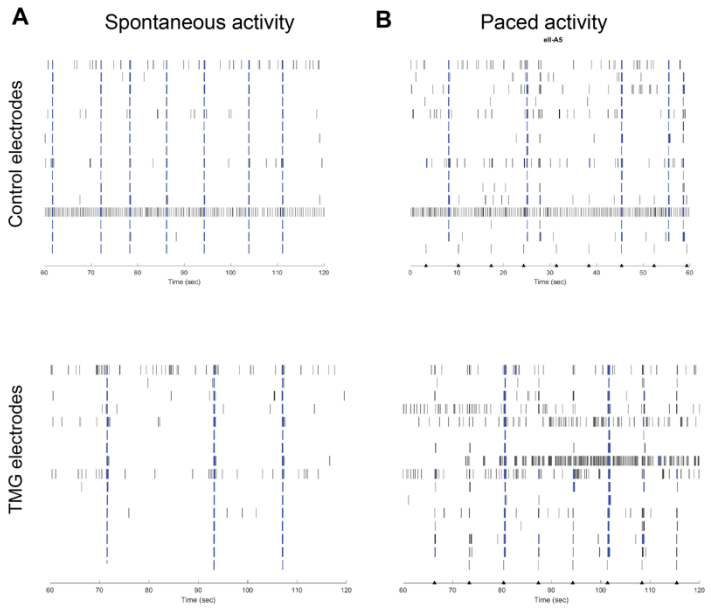

Figure 3.3 Representative neuronal activity recording and spike events recorded by microelectrode array.

(A) Spontaneous spike and burst patterns from Control (top) and TMG treated (bottom) cultured hippocampal neurons on MEA plates. **(B)** Neurons, cultured on MEA plate were stimulated every 7 seconds, as indicated with black arrowheads on the X-axis. Post-stimulation (400 AP, 500 mV) spike patterns from Control (top) and TMG treated (bottom) cultured hippocampal neurons on MEA plates.
N=8 separate wells for each condition from one independent neuronal dissection.

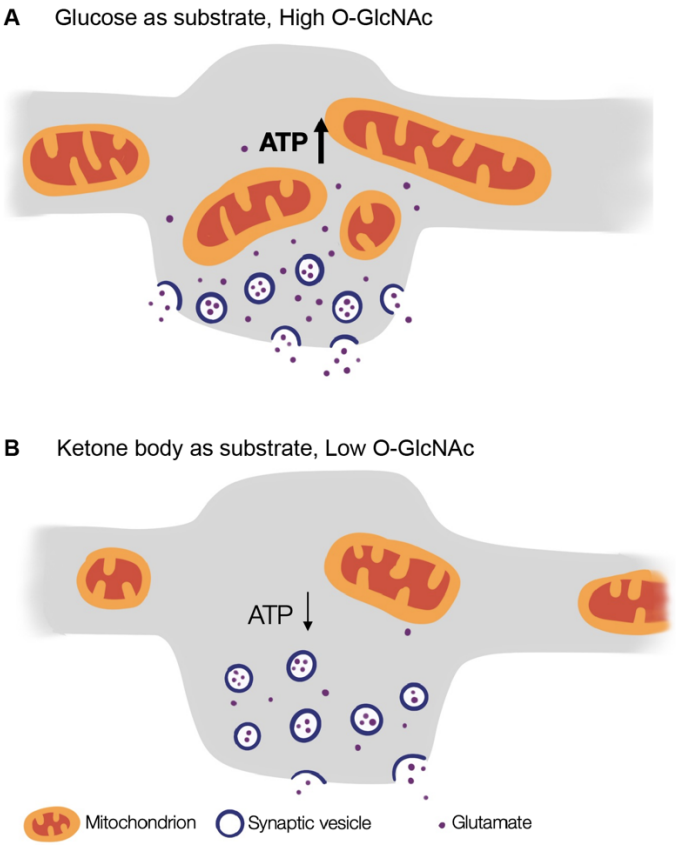

Figure 3.4 Working model of synaptic excitability in neurons fueled by glucose or ketone bodies.

Mitochondria and metabolism-centric hypothetical model demonstrates why ketone body utilization causes less excitability in neurons, and the role of O-GlcNAcylation. **(A)** When neurons are exposed to an abundant amount of glucose, O-GlcNAcylated mitochondria stop at glucose enriched regions such as pre-synaptic boutons, providing more ATP as well as amino acids like glutamate. More ATP and glutamate availability leads to synapses that can fire more efficiently. **(B)** When neurons are starved of glucose, they seek alternative fuel, such as ketone bodies. Less O-GlcNAcylation mobilizes mitochondria, which causes less local ATP and glutamate that can readily be used. This would result in overall less excitability for neurons.

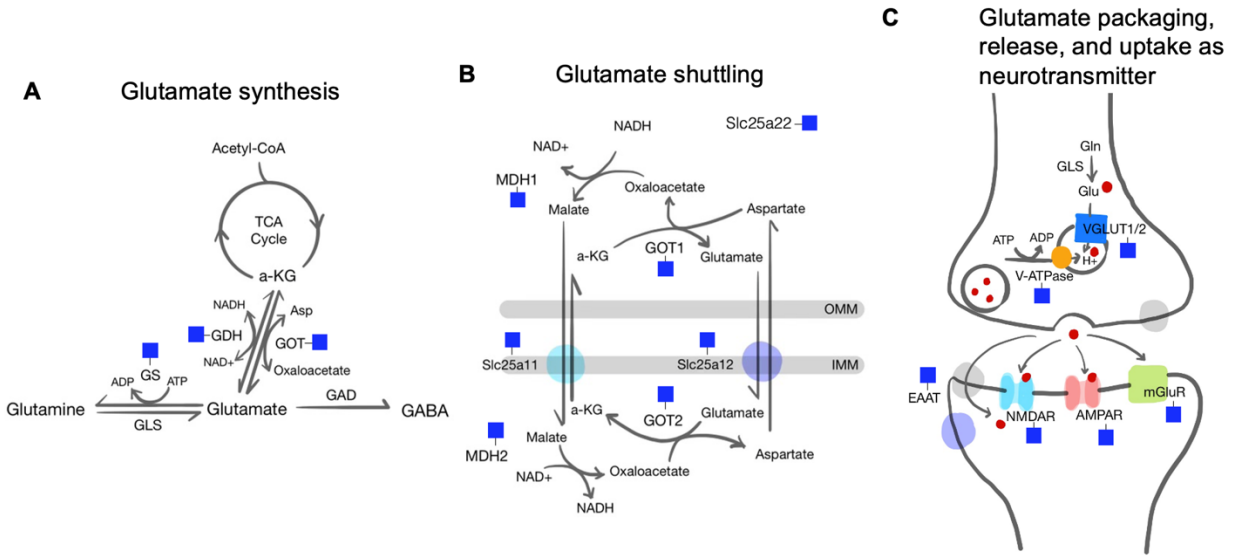

Figure 3.5 O-GlcNAcylated proteins involved in glutamate metabolism.

Representative pathways involved in glutamate synthesis **(A)**, shuttling of glutamate between cytoplasm and mitochondria (malate aspartate shuttle) **(B)**, and glutamate as a neurotransmitter **(C)** are demonstrated. Proteins/complexes identified as O-GlcNAcylated (from Chapter 2 proteome data or previous publications) are indicated with blue square (universal symbol for O-GlcNAc modification) (Clark et al., 2008; Lee et al., 2020; Ma et al., 2016, 2015; Wu et al., 2017).

Acknowledgements

Chapter 3 contains unpublished material coauthored with Ajit S. Divakaruni and Gulcin Pekkurnaz. The dissertation author was the primary investigator and author of this chapter.

Author contributions

Conceptualization: S.B.Y., G.P.; Methodology: S.B.Y., A.S.D, and G.P.; Data acquisition and analysis: S.B.Y., A.S.D.; Supervision: G.P.; Funding acquisition: A.S.D. and G.P.

CHAPTER 4: ROLE OF SIRTUIN 5 IN CROSSTALK BETWEEN TWO POST TRANSLATIONAL MODIFICATIONS

INTRODUCTION

There are multiple metabolic sensor enzymes that regulate cellular signaling pathways in addition to OGT and O-GlcNAcylation. The major metabolic sensor enzymes include: mammalian target of rapamycin (mTOR), AMPK, Phosphoinositide 3-kinase(PI3K), Protein kinase B family (Akt), and Sirtuins (SIRTs) (Houtkooper et al., 2012; Pillai et al., 2014; Sadria and Layton, 2021). While a known and well-established regulator of OGT's activity is nutrient flux through the hexosamine pathway, there is also evidence that other metabolic sensor enyzmes, such as mTOR and Akt, can alter OGT's activity. It has been thought that regulators are important for OGT's bias towards specific substrate groups, however mechanistically, little is known. OGT also has been shown to regulate mTOR, AMPK, and PI3K activity as well as intracellular distribution. Together, close collaboration of multiple metabolic sensing pathways maintains cellular homeostasis.

One of the SIRT family members, SIRT5, is identified in our mitochondrial O-GlcNAcome (Figure 2.11). Sirtuins are mammalian homologs of the yeast protein Silent information regulator 2 (Sir2), which are indicated in both lifespan expansion and metabolic regulation. The whole family of Sirtuin is characterized by its activation with caloric restriction and usage of NAD+ as a substrate. Amongst them, SIRT5 is one of three Sirtuin family proteins that are predominantly localized in mitochondria (Houtkooper et al., 2012; Ji et al., 2022). SIRT5 functions as NAD+-dependent deacylase that specifically removes acyl (succinyl, malonyl, and glutaryl) groups from lysine residues of proteins, whereas its deacetylation activity is fairly limited (Du et al., 2011; Hirschey and Zhao, 2015). Its target proteins are mainly found in the liver: ketogenic enzymes, glycolytic enzymes, and ETC subunits, encompassing a myriads of pathways (Park et al., 2013;

Rardin et al., 2013; Nishida et al., 2015). In the brain, SIRT5 is highly expressed in neurons and affects multiple metabolic pathways downstream of PKC signaling and plays a neuroprotective role under ischemic conditions (Koronowski et al., 2018; Morris-Blanco et al., 2016). Although it has extensive roles, there are a finite number of studies on how SIRT5 and related PTMs affect the central nervous system. Our goal was to reveal how SIRT5 activity is modified by O-GlcNAcylation and how this modification alters SIRT5-mediated neuronal metabolism regulation.

RESULTS

SIRT5 is O-GlcNAc-modified

To validate SIRT5 O-GlcNAcylation biochemically, we expressed HA-tagged human SIRT5 in HEK293T cells. The ectopic expression of the tagged SIRT5 allowed us to perform immunoprecipitation with an HA-tag and evaluate O-GlcNAc level with anti-O-GlcNAc (RL2) antibody (Figure 4.1A-B). Under baseline state, we observed minimal amount of O-GlcNAc modified SIRT5. Blocking the OGA enzyme with TMG treatment overnight caused ~2 fold increase in SIRT5 O-GlcNAcylation, specifically in HEK293T cells. To further ensure the protein is detected and O-GlcNAcylated in other cell types, all O-GlcNAcylated proteins were pulled down with anti-O-GlcNAc antibody (RL2), then probed with SIRT5 (Figure 4.1C). The change in O-GlcNAcayltion level with TMG was minimally detected on endogenous SIRT5 Intriguingly, in INS1 cells, when we used sWGA bead to capture endogenous O-GlcNAcylated SIRT5 protein (as described in Chapter 2), glucose stimulated conditions (Shum et al., 2022) displayed noticeably higher O-GlcNAcylation of SIRT5 (Figure 4.1D).

To test whether the expression level or subcellular location of SIRT5 is altered via O-GlcNAcylation, we purified mitochondria from the neurons treated with or without TMG (Figure

4.2A-B). Increasing O-GlcNAcylation with TMG did not cause any change in SIRT5 protein level or subcellular location. This result was also confirmed by immunostained COS7 cells, which displayed mitochondrial localization of SIRT5 under both conditions (Figure 4.2C).

SIRT5 alters cellular metabolism

We transiently expressed SIRT5 in various cell types and evaluated its impact on mitochondrial respiration. First, we confirmed the mitochondrial localization of ectopically expressed HA-tagged SIRT5. In neurons, SIRT5 overexpression did not induce significant changes in mitochondrial morphology and density in neuronal processes (data not shown). The same trend was also observed in COS7 cells, where mitochondria retained similar distribution, mass, and morphology (Figure 4.3A). Then we moved onto overexpressing SIRT5 in HEK293T cells and examined their metabolic changes via Seahorse metabolic flux analyzer. Despite having similar mitochondrial morphology, when expressed in HEK293T cells, SIRT5 caused an increase in basal cellular respiration, measured by oxygen consumption rate. Upregulation of O-GlcNAcylation with TMG treatment blocked this SIRT5-dependent increase (Figure 4.3B). Glycolysis, measured by extracellular acidification rate, displayed almost no change under both conditions. These results led us to conclude that global upregulation of O-GlcNAcylation has an inhibitory effect on SIRT5 activity. The target substrates of SIRT5 responsible from enhanced mitochondrial respiration is yet to be elucidated.

O-GlcNAcylation and succinylation crosstalk by SIRT5

As mentioned above, SIRT5 removes succinyl, malonyl, and a limited number of acetyl groups from its target proteins. Although ubiquitously expressed in every cell, SIRT5 activity

varies, thus acyl-modified protein composition varies across cell types and tissues. SIRT5 deficiency, in the knock-out mouse model, causes enhanced succinylation level in the brain, (Nishida et al., 2015). In the subcellular level, succinylation was highly enriched in mitochondria in contrast to malonylation and acetylation. Therefore, we hypothesized that suppression of SIRT5 activity via O-GlcNAcylation may alter succinylation of neuronal mitochondria.

To test our hypothesis, we cultured hippocampal neurons on microfluidic devices to be able to sparsely immunolabel axonal mitochondria with mitochondrial marker Mito-tracker green, anti-O-GlcNAc, and anti-lysine-succinylation (K-succ) antibodies. Our results confirmed that lysine-succinylation, similar to O-GlcNAcylation, is enriched on mitochondria (Figure 4.4A). Although the staining patterns displayed some differences, overall succinylation and O-GlcNAcylation intensity increased in response to TMG treatment (Figure 4.4B-C). We also examined succinylation and O-GlcNAcylation patterns in cortical mouse brain slices that have gone through the feeding-fasting regime as demonstrated in Figure 4.5A. Both O-GlcNAcylation and succinylation in cortical neurons followed the blood glucose level trend—downregulated with 24 hours of fasting, then increased with 24 hours of refeeding (Figure 4.5B-C). These results indicate the possible co-regulatory mechanism of succinylation and O-GlcNAcylation in the mammalian brain for the first time.

CONCLUDING REMARKS

Our preliminary results suggest O-GlcNAcylation exerts an inhibitory role on SIRT5 activity. The inhibition of SIRT5's desuccinylase activity may mediate the upregulation of succinylation in response to nutrient availability and enhanced O-GlcNAcylation in neurons. More studies are required to identify the O-GlcNAc modification sites for SIRT5 to elucidate the

molecular mechanism underlying the SIRT5 activity change. It is known that SIRT5 activity is regulated by the NAD+ level. Typically, NAD+ levels are augmented by glucose deprivation and caloric restriction—the conditions where O-GlcNAcylation is expected to be reduced (Cantó et al., 2015, 2010; Fulco et al., 2008). This may imply an interplay between O-GlcNAcylation and NAD+ level that eventually signals SIRT5 of nutrient status of the cell. The physiological implications of the potential crosstalk between the two PTMs will be further discussed in Chapter 5.

Materials and methods

Immunoprecipitation of SIRT5 for O-GlcNAcylation analysis:

Experiments with ectopically expressed SIRT5 in HEK293T cells: HEK293T cells were plated in 6-well plate at the density of 6×10^5 cells per well and cultured in DMEM media containing 5mM, 10% FBS, L-glutamine and penicillin/streptomycin. A day after plating, the cells were transfected with HA-tagged human SIRT5 plasmid using calcium phosphate transfection method. 48hours after transfections, cells were lysed with lysis buffer described in Chapter 2 and immunoprecipitations were performed as previously described (Pekkurnaz et al., 2014). Briefly, the cell lysates were tumbled together with anti-HA antibody (Roche) for 2 hours at 4 °C, followed by 1 hour tumbling with protein A Sepharose beads (GE Healthcare). The tumbled beads were then washed 3-4 times with the lysis buffer. Then the beads were resuspended in 4x Laemmli buffer with lysis buffer to make final concentration of 1x Laemmli. The beads with Laemmli buffer were boiled at 100 °C for 5 min to elute immunoprecipitated proteins, then analyzed by quantitative western blot.

Experiments with endogenous SIRT5 in HEK293T and Neuro2A cells: Both HEK293T cells and Neuro2A cells, cultured on 6-well plates as described above in DMEM containing 5mM glucose, and treated with or without TMG a day before the immunoprecipitation. After reaching 80-90% confluency, cells were lysed and immunoprecipitations were performed with anti-O-GlcNAc antibody (RL2), that specifically targets O-GlcNAcylated proteins.

Endogenous SIRT5 in glucose stimulated INS1 cells: INS1 cells were cultured in RPMI1640 medium supplemented with 5mM glucose until the day of experiment. Glucose stimulation for insulin secretion (GSIS) was utilized to induce insulin secretion for INS1 cells. Prior to GSIS, INS1 cells were culture in 2mM glucose in RPMI medium without serum for 2

hours. The culture medium was washed and incubated for 30 min in DMEM (XF assay medium for Seahorse Biosciences), containing 2mM glucose, 0.05% BSA, at pH 7.4. Then for GSIS, the cell culture medium was further changed to and incubated for 15 min in 16.7mM glucose in XF Seahorse DMEM medium (For control, 2mM glucose in XF Seahorse DMEM was used), containing 0.05% BSA. After GSIS, the cells were lysed and O-GlcNAcylated proteins were pulled down with sWGA beads as described in Chapter 2, then analyzed by quantitative western blot.

Plating of transfected HEK293T cells for Seahorse metabolic flux assay: HEK293T cells were transfected two days before the assay using the calcium phosphate method and incubated overnight at 37 °C, 5 % CO_2 incubator. Seahorse XF96 Cell Culture Microplates (Agilent) was coated with 40 μg/mL poly-L-lysine at room temperature overnight. After the overnight incubation, HEK293T cells were trypsinized, counted, and plated at density of 5×10^5 cells/mL (=40,000 cells / 80 μL). The plate with the HEK293T was centrifuged at 1000 xg at 5 min to pull down and adhere the cells at the bottom of the plate. The centrifuged plate was incubated for 2 hours at 37 °C in 5 % CO_2 incubator, then additional 120 μL of DMEM medium supplemented with FBS and Pen/Strep was added to each well. Pre-treatment of DMSO (Control) or 2 μM TMG was applied at this point. On the day of experiment, Seahorse XF Cell Mito Stress Test was carried out as described in Chapter 2.

Hippocampal neuron culture experiments with microfluidics: Hippocampal neurons were prepared as described in Chapter 2. But instead of plating them directly on coverslips, microfluidic devices (Xona microfluidics, Durham, NC) were utilized to separate axonal processes and

somatodendritic regions of neurons (Pekkurnaz et al., 2014; Taylor et al., 2005). First, round coverslips with diameter of 25mm were coated with 20 μg/mL poly-L-lysine (PLL, Sigma-Aldrich) and 3.5 μg/mL Laminin (Life Technologies) overnight in 6-well plate. After washed twice with ddH_2O, the coverslips were air-dried until completely dry, then the microfluidic devices were attached onto the coated surface of coverslips tightly. To ensure that medium was flowing through chambers, Neurobasal medium supplemented with L-glutamine, penicillin/streptomycin (PSG, Life Technologies) was pipetted through chambers several times before plating the cells. Subsequently, 1×10^6 cells in 50 μL of Neurobasal media supplemented with PSG were pipetted into the "somatodendritic" side of the microfluidic device, leaving the other side of the chamber empty for axonal growth. The plated cells were incubated in a tissue culture incubator (5 % CO_2, 37 °C) for 10 min to make sure the neuros were attached. Then, more maintenance medium (Neurobasal with B27, GlutaMAX, and PSG) was pipetted simultaneously into both chambers to fill the whole device. After making sure neurons were stably placed inside the plated chamber, they were put into the cell culture incubator for DIV 7-10. The maintenance medium was exchanged with new medium every 3 days. Immunostaining with indicated antibodies was performed as described in Chapter 2.

Feeding and fasting of animals for immunohistochemistry: Age matched (8-10 weeks old) male/female C57Bl/6J mice were housed using 12h light/dark cycles with ad libitum access to standard chow diet and water. The care of animals and diet change protocols were approval by the University of California San Diego Institutional Animal Care and Use Committee. For fasting and refeeding experiments, food access was removed for 24 hours and replaced. Before tissue collection, blood samples were collected from tail vein to perform glucose measurements. For

tissue harvesting, the mice were anesthetized with isoflurane (MWI Veterinary) then transcardially perfused with cold phosphate-buffered saline (PBS) followed by 4% paraformaldehyde (PFA) in PBS. The brains were post-fixed in 4% PFA, dehydrated, sliced and stained as described in Chapter 2.

Figures

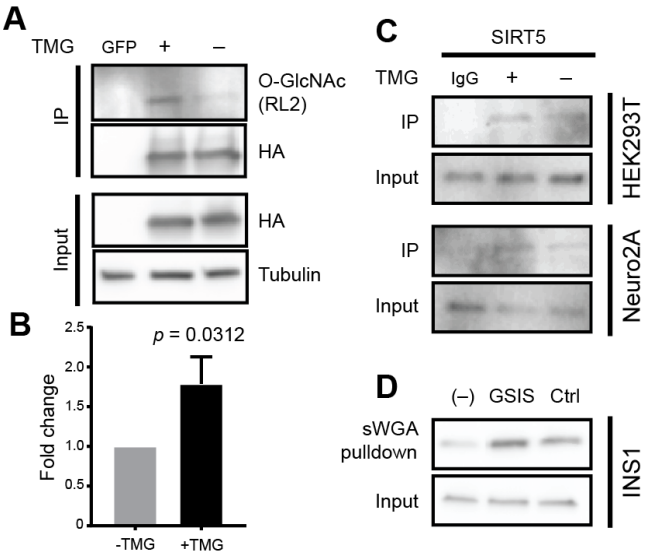

Figure 4.1 Regulation of SIRT5 O-GlcNAcylation.

(A-B) Regulation of SIRT5 O-GlcNAcylation in HEK293T cells. Cells were transfected HA-tagged SIRT5, and treated as indicated. HA-SIRT5 was immunoprecipitated with Anti-HA antibody from cells treated with or without 2 μM TMG. The band intensities were quantified in the linear range, and intensity of each GlcNAc band was normalized to the intensity of HA bands. GlcNAc level was set to 1 in untreated cells, and fold change was calculated. N=5, p value was determined from Wilcoxon matched-pairs signed rank test. **(C)** Regulation of endogenous SIRT5 O-GlcNAcylation. Immunoprecipitation was performed with anti-O-GlcNAc antibody (RL2) from HEK293T cells and Neuro2A cells, and blots were probed with Anti-SIRT5 antibody (N=2). **(D)** Probing of endogenous SIRT5, after enrichment of O-GlcNAcylated proteins with sWGA beads. INS1 cells at normal (Ctrl) and Glucose-stimulated insulin secretion (GSIS) states. (-) indicates negative control for pulldown with free-floating GlcNAc moiety in the sample (N=3).

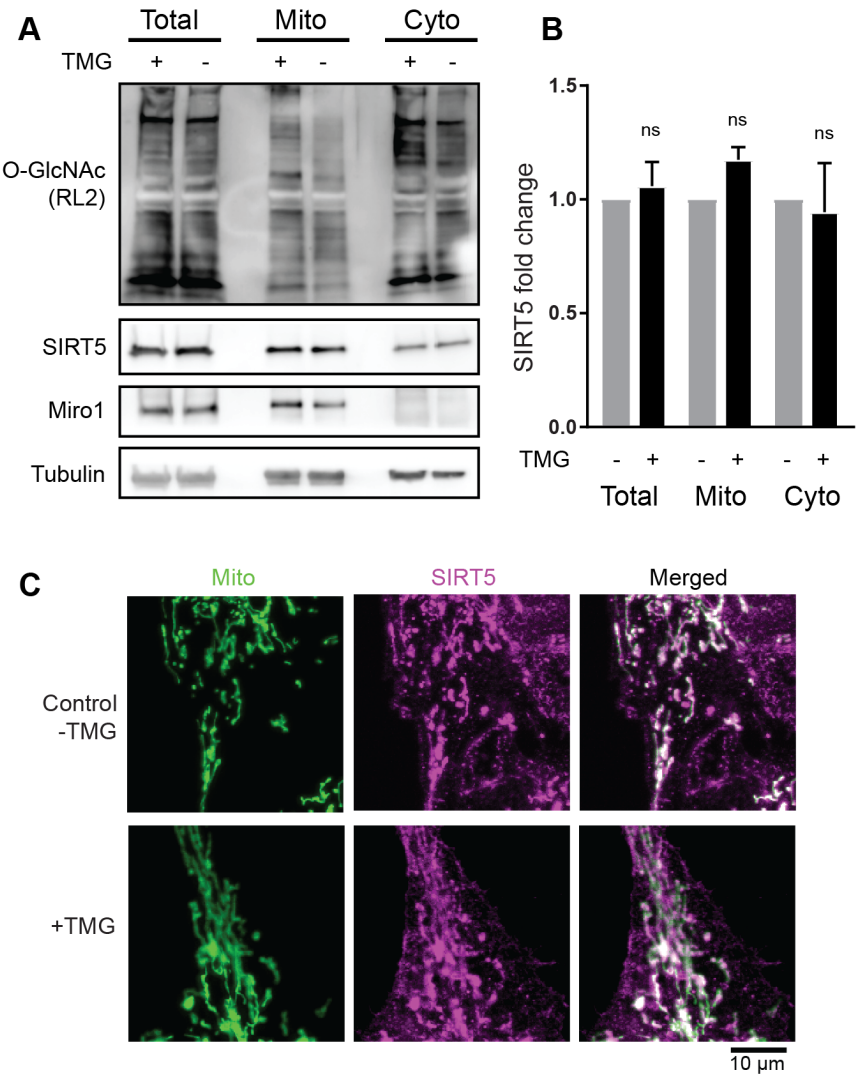

Figure 4.2 O-GlcNAcylation does not alter mitochondrial localization of SIRT5.

(A) SIRT5 and O-GlcNAcylated level of proteins probed from total cell lysate, and mitochondrial and cytoplasmic fractions isolated from cortical neurons. **(B)** The band intensities were quantified in the linear range with Anti-SIRT5, Anti-Miro (mitochondrial marker) and Anti-tubulin antibodies. The intensity of each SIRT5 band was normalized to the intensity of Miro for mitochondrial fractions and tubulin for cytoplasmic fraction and total cell lysate. SIRT5 levels in each fraction does not change with the TMG treatment in cortical neurons (Wilcoxon matched-pairs signed rank test. N=3-5 independent neuronal cultures). **(C)** Immunostaining of SIRT5 in COS7 cells, transfected with Mito-DsRed to also label mitochondria (with or without TMG treatments).

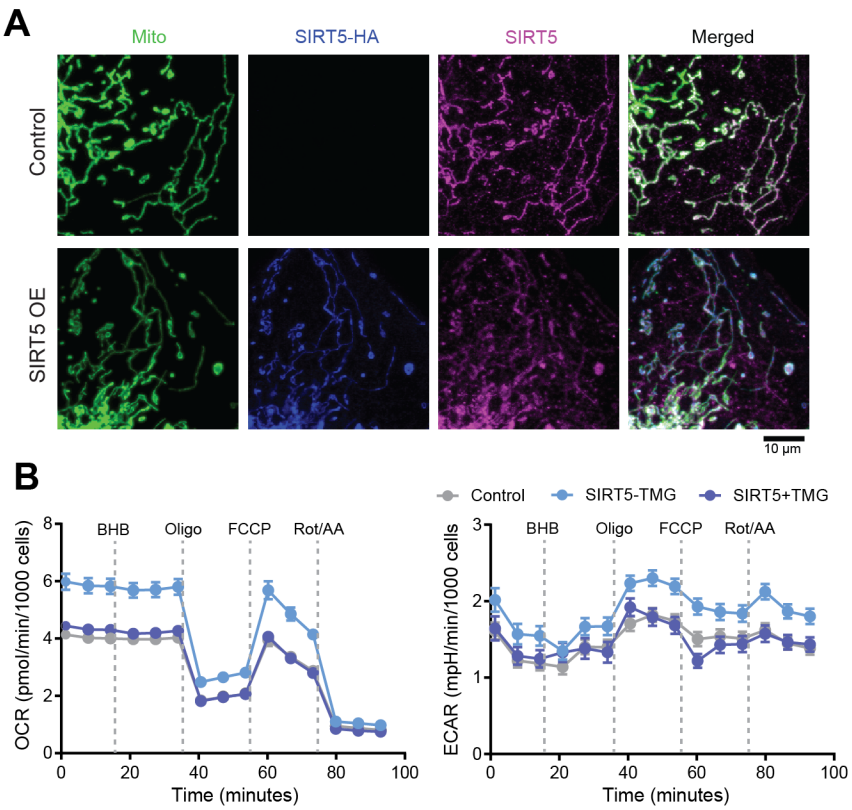

Figure 4.3 SIRT5 enhances mitochondrial respiration.

(A) Mitochondrial morphology and distribution in COS7 cells with endogenous or overexpressed SIRT5 levels. **(B)** Metabolic flux analysis showing HEK293T mitochondrial respiration and glycolysis changes with SIRT5 overexpression with or without TMG treatment. Oxygen consumption rate (OCR) and extracellular acidification rate (ECAR) describes mitochondrial respiration rate and glycolytic rate, respectively. Points in the graph represent mean values ± SEM of each measurement at given time point, with lines connecting all the points. N=14-18 wells per condition from three independent cultures.

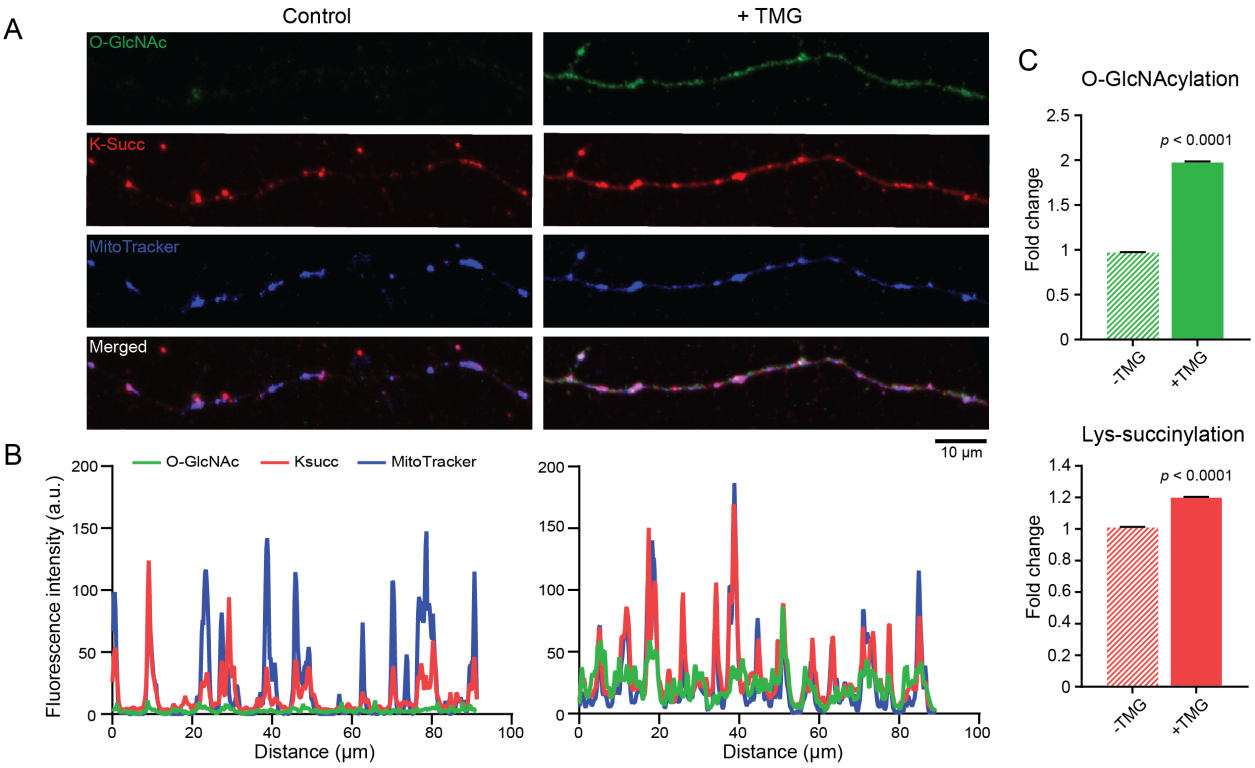

Figure 4.4 Upregulation of O-GlcNAcylation enhances succinylation level in neurons.

(A) Axonal mitochondria (MitoTracker) immunostained with Anti-O-GlcNAc and Anti-Lys-succinylation antibodies. **(B)** Intensity profiles of O-GlcNAcylation, succinylation and MitoTracker were plotted from the represented neuronal axon. **(C)** Quantification of O-GlcNAc and succinyl modifications per axonal mitochondrion. The bar graphs represent mean values ± SEM with indicated p-values calculated by y Mann-Whitney U test. N=9,747-14,933 individual axonal mitochondria from three independent neuronal dissections.

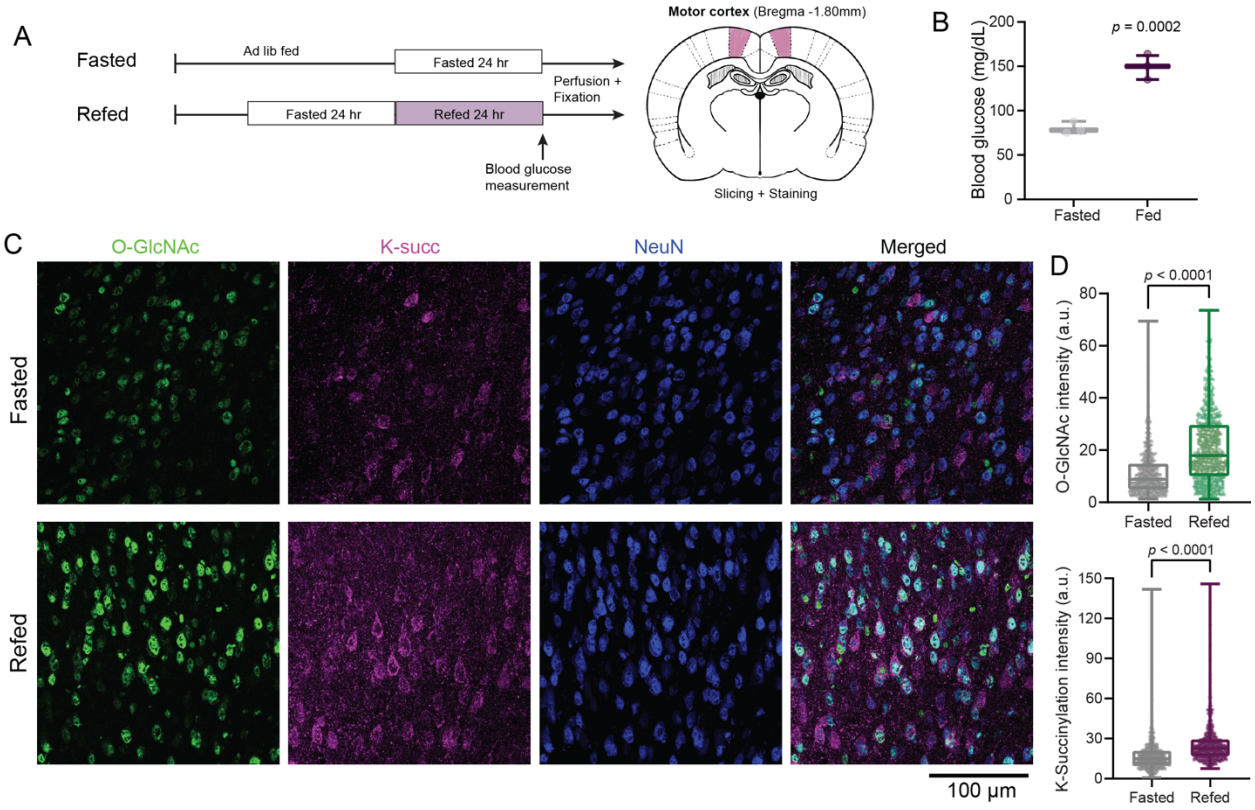

Figure 4.5 O-GlcNAcylation and succinylation levels mouse brain are altered by feeding.

(A) Scheme summarizing the mice fasting/feeding paradigm and the sample collection process. **(B)** Blood glucose level of animals after fasting for 24 hr and refeeding for 24hr. **(C)** Anti-O-GlcNAc and Anti-Lys-succinylation staining of the mouse motor cortex (specific coordinates are indicated) after the fasting/feeding. **(D)** Quantification of O-GlcNAc and succinyl modifications on NeuN-positive cortical neurons. All graphs were indicated as Min-Max plot with individual datapoints. Indicated p-values are computed by Mann-Whitney U test. N=671-776 neurons from three independent animals for each condition.

Acknowledgements

Chapter 4 contains unpublished material coauthored with Arlina de Lugo and Gulcin Pekkurnaz. The dissertation author was the primary investigator and author of this chapter.

Author contributions

Conceptualization: S.B.Y. and G.P.; Methodology: S.B.Y. and G.P.; Data acquisition and analysis: S.B.Y. and A.D.L.; Supervision: G.P.; Funding acquisition: G.P.

CHAPTER 5: CONCLUSIONS AND FUTURE DIRECTIONS

It is fundamental to coordinate energy consumption with nutrient availability to achieve metabolic homeostasis in cells. Metabolic signaling pathways such as AMPK and mTOR incorporate energetic stress signals into modulating cellular activities, eventually balancing the energy supply and consumption (Inoki et al., 2012). AMPK and mTOR both are kinases that convey the nutrient status to their downstream targets via phosphorylation. Hundreds of those protein targets are involved in myriads of metabolic pathways to be fine-tuned according to the nutrient status. Similar to these pathways, hexosamine biosynthetic pathway (HBP) allows glucose to act as a nutrient signaling molecule by converting glucose into the end product, UDP-GlcNAc. UDP-GlcNAc actively regulates post-translational modification (PTM) O-GlcNAcylation by altering OGT activity, which propagates the signal of glucose availability to its thousands of target proteins. Given the fact that over 8,000 proteins are regulated via OGT, O-GlcNAcylation emerged as another master regulator of nutrient sensing and a new promising therapeutic target for metabolic and neurodegenerative diseases (Bullen et al., 2014; Tan et al., 2017; Zhu and Hart, 2021).

Despite their crucial role in glucose sensing, only recently has the metabolic regulatory aspect of O-GlcNAcylation been shed light on. Especially over the last decade, studies emerged regarding O-GlcNAc-mediated regulation of neuronal synapses and how O-GlcNAcylation alters synaptic protein functions (Alfaro et al., 2012; Lagerlof et al., 2016; Lagerlöf et al., 2017; Rexach et al., 2012; Tallent et al., 2009; Taylor et al., 2014; Wheatley et al., 2019). However, these studies mainly used genetic or pharmacological manipulations of the two enzymes responsible for O-GlcNAc cycling; OGT and OGA. Such perturbations are far from representing physiological range of GlcNAc cycling in terms of timing and duration. Therefore, it is not surprising that nervous

system specific deletion of OGT causes early postnatal lethality and neurodegeneration (O'Donnell et al., 2004; Wang et al., 2016). It still remained inconclusive how O-GlcNAcylation is spatiotemporally regulated by neuronal activity until my thesis research. In my dissertation, I focused on the metabolic sensing role of O-GlcNAcylation in neurons. I have dissected out (1) how neuronal activity itself can modulate O-GlcNAcylation to support energy demand in Chapter 2, (2) the role of O-GlcNAcylation in mitochondrial fuel utilization in Chapter 3, and (3) how O-GlcNAcylation cross-talks with metabolic sensor enzyme SIRT5.

O-GlcNAcylation links neuronal activity and glucose metabolism

Glucose is the major fuel for the brain. Because the brain has limited glucose storage capacity, fluctuations of glucose levels cause cognitive decline and dysfunction (Ashrafi and Ryan, 2017; Bentsen et al., 2019; Yellen, 2018). Once glucose enters the cell through glucose transporters, the key pathway that allows glucose to also become a signaling molecule is HBP and O-GlcNAcylation. Our results (Figure 4.5) suggest that the O-GlcNAcylation level in the neurons follows the alterations in the blood glucose level based on the feeding state of the animal. Neurons maintain their O-GlcNAcylation level constantly, with small fluctuations to match the local needs (Akan et al., 2018; Ong et al., 2018; Yang and Qian, 2017). However, we showed that when neuronal activity is accelerated, the metabolic demands as well as the O-GlcNAcylation levels increase, especially during prolonged activities (Figure 2.1-2.2 and 2.4) and in response to acute electrical stimulations (Figure 2.7-2.8).

We reasoned that the increment in O-GlcNAcylation is the result of additional glucose flux triggered by neuronal activity. For neuronal activity to be sustained, more glucose is needed as fuel. It has already been demonstrated that glucose utilization can be boosted by kainic acid-

induced chronic activation, as well as transient electrical field stimulation (Frederick Wooten and Collins, 1980; Bak et al., 2009; Díaz-García et al., 2017). It was confirmed that the boost in glucose utilization is assisted by GLUT4-mediated glucose flux into the stimulated neurons (Ashrafi et al., 2017). Our data with the FBP sensor demonstrates that neurons enhance glucose utilization with neuronal activity (Figure 2.7A-D). Further experiments are necessary to connect glucose consumption through the HBP pathways to O-GlcNAc upregulation in stimulated neurons (Figure 2.7E-F). Currently, experiments with the inhibitor of fructose-6-phosphate-aminotransferase (GFAT) (the rate-limiting enzyme of HBP) are in the works to test whether blocking HBP alters downstream O-GlcNAcylation and the associated mitochondrial functions.

Glycolytic pathway regulation via O-GlcNAcylation

In addition to mitochondria, proteins in other subcellular compartments, including endoplasmic reticulum, lysosomes, and synaptosomes, are O-GlcNAc modified. Furthermore, our O-GlcNAcome data suggest that some key glycolytic proteins, including phosphofructokinase (PFK), glyceraldehyde-3-phosphate dehydrogenase (GAPDH), and enolase 1 (ENO1) (Figure 2.12C-D) are also substrates of OGT. These glycolytic enzymes are already verified to be O-GlcNAcylated, but are mostly studied in the context of cancer metabolism (Chiaradonna et al., 2018; Mueller et al., 2021). For example, O-GlcNAcylation of PFK at Serine 529 residue inhibits its activity and promotes the redirection of glucose metabolism to the pentose phosphate pathway (PPP) in cancer cells (Yi et al., 2012). While O-GlcNAcylation helps bypass the glycolytic pathway in the cancer environment, more studies are needed in neurons to confirm whether the modification sites and the functional modulations of the neuronal isoform of PFK are conserved. Unpublished data from our lab suggests that hexokinase1 (HK1) is O-GlcNAcylated, and this

modification accelerates glucose phosphorylation and glycolysis. In *Caenorhabditis elegans* (C. elegans), it has been demonstrated that axon regeneration depends on glycolysis as well as mitochondrial functions, and perturbation of O-GlcNAcylation halts the axons regeneration rate (Taub et al., 2018). Thus, it is also likely that other identified glycolytic enzymes are modified to support metabolic adaptations in neurons.

Further studies *in vivo* will also be important to capture dynamic neuronal O-GlcNAcome. It will be intriguing to identify both mitochondrial and glycolytic O-GlcNAcome from stimulated brain parts, such as those from KA injected hippocampus, compared to neurons in a normal, resting state. The results from such proteome would hint us better towards how glycolysis and mitochondrial proteome are coupled together by O-GlcNAcylation in highly activated neurons.

How does mitochondrial O-GlcNAcylation control ATP production?

We demonstrated that mitochondrial O-GlcNAcylation promotes ATP production. Our mitochondrial O-GlcNAcome data represent that electron transport chain complex (ETC) subunits including ATP synthase are O-GlcNAcylated (Figure 2.11E). Upregulation of mitochondrial O-GlcNAcylation enhances mitochondrial respiratory capacity (Figure 2.9C-E) and mitochondrial membrane potential $\Delta\Psi m$ (Figure 2.9A-B). Our results are consistent with the rat cardiomyocyte studies demonstrating TMG-mediated upregulation of O-GlcNAcylation promotes mitochondrial bioenergetics (Ma et al., 2015). Thus, it may be a conserved mechanism utilized by multiple cell types. Perhaps, O-GlcNAcylation of ETC subunits leads to more active pumping of protons by Complex I, III, and IV. It will work as (1) more potent reserve of proton gradient for ATP synthase that makes it (2) more likely to drive ATP^{4-} and ADP^{3-} exchange by adenine nucleotide transporters (ANT) due to its nature of net charge imbalance (Zorova et al., 2018). This prolonged

elevation of ΔΨm is an abnormal state achieved by chronic TMG treatment and we predict it may not be retained on a physiological time scale. Rather, with the transient electrical stimulation like in Figure 2.13, I would expect a transitory O-GlcNAcylation on those mitochondrial proteins would induce ΔΨm increase that can be utilized right away for ATP generation and transport out of mitochondria on the realistic, physiological time scale within a few minutes.

However, it remains elusive why O-GlcNAcylation of such proteins can accommodate much more efficient ETC activity or ATP production. One possibility is that subunits that are O-GlcNAcylated may undergo a conformational change to favor substrate binding, or even binding to other subunits in the same complex. Previously, it has been demonstrated that O-GlcNAcylation of ATP synthase subunit ATP5A1 prevents Amyloid-beta (Aβ) binding to the subunit and dysregulation of this modification is observed in Alzheimer's disease brains (Cha et al., 2015). Identification other O-GlcNAcylated ETC subunits, in addition to ATP synthase, may indicate that the modified subunits can restructure the complex and further participate in mitochondrial supercomplex formation, which needs further investigation.

Neuronal activity-dependent O-GlcNAcylation may also stimulate denser cristae formation, which then may act as a scaffold for the organization of the respiratory chain complexes. It has been recently reported that OGT induces cristae formation in response to cold-stress by promoting the import of a subunit of mitochondrial contact site and cristae organizing system (MICOS) (Latorre-Muro et al., 2021). Although the signaling cascade and model system is far from our neuronal activity model, it still highlights the potential role of O-GlcNAcylation in shaping mitochondrial cristae/structure. It is another interesting direction that requires proper examination by using electron microscopy images of mitochondria (for cristae morphologies) and blue native gel analysis (for supercomplex characterization) from stimulated neurons.

Substrate specific regulation of synaptoenergetics

Mitochondria are enriched at high energy demanding areas of neurons, such as presynaptic terminals or boutons, to offset high local energy consumption with more ATP generated by mitochondria in proximity (Li and Sheng, 2022; Rossi and Pekkurnaz, 2019). In addition to conventional factors regulating mitochondrial localization, like Ca^{2+} influx or ADP depletion, Pekkurnaz et al. previously showed that the fuel source can also control mitochondrial positioning in neurons (Li and Sheng, 2022; Pekkurnaz et al., 2014). Based on this previous work, I investigated ketone body- dependent regulation of mitochondrial transport and concluded that ketone body metabolism does not cause mitochondrial motility arrest (Figure 3.2). For future direction, it may be critical to evaluate whether mitochondrial density in presynaptic boutons is reduced in neurons using ketone bodies as the primary fuel source. This could be achieved by co-labeling mitochondria and synapses with markers such as vGLUT1-mVenus or Synaptophysin-GFP and analyzing their co-localization by live and fixed imaging. These experiments would provide us insight on how mitochondrial motility is acutely regulated near energy demanding boutons (Courchet et al., 2013; Sun et al., 2013). ATP sensors could also be targeted to presynaptic regions to evaluate how ketone body utilization may alter local synaptoenergetics in neurons.

Possible role of O-GlcNAcylation in glutamate metabolism

I demonstrated that the intracellular amino acid abundance is altered via O-GlcNAcylation (Figure 3.1C). Two of those particular amino acids that showed significantly elevated amounts were glutamate and aspartate, which can work as neurotransmitters in neurons. These results may indicate that O-GlcNAcylation primes neurons for more active neurotransmission, supported by

the dynamic O-GlcNAc modifications on glutamate-related proteins (Figure 3.5). For example, deletion of OGT in neurons cause downregulation of AMPA receptor subunits, GluA2 and GluA3, which further supports the crucial role of OGT and O-GlcNAcylation for synaptic function (Lagerlöf et al., 2017). In addition to glutamate receptors already validated by our data and previous works, many neuronal or mitochondrial proteins involved in glutamate metabolism are O-GlcNAcylated. These proteins include: glutamate transporters (both neuronal and mitochondrial), glutamate oxaloacetate transaminase (GOT2), and glutamate dehydrogenase (GDH) (Chiaradonna et al., 2018; Ma et al., 2016, 2015). The aforementioned proteins are either part of the glutamine-glutamate synthesis pathway or malate-aspartate shuttle (MAS), a major electron transport gate in and out of mitochondria (Figure 3.5A and B). How O-GlcNAcylation on these proteins affect their function and contribute to glutamate abundance requires further investigations. However, it is tempting to hypothesize that glutamate synthesis from the TCA cycle, as known as glutamate anabolic formation, is activated via O-GlcNAcylation, given the previous finding of cellular NAD+/NADH ratio increase in TMG treated rat cardiomyocytes (Tan et al., 2017) and our corresponding preliminary data from TMG treated neurons. To validate the hypothesis, the effect of O-GlcNAcylation on GDH—the key enzyme for glutamate biosynthesis from alpha-ketoglutarate (α-KG)—needs to be systematically evaluated.

So it leaves an important question unanswered: what is source of glutamate when O-GlcNAcylation is augmented in neurons? There are several possible pathways: (1) it is recycled from the synaptic cleft, (2) it could be taken up from the non-neuronal cells in the form of glutamine, which is rapidly converted back to glutamate by mitochondria, or (3) it is newly synthesized by mitochondria. To answer this question, we need spatial information of where glutamate is enriched. The first potential pathway, with glutamate coming from extracellular space,

can be easily evaluated by the use of a conventional glutamate sensor, iGluSnFR (Marvin et al., 2018, 2013). However, to investigate the second and third potential pathways, it would be necessary to target iGluSnFR to mitochondrial matrix in a similar way with iGABASnFR derivative targeting the mitochondria (mito-iGABASnFR.F102Y.Y137L) (Marvin et al., 2019). This approach would shed a light on detecting glutamate content and source in and out of mitochondria, eventually identifying how glutamate abundance changes with O-GlcNAcylation.

Our working model (Figure 3.4) goes in parallel with long-held views in the field that ketogenic diet or caloric restriction is effective in relieving seizure-like activities. At the cellular level, less excitability was observed in neurons from the subjects fed with ketogenic diet, either by downregulating excitatory synaptic activity or upregulating inhibitory synaptic transmissions (Juge et al., 2010; Lutas and Yellen, 2013; Ma et al., 2007; Yudkoff et al., 2007). Intriguingly, this anti-convulsant effect of the ketogenic diet is overturned by glucose infusion (Huttenlocher, 1976). This strongly implies that neuronal excitability is highly dependent on the fuel. Our working model highlights O-GlcNAcylation as a key player in this substrate-dependent neuronal excitability. It will further build to the clinical implication of O-GlcNAcylation as a therapeutic target for an epileptic seizure.

O-GlcNAcylation of SIRT5: Co-regulations of multiple PTMs

We identified that SIRT5 is O-GlcNAcylated (Figure 2.11B and Figure 4.1). SIRT5 is one of the Sirtuin family proteins responsible for removing acyl groups (succinyl-, malonyl- and glutaryl-) in an NAD+ dependent manner (Cantó et al., 2015; Houtkooper et al., 2012; Ji et al., 2022). Thus, SIRT5 is an important player of cellular metabolism. I have demonstrated that the

metabolic role of SIRT5 can be downregulated with higher O-GlcNAcylation by using metabolic flux anlaysis (Figure 4.3B) and immunostaining of its target PTM, succinylation (Figure 4.4-4.5). Since it is known that SIRT5 functions by NAD+ availability, a critical question remains: how does O-GlcNAcylation modulate SIRT5 activity in parallel to cellular NAD+ levels? Our data together with previous literatures (Durgan et al., 2011; Hwang and Song, 2017; Tan et al., 2017) suggest that O-GlcNAcylation may overrule the NAD+-activation of SIRT5 and work as an ultimate SIRT5 activity regulator, but this hypothesis needs thorough investigation in the future.

One caveat of my experimental design was the use of "succinylated" WGA to enrich O-GlcNAcylated proteins. Perhaps, non-specific attachment of SIRT5 on "succinylated" moieties on WGA may have caused SIRT5's detection in our proteomics data. To circumvent this problem, we can utilize Click-iT O-GlcNAc Enzyme Labeling System to label O-GlcNAc modified proteins with azide, instead of sWGA beads, which would allow tagging of these proteins with biotin to enable specific detection. The identification of O-GlcNAc modification sites of SIRT5 in neurons will be necessary for further mechanistic studies.

Despite its important role in metabolic homeostasis, succinylation is a remarkably understudied PTM. It is a larger PTM (~100 Da) compared to methylation (~14 Da) or acetylation (~40 Da) that alters the positively charged lysine residue to be negatively charged, which would yield more drastic changes in protein structure (Yang and Gibson, 2019). At present, there are only a few studies addressing how this modification changes protein structures or enzyme activity involved in key mitochondrial bioenergetics pathways (Lin et al., 2013; Park et al., 2013; Rardin et al., 2013; Zhang et al., 2017). This observation is consistent with our data that the succinylation staining pattern resembles that of mitochondria in neurons, implying high enrichment of modification in mitochondria and their major metabolic pathways (Figure 4.4-4.5).

The mechanisms regulating succinylation levels in the central nervous system is not well known. Only recently, alpha-ketoglutarate dehydrogenase complex (KGDHC) activity in primary cultured neurons is associated with succinylation (Gibson et al., 2015; Yang and Gibson, 2019). A very recent study by Yang et al. revealed a global change in succinylation level in Alzheimer's disease (AD) models in a subcellular specific manner—mostly downregulated in mitochondria and upregulated succinylation in the cytoplasm (Yang et al., 2022). The study attributed this particular change in AD to reduced brain glucose metabolism and disrupted KGDHC activity. Although indirect, this evidence hinted us to the involvement of glucose metabolism in regulating succinylation. Combined with our results, it is our speculation that O-GlcNAcylation, as a major glucose signaling pathway, would play a vital role in controlling succinylation, which can further tailor mitochondrial metabolism. Intriguingly, multiple proteins identified in mitochondrial O-GlcNAcome are also found to be succinylated (Nishida et al., 2015; Rardin et al., 2013). It coincides with the fact that there is no other protein identified to remove succinyl modification besides SIRT7, which is predominantly localized in the nucleus. Thus, for mitochondrial proteins that are succinylated, it is highly likely that the proteins are interactors of SIRT5. Regulation of SIRT5 via O-GlcNAcylation will be an interesting research direction that will provide us with a new mechanism that allows tight neurometabolism control by glucose metabolism.

Concluding perspectives

Roaming around the main theme of O-GlcNAcylation with its glucose sensing role, my doctorate work has demonstrated that mitochondrial metabolism is tightly regulated to accommodate neuronal activity (Chapter 2), substrate specificity (Chapter 3), and crosstalk between two PTMs (Chapter 4). The evidence that I have accumulated here point to the new

possible research paradigm of nutrient sensing for metabolic homeostasis, a step forward from the conventional paradigm of energetic stress in the field of neuronal metabolism. I am suggesting that O-GlcNAcylation is the mechanism that signals mitochondria to shift gears for glucose availability, the resource that mitochondria eventually have to utilize to generate energy accordingly.

My findings also suggest a tight link between glucose metabolism and mitochondrial bioenergetics, mediated by O-GlcNAcylation. This findings will particularly provide the key to identifying the crosstalk between glycolysis and mitochondria in neurons, which must be coordinated together for the proper energy supplies. For example, O-GlcNAcylation may imply a molecular mechanism of transition between the neuron's highly activated state, in which glycolysis takes over most of the synaptic ATP burden, and the normal OXPHOS-dominant state afterwards. My speculation is that O-GlcNAcylation may play an important role in this change in prioritizing ATP generating machineries, first by modifying glycolytic proteins and then propagating to mitochondrial O-GlcNAcylation. This will need further investigation in combination of proteomics analysis and live imaging with genetically modified sensors.

Finally, an additional effort of my doctoral research includes identifying the spontaneous O-GlcNAcylation changes by neuronal activity. Because most of neuronal activity like spiking and synaptic transmissions entails the millisecond to second timescales (Boyden et al., 2005), the molecular pathway that sustains those events must be as transient. Albeit our results revealing the capability of O-GlcNAc addition after one minute of robust stimulation, I would assume much more transient addition and removal of modification will happen with more physiological stimulations. It underscores the importance of monitoring O-GlcNAcylation, or even its donor substrate UDP-GlcNAc, in a more temporal manner.

To sum up, the work of my doctorate has opened the door for a new molecular pathway that couples glucose metabolism to metabolic regulations of mitochondria in neurons. It can further lead to the possible contribution to the field of neurodegeneration and aging, where both hypo-glucose metabolism and dysfunctional mitochondria are implicated. Therefore, the mediator of these two pathways, O-GlcNAcylation, can work as an impactful therapeutic target for such pathological conditions.

REFERENCES

Akan, I., Olivier-Van Stichelen, S., Bond, M.R., Hanover, J.A., 2018. Nutrient-driven *O* -GlcNAc in proteostasis and neurodegeneration. J. Neurochem. 144, 7–34. https://doi.org/10.1111/jnc.14242

Alfaro, J.F., Gong, C.-X., Monroe, M.E., Aldrich, J.T., Clauss, T.R.W., Purvine, S.O., Wang, Z., Camp, D.G., Shabanowitz, J., Stanley, P., Hart, G.W., Hunt, D.F., Yang, F., Smith, R.D., 2012. Tandem mass spectrometry identifies many mouse brain O-GlcNAcylated proteins including EGF domain-specific O-GlcNAc transferase targets. Proc. Natl. Acad. Sci. 109, 7280–7285. https://doi.org/10.1073/pnas.1200425109

Ansari, S.A., Emerald, B.S., 2019. The Role of Insulin Resistance and Protein O-GlcNAcylation in Neurodegeneration. Front. Neurosci. 13, 473. https://doi.org/10.3389/fnins.2019.00473

Ashrafi, G., de Juan-Sanz, J., Farrell, R.J., Ryan, T.A., 2020. Molecular Tuning of the Axonal Mitochondrial Ca2+ Uniporter Ensures Metabolic Flexibility of Neurotransmission. Neuron 105, 678-687.e5. https://doi.org/10.1016/j.neuron.2019.11.020

Ashrafi, G., Ryan, T.A., 2017. Glucose metabolism in nerve terminals. Curr. Opin. Neurobiol. 45, 156–161. https://doi.org/10.1016/j.conb.2017.03.007

Ashrafi, G., Schlehe, J.S., LaVoie, M.J., Schwarz, T.L., 2014. Mitophagy of damaged mitochondria occurs locally in distal neuronal axons and requires PINK1 and Parkin. J. Cell Biol. 206, 655–670. https://doi.org/10.1083/jcb.201401070

Ashrafi, G., Wu, Z., Farrell, R.J., Ryan, T.A., 2017. GLUT4 Mobilization Supports Energetic Demands of Active Synapses. Neuron 93, 606-615.e3. https://doi.org/10.1016/j.neuron.2016.12.020

Bak, L.K., Walls, A.B., Schousboe, A., Ring, A., Sonnewald, U., Waagepetersen, H.S., 2009. Neuronal glucose but not lactate utilization is positively correlated with NMDA-induced neurotransmission and fluctuations in cytosolic Ca^{2+} levels. J. Neurochem. 109, 87–93. https://doi.org/10.1111/j.1471-4159.2009.05943.x

Banerjee, P.S., Ma, J., Hart, G.W., 2015. Diabetes-associated dysregulation of *O* -GlcNAcylation in rat cardiac mitochondria. Proc. Natl. Acad. Sci. 112, 6050–6055. https://doi.org/10.1073/pnas.1424017112

Basu, H., Ding, L., Pekkurnaz, G., Cronin, M., Schwarz, T.L., 2020. Kymolyzer, a Semi-Autonomous Kymography Tool to Analyze Intracellular Motility. Curr. Protoc. Cell Biol. 87. https://doi.org/10.1002/cpcb.107

Basu, H., Pekkurnaz, G., Falk, J., Wei, W., Chin, M., Steen, J., Schwarz, T.L., 2021. FHL2 anchors mitochondria to actin and adapts mitochondrial dynamics to glucose supply. J. Cell Biol. 220, e201912077. https://doi.org/10.1083/jcb.201912077

Bateup, H.S., Johnson, C.A., Denefrio, C.L., Saulnier, J.L., Kornacker, K., Sabatini, B.L., 2013. Excitatory/Inhibitory Synaptic Imbalance Leads to Hippocampal Hyperexcitability in Mouse Models of Tuberous Sclerosis. Neuron 78, 510–522. https://doi.org/10.1016/j.neuron.2013.03.017

Benjamini, Y., Hochberg, Y., 1995. Controlling the False Discovery Rate: A Practical and Powerful Approach to Multiple Testing. J. R. Stat. Soc. Ser. B Methodol. 57, 289–300. https://doi.org/10.1111/j.2517-6161.1995.tb02031.x

Bentsen, M.A., Mirzadeh, Z., Schwartz, M.W., 2019. Revisiting How the Brain Senses Glucose—And Why. Cell Metab. 29, 11–17. https://doi.org/10.1016/j.cmet.2018.11.001

Boyden, E.S., Zhang, F., Bamberg, E., Nagel, G., Deisseroth, K., 2005. Millisecond-timescale, genetically targeted optical control of neural activity. Nat. Neurosci. 8, 1263–1268. https://doi.org/10.1038/nn1525

Bullen, J.W., Balsbaugh, J.L., Chanda, D., Shabanowitz, J., Hunt, D.F., Neumann, D., Hart, G.W., 2014. Cross-talk between Two Essential Nutrient-sensitive Enzymes. J. Biol. Chem. 289, 10592–10606. https://doi.org/10.1074/jbc.M113.523068

Bullitt, E., 1990. Expression of c-fos-like protein as a marker for neuronal activity following noxious stimulation in the rat. J. Comp. Neurol. 296, 517–530. https://doi.org/10.1002/cne.902960402

Cahill, G.F., 2006. Fuel Metabolism in Starvation. Annu. Rev. Nutr. 26, 1–22. https://doi.org/10.1146/annurev.nutr.26.061505.111258

Cantó, C., Jiang, L.Q., Deshmukh, A.S., Mataki, C., Coste, A., Lagouge, M., Zierath, J.R., Auwerx, J., 2010. Interdependence of AMPK and SIRT1 for Metabolic Adaptation to Fasting and Exercise in Skeletal Muscle. Cell Metab. 11, 213–219. https://doi.org/10.1016/j.cmet.2010.02.006

Cantó, C., Menzies, K.J., Auwerx, J., 2015. NAD+ Metabolism and the Control of Energy Homeostasis: A Balancing Act between Mitochondria and the Nucleus. Cell Metab. 22, 31–53. https://doi.org/10.1016/j.cmet.2015.05.023

Cha, M.-Y., Cho, H.J., Kim, C., Jung, Y.O., Kang, M.J., Murray, M.E., Hong, H.S., Choi, Y.-J., Choi, Heesun, Kim, D.K., Choi, Hyunjung, Kim, Jisoo, Dickson, D.W., Song, H.K., Cho, J.W., Yi, E.C., Kim, Jungsu, Jin, S.M., Mook-Jung, I., 2015. Mitochondrial ATP

synthase activity is impaired by suppressed *O* -GlcNAcylation in Alzheimer's disease. Hum. Mol. Genet. 24, 6492–6504. https://doi.org/10.1093/hmg/ddv358

Chen, T.-W., Wardill, T.J., Sun, Y., Pulver, S.R., Renninger, S.L., Baohan, A., Schreiter, E.R., Kerr, R.A., Orger, M.B., Jayaraman, V., Looger, L.L., Svoboda, K., Kim, D.S., 2013. Ultrasensitive fluorescent proteins for imaging neuronal activity. Nature 499, 295–300. https://doi.org/10.1038/nature12354

Chiaradonna, F., Ricciardiello, F., Palorini, R., 2018. The Nutrient-Sensing Hexosamine Biosynthetic Pathway as the Hub of Cancer Metabolic Rewiring. Cells 7, 53. https://doi.org/10.3390/cells7060053

Chowdhury, G.M., Jiang, L., Rothman, D.L., Behar, K.L., 2014. The Contribution of Ketone Bodies to Basal and Activity-Dependent Neuronal Oxidation *in Vivo*. J. Cereb. Blood Flow Metab. 34, 1233–1242. https://doi.org/10.1038/jcbfm.2014.77

Clark, P.M., Dweck, J.F., Mason, D.E., Hart, C.R., Buck, S.B., Peters, E.C., Agnew, B.J., Hsieh-Wilson, L.C., 2008. Direct In-Gel Fluorescence Detection and Cellular Imaging of *O* -GlcNAc-Modified Proteins. J. Am. Chem. Soc. 130, 11576–11577. https://doi.org/10.1021/ja8030467

Clarke, D.D., Sokoloff, L., 1999. Circulation and energy metabolism in the brain / Donald D. Clarke and Louis Sokoloff 34.

Cordes, T., Metallo, C.M., 2019. Quantifying Intermediary Metabolism and Lipogenesis in Cultured Mammalian Cells Using Stable Isotope Tracing and Mass Spectrometry, in: D'Alessandro, A. (Ed.), High-Throughput Metabolomics, Methods in Molecular Biology. Springer New York, New York, NY, pp. 219–241. https://doi.org/10.1007/978-1-4939-9236-2_14

Courchet, J., Lewis, T.L., Lee, S., Courchet, V., Liou, D.-Y., Aizawa, S., Polleux, F., 2013. Terminal Axon Branching Is Regulated by the LKB1-NUAK1 Kinase Pathway via Presynaptic Mitochondrial Capture. Cell 153, 1510–1525. https://doi.org/10.1016/j.cell.2013.05.021

Cunnane, S.C., Trushina, E., Morland, C., Prigione, A., Casadesus, G., Andrews, Z.B., Beal, M.F., Bergersen, L.H., Brinton, R.D., de la Monte, S., Eckert, A., Harvey, J., Jeggo, R., Jhamandas, J.H., Kann, O., la Cour, C.M., Martin, W.F., Mithieux, G., Moreira, P.I., Murphy, M.P., Nave, K.-A., Nuriel, T., Oliet, S.H.R., Saudou, F., Mattson, M.P., Swerdlow, R.H., Millan, M.J., 2020. Brain energy rescue: an emerging therapeutic concept for neurodegenerative disorders of ageing. Nat. Rev. Drug Discov. 19, 609–633. https://doi.org/10.1038/s41573-020-0072-x

Díaz-García, C.M., Mongeon, R., Lahmann, C., Koveal, D., Zucker, H., Yellen, G., 2017. Neuronal Stimulation Triggers Neuronal Glycolysis and Not Lactate Uptake. Cell Metab. 26, 361-374.e4. https://doi.org/10.1016/j.cmet.2017.06.021

Dietrich, M.O., Liu, Z.-W., Horvath, T.L., 2013. Mitochondrial Dynamics Controlled by Mitofusins Regulate Agrp Neuronal Activity and Diet-Induced Obesity. Cell 155, 188–199. https://doi.org/10.1016/j.cell.2013.09.004

Divakaruni, A.S., Wallace, M., Buren, C., Martyniuk, K., Andreyev, A.Y., Li, E., Fields, J.A., Cordes, T., Reynolds, I.J., Bloodgood, B.L., Raymond, L.A., Metallo, C.M., Murphy, A.N., 2017. Inhibition of the mitochondrial pyruvate carrier protects from excitotoxic neuronal death. J. Cell Biol. 216, 1091–1105. https://doi.org/10.1083/jcb.201612067

Du, J., Zhou, Y., Su, X., Yu, J.J., Khan, S., Jiang, H., Kim, J., Woo, J., Kim, J.H., Choi, B.H., He, B., Chen, W., Zhang, S., Cerione, R.A., Auwerx, J., Hao, Q., Lin, H., 2011. Sirt5 Is a NAD-Dependent Protein Lysine Demalonylase and Desuccinylase. Science 334, 806–809. https://doi.org/10.1126/science.1207861

Durgan, D.J., Pat, B.M., Laczy, B., Bradley, J.A., Tsai, J.-Y., Grenett, M.H., Ratcliffe, W.F., Brewer, R.A., Nagendran, J., Villegas-Montoya, C., Zou, C., Zou, L., Johnson, R.L., Dyck, J.R.B., Bray, M.S., Gamble, K.L., Chatham, J.C., Young, M.E., 2011. O-GlcNAcylation, Novel Post-Translational Modification Linking Myocardial Metabolism and Cardiomyocyte Circadian Clock. J. Biol. Chem. 286, 44606–44619. https://doi.org/10.1074/jbc.M111.278903

Frederick Wooten, G., Collins, R.C., 1980. Regional brain glucose utilization following intrastriatal injections of kainic acid. Brain Res. 201, 173–184. https://doi.org/10.1016/0006-8993(80)90782-9

Fulco, M., Cen, Y., Zhao, P., Hoffman, E.P., McBurney, M.W., Sauve, A.A., Sartorelli, V., 2008. Glucose Restriction Inhibits Skeletal Myoblast Differentiation by Activating SIRT1 through AMPK-Mediated Regulation of Nampt. Dev. Cell 14, 661–673. https://doi.org/10.1016/j.devcel.2008.02.004

Ge, Y., Ramirez, D.H., Yang, B., D'Souza, A.K., Aonbangkhen, C., Wong, S., Woo, C.M., 2021. Target protein deglycosylation in living cells by a nanobody-fused split O-GlcNAcase. Nat. Chem. Biol. 17, 593–600. https://doi.org/10.1038/s41589-021-00757-y

Gerber, L., Melis, L.V.J., Kleef, R.G.D.M., Groot, A., Westerink, R.H.S., 2021. Culture of Rat Primary Cortical Cells for Microelectrode Array (MEA) Recordings to Screen for Acute and Developmental Neurotoxicity. Curr. Protoc. 1. https://doi.org/10.1002/cpz1.158

Gibson, G.E., Xu, H., Chen, H.-L., Chen, W., Denton, T.T., Zhang, S., 2015. Alpha-ketoglutarate dehydrogenase complex-dependent succinylation of proteins in neurons and neuronal cell lines. J. Neurochem. 134, 86–96. https://doi.org/10.1111/jnc.13096

Graveling, A.J., Deary, I.J., Frier, B.M., 2013. Acute Hypoglycemia Impairs Executive Cognitive Function in Adults With and Without Type 1 Diabetes. Diabetes Care 36, 3240–3246. https://doi.org/10.2337/dc13-0194

Gusel'nikova, V.V., Korzhevskiy, D.E., 2015. NeuN As a Neuronal Nuclear Antigen and Neuron Differentiation Marker. Acta Naturae 7, 42–47.

Halim, N.D., Mcfate, T., Mohyeldin, A., Okagaki, P., Korotchkina, L.G., Patel, M.S., Jeoung, N.H., Harris, R.A., Schell, M.J., Verma, A., 2010. Phosphorylation status of pyruvate dehydrogenase distinguishes metabolic phenotypes of cultured rat brain astrocytes and neurons: Inhibited Glucose Oxidation in Astrocytes. Glia 58, 1168–1176. https://doi.org/10.1002/glia.20996

Hall, C.N., Klein-Flugge, M.C., Howarth, C., Attwell, D., 2012. Oxidative Phosphorylation, Not Glycolysis, Powers Presynaptic and Postsynaptic Mechanisms Underlying Brain Information Processing. J. Neurosci. 32, 8940–8951. https://doi.org/10.1523/JNEUROSCI.0026-12.2012

Hanover, J.A., Yu, S., Lubas, W.B., Shin, S.-H., Ragano-Caracciola, M., Kochran, J., Love, D.C., 2003. Mitochondrial and nucleocytoplasmic isoforms of O-linked GlcNAc transferase encoded by a single mammalian gene. Arch. Biochem. Biophys. 409, 287–297. https://doi.org/10.1016/S0003-9861(02)00578-7

Hirschey, M.D., Zhao, Y., 2015. Metabolic Regulation by Lysine Malonylation, Succinylation, and Glutarylation. Mol. Cell. Proteomics 14, 2308–2315. https://doi.org/10.1074/mcp.R114.046664

Houtkooper, R.H., Pirinen, E., Auwerx, J., 2012. Sirtuins as regulators of metabolism and healthspan. Nat. Rev. Mol. Cell Biol. 13, 225–238. https://doi.org/10.1038/nrm3293

Huttenlocher, P.R., 1976. Ketonemia and Seizures: Metabolic and Anticonvulsant Effects of Two Ketogenic Diets in Childhood Epilepsy. Pediatr. Res. 10, 536–540. https://doi.org/10.1203/00006450-197605000-00006

Hwang, E.S., Song, S.B., 2017. Nicotinamide is an inhibitor of SIRT1 in vitro, but can be a stimulator in cells. Cell. Mol. Life Sci. 74, 3347–3362. https://doi.org/10.1007/s00018-017-2527-8

Hwang, H., Rhim, H., 2019. Acutely elevated O-GlcNAcylation suppresses hippocampal activity by modulating both intrinsic and synaptic excitability factors. Sci. Rep. 9, 7287. https://doi.org/10.1038/s41598-019-43017-9

Inoki, K., Kim, J., Guan, K.-L., 2012. AMPK and mTOR in Cellular Energy Homeostasis and Drug Targets. Annu. Rev. Pharmacol. Toxicol. 52, 381–400. https://doi.org/10.1146/annurev-pharmtox-010611-134537

Jackson, D.A., Michael, T., Vieira de Abreu, A., Agrawal, R., Bortolato, M., Fisher, S.J., 2018. Prevention of Severe Hypoglycemia-Induced Brain Damage and Cognitive Impairment With Verapamil. Diabetes 67, 2107–2112. https://doi.org/10.2337/db18-0008

Ji, Z., Liu, G.-H., Qu, J., 2022. Mitochondrial sirtuins, metabolism, and aging. J. Genet. Genomics 49, 287–298. https://doi.org/10.1016/j.jgg.2021.11.005

Juge, N., Gray, J.A., Omote, H., Miyaji, T., Inoue, T., Hara, C., Uneyama, H., Edwards, R.H., Nicoll, R.A., Moriyama, Y., 2010. Metabolic Control of Vesicular Glutamate Transport and Release. Neuron 68, 99–112. https://doi.org/10.1016/j.neuron.2010.09.002

Khidekel, N., Ficarro, S.B., Clark, P.M., Bryan, M.C., Swaney, D.L., Rexach, J.E., Sun, Y.E., Coon, J.J., Peters, E.C., Hsieh-Wilson, L.C., 2007. Probing the dynamics of O-GlcNAc glycosylation in the brain using quantitative proteomics. Nat. Chem. Biol. 3, 339–348. https://doi.org/10.1038/nchembio881

Kolberg, L., Raudvere, U., Kuzmin, I., Vilo, J., Peterson, H., 2020. gprofiler2 -- an R package for gene list functional enrichment analysis and namespace conversion toolset g:Profiler. F1000Research 9, ELIXIR-709. https://doi.org/10.12688/f1000research.24956.2

Koronowski, K.B., Khoury, N., Morris-Blanco, K.C., Stradecki-Cohan, H.M., Garrett, T.J., Perez-Pinzon, M.A., 2018. Metabolomics Based Identification of SIRT5 and Protein Kinase C Epsilon Regulated Pathways in Brain. Front. Neurosci. 12, 32. https://doi.org/10.3389/fnins.2018.00032

Lagerlöf, O., Hart, G.W., Huganir, R.L., 2017. O-GlcNAc transferase regulates excitatory synapse maturity. Proc. Natl. Acad. Sci. 114, 1684–1689. https://doi.org/10.1073/pnas.1621367114

Lagerlof, O., Slocomb, J.E., Hong, I., Aponte, Y., Blackshaw, S., Hart, G.W., Huganir, R.L., 2016. The nutrient sensor OGT in PVN neurons regulates feeding. Science 351, 1293–1296. https://doi.org/10.1126/science.aad5494

Latorre-Muro, P., O'Malley, K.E., Bennett, C.F., Perry, E.A., Balsa, E., Tavares, C.D.J., Jedrychowski, M., Gygi, S.P., Puigserver, P., 2021. A cold-stress-inducible PERK/OGT

axis controls TOM70-assisted mitochondrial protein import and cristae formation. Cell Metab. 33, 598-614.e7. https://doi.org/10.1016/j.cmet.2021.01.013

Laughlin, S.B., de Ruyter van Steveninck, R.R., Anderson, J.C., 1998. The metabolic cost of neural information. Nat. Neurosci. 1, 36–41. https://doi.org/10.1038/236

Lazarus, B.D., Love, D.C., Hanover, J.A., 2006. Recombinant O-GlcNAc transferase isoforms: identification of O-GlcNAcase, yes tyrosine kinase, and tau as isoform-specific substrates. Glycobiology 16, 415–421. https://doi.org/10.1093/glycob/cwj078

Lee, B.E., Kim, H.Y., Kim, H.-J., Jeong, H., Kim, B.-G., Lee, H.-E., Lee, J., Kim, H.B., Lee, S.E., Yang, Y.R., Yi, E.C., Hanover, J.A., Myung, K., Suh, P.-G., Kwon, T., Kim, J.-I., 2020. *O*- GlcNAcylation regulates dopamine neuron function, survival and degeneration in Parkinson disease. Brain 143, 3699–3716. https://doi.org/10.1093/brain/awaa320

Lee, J.-Y., Kapur, M., Li, M., Choi, M.-C., Choi, S., Kim, H.-J., Kim, I., Lee, E., Taylor, J.P., Yao, T.-P., 2014. MFN1 deacetylation activates adaptive mitochondrial fusion and protects metabolically challenged mitochondria. J. Cell Sci. jcs.157321. https://doi.org/10.1242/jcs.157321

Lee, W.-L., Hablitz, J.J., 1989. Involvement of non-NMDA receptors in picrotoxin-induced epileptiform activity in the hippocampus. Neurosci. Lett. 107, 129–134. https://doi.org/10.1016/0304-3940(89)90804-5

Lévesque, M., Avoli, M., 2013. The kainic acid model of temporal lobe epilepsy. Neurosci. Biobehav. Rev. 37, 2887–2899. https://doi.org/10.1016/j.neubiorev.2013.10.011

Lewis, T.L., Kwon, S.-K., Lee, A., Shaw, R., Polleux, F., 2018. MFF-dependent mitochondrial fission regulates presynaptic release and axon branching by limiting axonal mitochondria size. Nat. Commun. 9, 5008. https://doi.org/10.1038/s41467-018-07416-2

Li, S., Sheng, Z.-H., 2022. Energy matters: presynaptic metabolism and the maintenance of synaptic transmission. Nat. Rev. Neurosci. 23, 4–22. https://doi.org/10.1038/s41583-021-00535-8

Li, S., Xiong, G.-J., Huang, N., Sheng, Z.-H., 2020. The cross-talk of energy sensing and mitochondrial anchoring sustains synaptic efficacy by maintaining presynaptic metabolism. Nat. Metab. 2, 1077–1095. https://doi.org/10.1038/s42255-020-00289-0

Liakath-Ali, K., Südhof, T.C., 2021. The Perils of Navigating Activity-Dependent Alternative Splicing of Neurexins. Front. Mol. Neurosci. 14, 659681. https://doi.org/10.3389/fnmol.2021.659681

Lin, Y., Bloodgood, B.L., Hauser, J.L., Lapan, A.D., Koon, A.C., Kim, T.-K., Hu, L.S., Malik, A.N., Greenberg, M.E., 2008. Activity-dependent regulation of inhibitory synapse development by Npas4. Nature 455, 1198–1204. https://doi.org/10.1038/nature07319

Lin, Z.-F., Xu, H.-B., Wang, J.-Y., Lin, Q., Ruan, Z., Liu, F.-B., Jin, W., Huang, H.-H., Chen, X., 2013. SIRT5 desuccinylates and activates SOD1 to eliminate ROS. Biochem. Biophys. Res. Commun. 441, 191–195. https://doi.org/10.1016/j.bbrc.2013.10.033

Lobas, M.A., Tao, R., Nagai, J., Kronschläger, M.T., Borden, P.M., Marvin, J.S., Looger, L.L., Khakh, B.S., 2019. A genetically encoded single-wavelength sensor for imaging cytosolic and cell surface ATP. Nat. Commun. 10, 711. https://doi.org/10.1038/s41467-019-08441-5

Lutas, A., Yellen, G., 2013. The ketogenic diet: metabolic influences on brain excitability and epilepsy. Trends Neurosci. 36, 32–40. https://doi.org/10.1016/j.tins.2012.11.005

Ma, J., Banerjee, P., Whelan, S.A., Liu, T., Wei, A.-C., Ramirez-Correa, G., McComb, M.E., Costello, C.E., O'Rourke, B., Murphy, A., Hart, G.W., 2016. Comparative Proteomics Reveals Dysregulated Mitochondrial O-GlcNAcylation in Diabetic Hearts. J. Proteome Res. 15, 2254–2264. https://doi.org/10.1021/acs.jproteome.6b00250

Ma, J., Liu, T., Wei, A.-C., Banerjee, P., O'Rourke, B., Hart, G.W., 2015. O-GlcNAcomic Profiling Identifies Widespread O-Linked β-N-Acetylglucosamine Modification (O-GlcNAcylation) in Oxidative Phosphorylation System Regulating Cardiac Mitochondrial Function. J. Biol. Chem. 290, 29141–29153. https://doi.org/10.1074/jbc.M115.691741

Ma, W., Berg, J., Yellen, G., 2007. Ketogenic Diet Metabolites Reduce Firing in Central Neurons by Opening KATP Channels. J. Neurosci. 27, 3618–3625. https://doi.org/10.1523/JNEUROSCI.0132-07.2007

MacAskill, A.F., Rinholm, J.E., Twelvetrees, A.E., Arancibia-Carcamo, I.L., Muir, J., Fransson, A., Aspenstrom, P., Attwell, D., Kittler, J.T., 2009. Miro1 Is a Calcium Sensor for Glutamate Receptor-Dependent Localization of Mitochondria at Synapses. Neuron 61, 541–555. https://doi.org/10.1016/j.neuron.2009.01.030

Malard, F., Wulff-Fuentes, E., Berendt, R.R., Didier, G., Olivier-Van Stichelen, S., 2021. Automatization and self-maintenance of the O-GlcNAcome catalog: a smart scientific database. Database 2021, baab039. https://doi.org/10.1093/database/baab039

Marvin, J.S., Borghuis, B.G., Tian, L., Cichon, J., Harnett, M.T., Akerboom, J., Gordus, A., Renninger, S.L., Chen, T.-W., Bargmann, C.I., Orger, M.B., Schreiter, E.R., Demb, J.B., Gan, W.-B., Hires, S.A., Looger, L.L., 2013. An optimized fluorescent probe for

visualizing glutamate neurotransmission. Nat. Methods 10, 162–170. https://doi.org/10.1038/nmeth.2333

Marvin, J.S., Scholl, B., Wilson, D.E., Podgorski, K., Kazemipour, A., Müller, J.A., Schoch, S., Quiroz, F.J.U., Rebola, N., Bao, H., Little, J.P., Tkachuk, A.N., Cai, E., Hantman, A.W., Wang, S.S.-H., DePiero, V.J., Borghuis, B.G., Chapman, E.R., Dietrich, D., DiGregorio, D.A., Fitzpatrick, D., Looger, L.L., 2018. Stability, affinity, and chromatic variants of the glutamate sensor iGluSnFR. Nat. Methods 15, 936–939. https://doi.org/10.1038/s41592-018-0171-3

Marvin, J.S., Shimoda, Y., Magloire, V., Leite, M., Kawashima, T., Jensen, T.P., Kolb, I., Knott, E.L., Novak, O., Podgorski, K., Leidenheimer, N.J., Rusakov, D.A., Ahrens, M.B., Kullmann, D.M., Looger, L.L., 2019. A genetically encoded fluorescent sensor for in vivo imaging of GABA. Nat. Methods 16, 763–770. https://doi.org/10.1038/s41592-019-0471-2

Mergenthaler, P., Lindauer, U., Dienel, G.A., Meisel, A., 2013. Sugar for the brain: the role of glucose in physiological and pathological brain function. Trends Neurosci. 36, 587–597. https://doi.org/10.1016/j.tins.2013.07.001

Mink, J.W., Blumenschine, R.J., Adams, D.B., 1981. Ratio of central nervous system to body metabolism in vertebrates: its constancy and functional basis. Am. J. Physiol.-Regul. Integr. Comp. Physiol. 241, R203–R212. https://doi.org/10.1152/ajpregu.1981.241.3.R203

Misgeld, T., Schwarz, T.L., 2017. Mitostasis in Neurons: Maintaining Mitochondria in an Extended Cellular Architecture. Neuron 96, 651–666. https://doi.org/10.1016/j.neuron.2017.09.055

Morris-Blanco, K.C., Dave, K.R., Saul, I., Koronowski, K.B., Stradecki, H.M., Perez-Pinzon, M.A., 2016. Protein Kinase C Epsilon Promotes Cerebral Ischemic Tolerance Via Modulation of Mitochondrial Sirt5. Sci. Rep. 6, 29790. https://doi.org/10.1038/srep29790

Mueller, T., Ouyang, X., Johnson, M.S., Qian, W.-J., Chatham, J.C., Darley-Usmar, V., Zhang, J., 2021. New Insights Into the Biology of Protein O-GlcNAcylation: Approaches and Observations. Front. Aging 1, 620382. https://doi.org/10.3389/fragi.2020.620382

Nie, D., Sahin, M., 2012. A Genetic Model to Dissect the Role of Tsc-mTORC1 in Neuronal Cultures, in: Weichhart, T. (Ed.), MTOR, Methods in Molecular Biology. Humana Press, Totowa, NJ, pp. 393–405. https://doi.org/10.1007/978-1-61779-430-8_25

Nishida, Y., Rardin, M.J., Carrico, C., He, W., Sahu, A.K., Gut, P., Najjar, R., Fitch, M., Hellerstein, M., Gibson, B.W., Verdin, E., 2015. SIRT5 Regulates both Cytosolic and

Mitochondrial Protein Malonylation with Glycolysis as a Major Target. Mol. Cell 59, 321–332. https://doi.org/10.1016/j.molcel.2015.05.022

O'Donnell, N., Zachara, N.E., Hart, G.W., Marth, J.D., 2004. *Ogt* -Dependent X-Chromosome-Linked Protein Glycosylation Is a Requisite Modification in Somatic Cell Function and Embryo Viability. Mol. Cell. Biol. 24, 1680–1690. https://doi.org/10.1128/MCB.24.4.1680-1690.2004

Ong, Q., Han, W., Yang, X., 2018. O-GlcNAc as an Integrator of Signaling Pathways. Front. Endocrinol. 9, 599. https://doi.org/10.3389/fendo.2018.00599

Owen, O.E., Morgan, A.P., Kemp, H.G., Sullivan, J.M., Herrera, M.G., Cahill, G.F., 1967. Brain Metabolism during Fasting*. J. Clin. Invest. 46, 1589–1595. https://doi.org/10.1172/JCI105650

Park, J., Chen, Y., Tishkoff, D.X., Peng, C., Tan, M., Dai, L., Xie, Z., Zhang, Y., Zwaans, B.M.M., Skinner, M.E., Lombard, D.B., Zhao, Y., 2013. SIRT5-Mediated Lysine Desuccinylation Impacts Diverse Metabolic Pathways. Mol. Cell 50, 919–930. https://doi.org/10.1016/j.molcel.2013.06.001

Pekkurnaz, G., Trinidad, J.C., Wang, X., Kong, D., Schwarz, T.L., 2014. Glucose Regulates Mitochondrial Motility via Milton Modification by O-GlcNAc Transferase. Cell 158, 54–68. https://doi.org/10.1016/j.cell.2014.06.007

Pillai, V.B., Sundaresan, N.R., Gupta, M.P., 2014. Regulation of Akt Signaling by Sirtuins: Its Implication in Cardiac Hypertrophy and Aging. Circ. Res. 114, 368–378. https://doi.org/10.1161/CIRCRESAHA.113.300536

Pinho, T.S., Verde, D.M., Correia, S.C., Cardoso, S.M., Moreira, P.I., 2018. O-GlcNAcylation and neuronal energy status: Implications for Alzheimer's disease. Ageing Res. Rev. 46, 32–41. https://doi.org/10.1016/j.arr.2018.05.003

Piquereau, J., Caffin, F., Novotova, M., Lemaire, C., Veksler, V., Garnier, A., Ventura-Clapier, R., Joubert, F., 2013. Mitochondrial dynamics in the adult cardiomyocytes: which roles for a highly specialized cell? Front. Physiol. 4. https://doi.org/10.3389/fphys.2013.00102

Poole, A.C., Thomas, R.E., Andrews, L.A., McBride, H.M., Whitworth, A.J., Pallanck, L.J., 2008. The PINK1/Parkin pathway regulates mitochondrial morphology. Proc. Natl. Acad. Sci. 105, 1638–1643. https://doi.org/10.1073/pnas.0709336105

Raichle, M.E., Mintun, M.A., 2006. BRAIN WORK AND BRAIN IMAGING. Annu. Rev. Neurosci. 29, 449–476. https://doi.org/10.1146/annurev.neuro.29.051605.112819

Ramírez, S., Gómez-Valadés, A.G., Schneeberger, M., Varela, L., Haddad-Tóvolli, R., Altirriba, J., Noguera, E., Drougard, A., Flores-Martínez, Á., Imbernón, M., Chivite, I., Pozo, M., Vidal-Itriago, A., Garcia, A., Cervantes, S., Gasa, R., Nogueiras, R., Gama-Pérez, P., Garcia-Roves, P.M., Cano, D.A., Knauf, C., Servitja, J.-M., Horvath, T.L., Gomis, R., Zorzano, A., Claret, M., 2017. Mitochondrial Dynamics Mediated by Mitofusin 1 Is Required for POMC Neuron Glucose-Sensing and Insulin Release Control. Cell Metab. 25, 1390-1399.e6. https://doi.org/10.1016/j.cmet.2017.05.010

Rangaraju, V., Calloway, N., Ryan, T.A., 2014. Activity-Driven Local ATP Synthesis Is Required for Synaptic Function. Cell 156, 825–835. https://doi.org/10.1016/j.cell.2013.12.042

Rardin, M.J., He, W., Nishida, Y., Newman, J.C., Carrico, C., Danielson, S.R., Guo, A., Gut, P., Sahu, A.K., Li, B., Uppala, R., Fitch, M., Riiff, T., Zhu, L., Zhou, J., Mulhern, D., Stevens, R.D., Ilkayeva, O.R., Newgard, C.B., Jacobson, M.P., Hellerstein, M., Goetzman, E.S., Gibson, B.W., Verdin, E., 2013. SIRT5 Regulates the Mitochondrial Lysine Succinylome and Metabolic Networks. Cell Metab. 18, 920–933. https://doi.org/10.1016/j.cmet.2013.11.013

Rath, S., Sharma, R., Gupta, R., Ast, T., Chan, C., Durham, T.J., Goodman, R.P., Grabarek, Z., Haas, M.E., Hung, W.H.W., Joshi, P.R., Jourdain, A.A., Kim, S.H., Kotrys, A.V., Lam, S.S., McCoy, J.G., Meisel, J.D., Miranda, M., Panda, A., Patgiri, A., Rogers, R., Sadre, S., Shah, H., Skinner, O.S., To, T.-L., Walker, M.A., Wang, H., Ward, P.S., Wengrod, J., Yuan, C.-C., Calvo, S.E., Mootha, V.K., 2021. MitoCarta3.0: an updated mitochondrial proteome now with sub-organelle localization and pathway annotations. Nucleic Acids Res. 49, D1541–D1547. https://doi.org/10.1093/nar/gkaa1011

Raudvere, U., Kolberg, L., Kuzmin, I., Arak, T., Adler, P., Peterson, H., Vilo, J., 2019. g:Profiler: a web server for functional enrichment analysis and conversions of gene lists (2019 update). Nucleic Acids Res. 47, W191–W198. https://doi.org/10.1093/nar/gkz369

Rexach, J.E., Clark, P.M., Mason, D.E., Neve, R.L., Peters, E.C., Hsieh-Wilson, L.C., 2012. Dynamic O-GlcNAc modification regulates CREB-mediated gene expression and memory formation. Nat. Chem. Biol. 8, 253–261. https://doi.org/10.1038/nchembio.770

Ritchie, M.E., Phipson, B., Wu, D., Hu, Y., Law, C.W., Shi, W., Smyth, G.K., 2015. limma powers differential expression analyses for RNA-sequencing and microarray studies. Nucleic Acids Res. 43, e47–e47. https://doi.org/10.1093/nar/gkv007

Rossi, M.J., Pekkurnaz, G., 2019. Powerhouse of the mind: mitochondrial plasticity at the synapse. Curr. Opin. Neurobiol. 57, 149–155. https://doi.org/10.1016/j.conb.2019.02.001

Sacoman, J.L., Dagda, R.Y., Burnham-Marusich, A.R., Dagda, R.K., Berninsone, P.M., 2017. Mitochondrial O-GlcNAc Transferase (mOGT) Regulates Mitochondrial Structure, Function, and Survival in HeLa Cells. J. Biol. Chem. 292, 4499–4518. https://doi.org/10.1074/jbc.M116.726752

Sadria, M., Layton, A.T., 2021. Interactions among mTORC, AMPK and SIRT: a computational model for cell energy balance and metabolism. Cell Commun. Signal. 19, 57. https://doi.org/10.1186/s12964-021-00706-1

Schindelin, J., Arganda-Carreras, I., Frise, E., Kaynig, V., Longair, M., Pietzsch, T., Preibisch, S., Rueden, C., Saalfeld, S., Schmid, B., Tinevez, J.-Y., White, D.J., Hartenstein, V., Eliceiri, K., Tomancak, P., Cardona, A., 2012. Fiji: an open-source platform for biological-image analysis. Nat. Methods 9, 676–682. https://doi.org/10.1038/nmeth.2019

Schneeberger, M., Dietrich, M.O., Sebastián, D., Imbernón, M., Castaño, C., Garcia, A., Esteban, Y., Gonzalez-Franquesa, A., Rodríguez, I.C., Bortolozzi, A., Garcia-Roves, P.M., Gomis, R., Nogueiras, R., Horvath, T.L., Zorzano, A., Claret, M., 2013. Mitofusin 2 in POMC Neurons Connects ER Stress with Leptin Resistance and Energy Imbalance. Cell 155, 172–187. https://doi.org/10.1016/j.cell.2013.09.003

Shannon, P., Markiel, A., Ozier, O., Baliga, N.S., Wang, J.T., Ramage, D., Amin, N., Schwikowski, B., Ideker, T., 2003. Cytoscape: A Software Environment for Integrated Models of Biomolecular Interaction Networks. Genome Res. 13, 2498–2504. https://doi.org/10.1101/gr.1239303

Shevchenko, A., Wilm, M., Vorm, O., Mann, M., 1996. Mass spectrometric sequencing of proteins silver-stained polyacrylamide gels. Anal. Chem. 68, 850–858. https://doi.org/10.1021/ac950914h

Shum, M., Segawa, M., Gharakhanian, R., Viñuela, A., Wortham, M., Baghdasarian, S., Wolf, D.M., Sereda, S.B., Nocito, L., Stiles, L., Zhou, Z., Gutierrez, V., Sander, M., Shirihai, O.S., Liesa, M., 2022. Deletion of ABCB10 in beta-cells protects from high-fat diet induced insulin resistance. Mol. Metab. 55, 101403. https://doi.org/10.1016/j.molmet.2021.101403

Smith, A.C., Robinson, A.J., 2019. MitoMiner v4.0: an updated database of mitochondrial localization evidence, phenotypes and diseases. Nucleic Acids Res. 47, D1225–D1228. https://doi.org/10.1093/nar/gky1072

Stewart, L.T., Abiraman, K., Chatham, J.C., McMahon, L.L., 2020. Increased O-GlcNAcylation rapidly decreases GABAAR currents in hippocampus but depresses neuronal output. Sci. Rep. 10, 7494. https://doi.org/10.1038/s41598-020-63188-0

Südhof, T.C., 2018. Towards an Understanding of Synapse Formation. Neuron 100, 276–293. https://doi.org/10.1016/j.neuron.2018.09.040

Sun, T., Qiao, H., Pan, P.-Y., Chen, Y., Sheng, Z.-H., 2013. Motile Axonal Mitochondria Contribute to the Variability of Presynaptic Strength. Cell Rep. 4, 413–419. https://doi.org/10.1016/j.celrep.2013.06.040

Szklarczyk, D., Gable, A.L., Nastou, K.C., Lyon, D., Kirsch, R., Pyysalo, S., Doncheva, N.T., Legeay, M., Fang, T., Bork, P., Jensen, L.J., von Mering, C., 2021. The STRING database in 2021: customizable protein–protein networks, and functional characterization of user-uploaded gene/measurement sets. Nucleic Acids Res. 49, D605–D612. https://doi.org/10.1093/nar/gkaa1074

Tallent, M.K., Varghis, N., Skorobogatko, Y., Hernandez-Cuebas, L., Whelan, K., Vocadlo, D.J., Vosseller, K., 2009. In Vivo Modulation of O-GlcNAc Levels Regulates Hippocampal Synaptic Plasticity through Interplay with Phosphorylation. J. Biol. Chem. 284, 174–181. https://doi.org/10.1074/jbc.M807431200

Tan, E.P., McGreal, S.R., Graw, S., Tessman, R., Koppel, S.J., Dhakal, P., Zhang, Z., Machacek, M., Zachara, N.E., Koestler, D.C., Peterson, K.R., Thyfault, J.P., Swerdlow, R.H., Krishnamurthy, P., DiTacchio, L., Apte, U., Slawson, C., 2017. Sustained O-GlcNAcylation reprograms mitochondrial function to regulate energy metabolism. J. Biol. Chem. 292, 14940–14962. https://doi.org/10.1074/jbc.M117.797944

Taub, D.G., Awal, M.R., Gabel, C.V., 2018. O-GlcNAc Signaling Orchestrates the Regenerative Response to Neuronal Injury in Caenorhabditis elegans. Cell Rep. 24, 1931-1938.e3. https://doi.org/10.1016/j.celrep.2018.07.078

Taylor, A.M., Blurton-Jones, M., Rhee, S.W., Cribbs, D.H., Cotman, C.W., Jeon, N.L., 2005. A microfluidic culture platform for CNS axonal injury, regeneration and transport. Nat. Methods 2, 599–605. https://doi.org/10.1038/nmeth777

Taylor, E.W., Wang, K., Nelson, A.R., Bredemann, T.M., Fraser, K.B., Clinton, S.M., Puckett, R., Marchase, R.B., Chatham, J.C., McMahon, L.L., 2014. O-GlcNAcylation of AMPA Receptor GluA2 Is Associated with a Novel Form of Long-Term Depression at Hippocampal Synapses. J. Neurosci. 34, 10–21. https://doi.org/10.1523/JNEUROSCI.4761-12.2014

Tondera, D., Grandemange, S., Jourdain, A., Karbowski, M., Mattenberger, Y., Herzig, S., Da Cruz, S., Clerc, P., Raschke, I., Merkwirth, C., Ehses, S., Krause, F., Chan, D.C., Alexander, C., Bauer, C., Youle, R., Langer, T., Martinou, J.-C., 2009. SLP-2 is required for stress-induced mitochondrial hyperfusion. EMBO J. 28, 1589–1600. https://doi.org/10.1038/emboj.2009.89

Trinidad, J.C., Barkan, D.T., Thalhammer, A., Sali, A., 2012. Global Identification and Characterization of Both O-GlcNAcylation and Phosphorylation at the Murine Synapse 15.

Tyanova, S., Temu, T., Sinitcyn, P., Carlson, A., Hein, M.Y., Geiger, T., Mann, M., Cox, J., 2016. The Perseus computational platform for comprehensive analysis of (prote)omics data. Nat. Methods 13, 731–740. https://doi.org/10.1038/nmeth.3901

Vaccaro, V., Devine, M.J., Higgs, N.F., Kittler, J.T., 2017. Miro1-dependent mitochondrial positioning drives the rescaling of presynaptic Ca $^{2+}$ signals during homeostatic plasticity. EMBO Rep. 18, 231–240. https://doi.org/10.15252/embr.201642710

Wang, A.C., Jensen, E.H., Rexach, J.E., Vinters, H.V., Hsieh-Wilson, L.C., 2016. Loss of *O* -GlcNAc glycosylation in forebrain excitatory neurons induces neurodegeneration. Proc. Natl. Acad. Sci. 113, 15120–15125. https://doi.org/10.1073/pnas.1606899113

Wang, X., Schwarz, T.L., 2009. The Mechanism of Ca2+-Dependent Regulation of Kinesin-Mediated Mitochondrial Motility. Cell 136, 163–174. https://doi.org/10.1016/j.cell.2008.11.046

Wheatley, E.G., Albarran, E., White, C.W., Bieri, G., Sanchez-Diaz, C., Pratt, K., Snethlage, C.E., Ding, J.B., Villeda, S.A., 2019. Neuronal O-GlcNAcylation Improves Cognitive Function in the Aged Mouse Brain. Curr. Biol. 29, 3359-3369.e4. https://doi.org/10.1016/j.cub.2019.08.003

Wickham, H., 2016. ggplot2: Elegant Graphics for Data Analysis, 2nd ed. 2016. ed, Use R! Springer International Publishing : Imprint: Springer, Cham. https://doi.org/10.1007/978-3-319-24277-4

Wu, J.-L., Chiang, M.-F., Hsu, P.-H., Tsai, D.-Y., Hung, K.-H., Wang, Y.-H., Angata, T., Lin, K.-I., 2017. O-GlcNAcylation is required for B cell homeostasis and antibody responses. Nat. Commun. 8, 1854. https://doi.org/10.1038/s41467-017-01677-z

Wulff-Fuentes, E., Berendt, R.R., Massman, L., Danner, L., Malard, F., Vora, J., Kahsay, R., Olivier-Van Stichelen, S., 2021. The human O-GlcNAcome database and meta-analysis. Sci. Data 8, 25. https://doi.org/10.1038/s41597-021-00810-4

Yang, X., Qian, K., 2017. Protein O-GlcNAcylation: emerging mechanisms and functions. Nat. Rev. Mol. Cell Biol. 18, 452–465. https://doi.org/10.1038/nrm.2017.22

Yang, Y., Gibson, G.E., 2019. Succinylation Links Metabolism to Protein Functions. Neurochem. Res. 44, 2346–2359. https://doi.org/10.1007/s11064-019-02780-x

Yang, Y., Tapias, V., Acosta, D., Xu, H., Chen, H., Bhawal, R., Anderson, E.T., Ivanova, E., Lin, H., Sagdullaev, B.T., Chen, J., Klein, W.L., Viola, K.L., Gandy, S., Haroutunian, V., Beal, M.F., Eliezer, D., Zhang, S., Gibson, G.E., 2022. Altered succinylation of mitochondrial proteins, APP and tau in Alzheimer's disease. Nat. Commun. 13, 159. https://doi.org/10.1038/s41467-021-27572-2

Yang, Y.R., Song, S., Hwang, H., Jung, J.H., Kim, S.-J., Yoon, S., Hur, J.-H., Park, J.-I., Lee, C., Nam, D., Seo, Y.-K., Kim, J.-H., Rhim, H., Suh, P.-G., 2017. Memory and synaptic plasticity are impaired by dysregulated hippocampal O-GlcNAcylation. Sci. Rep. 7, 44921. https://doi.org/10.1038/srep44921

Yellen, G., 2018. Fueling thought: Management of glycolysis and oxidative phosphorylation in neuronal metabolism. J. Cell Biol. 217, 2235–2246. https://doi.org/10.1083/jcb.201803152

Yi, W., Clark, P.M., Mason, D.E., Keenan, M.C., Hill, C., Goddard, W.A., Peters, E.C., Driggers, E.M., Hsieh-Wilson, L.C., 2012. Phosphofructokinase 1 Glycosylation Regulates Cell Growth and Metabolism. Science 337, 975–980. https://doi.org/10.1126/science.1222278

Yu, S.B., Pekkurnaz, G., 2018. Mechanisms Orchestrating Mitochondrial Dynamics for Energy Homeostasis. J. Mol. Biol. 430, 3922–3941. https://doi.org/10.1016/j.jmb.2018.07.027

Yudkoff, M., Daikhin, Y., Melø, T.M., Nissim, Ilana, Sonnewald, U., Nissim, Itzhak, 2007. The Ketogenic Diet and Brain Metabolism of Amino Acids: Relationship to the Anticonvulsant Effect. Annu. Rev. Nutr. 27, 415–430. https://doi.org/10.1146/annurev.nutr.27.061406.093722

Zhang, J., Nuebel, E., Wisidagama, D.R.R., Setoguchi, K., Hong, J.S., Van Horn, C.M., Imam, S.S., Vergnes, L., Malone, C.S., Koehler, C.M., Teitell, M.A., 2012. Measuring energy metabolism in cultured cells, including human pluripotent stem cells and differentiated cells. Nat. Protoc. 7, 1068–1085. https://doi.org/10.1038/nprot.2012.048

Zhang, Y., Bharathi, S.S., Rardin, M.J., Lu, J., Maringer, K.V., Sims-Lucas, S., Prochownik, E.V., Gibson, B.W., Goetzman, E.S., 2017. Lysine desuccinylase SIRT5 binds to cardiolipin and regulates the electron transport chain. J. Biol. Chem. 292, 10239–10249. https://doi.org/10.1074/jbc.M117.785022

Zhu, Y., Hart, G.W., 2021. Targeting O-GlcNAcylation to develop novel therapeutics. Mol. Aspects Med. 79, 100885. https://doi.org/10.1016/j.mam.2020.100885

Zorova, L.D., Popkov, V.A., Plotnikov, E.Y., Silachev, D.N., Pevzner, I.B., Jankauskas, S.S., Babenko, V.A., Zorov, S.D., Balakireva, A.V., Juhaszova, M., Sollott, S.J., Zorov, D.B.,

2018. Mitochondrial membrane potential. Anal. Biochem. 552, 50–59. https://doi.org/10.1016/j.ab.2017.07.009